Modeling and Simulation of Lower Limb Spasticity in Motor-Impaired Individuals

by

Yesung Cha

A thesis

presented to the University of Waterloo

in fulfillment of the

thesis requirement for the degree of

Master of Applied Science

in

Mechanical and Mechatronics Engineering

Waterloo, Ontario, Canada, 2021

Author’s Declaration

This thesis consists of material all of which I authored or co-authored: see Statement of Contributions included in the thesis. This is a true copy of the thesis, including any required final revisions, as accepted by my examiners.

I understand that my thesis may be made electronically available to the public.

Statement of Contributions

Yesung Cha was the sole author of Chapters 3 and 5, under the supervision of Dr. Arash Arami.

Research presented in Chapters 1 and 2:

Chapters 1 and 2 contain excerpts from a publication [1] that was co-authored by Yesung Cha and Dr. Arash Arami in the peer-reviewed journal *Sensors*, for the special issue: "Body Worn Sensors and Special Applications" (September 5, 2020).

Research presented in Chapter 4:

Yesung Cha was the sole author and researcher for the development of a spastic controller for simulation environments, and the application of that controller in simulations of passive motion spasticity assessments.

The research for simulations of spastic walking agents was conducted by Yesung Cha and Jiacheng (Sola) Weng. Yesung Cha provided the adaptation of the previously developed spasticity controller for walking simulations and was the sole author of the analysis and discussion of the results. Jiacheng Weng provided the originally developed reinforcement-learning walking agent, integration of the spasticity controller into the Python environment and modification of the reinforcement-learning functions and training of the agents to achieve successful walking simulations.

Abstract

Spasticity is a symptom that impairs the ability to freely move and control one's limbs through increased tone and involuntary activations in the muscles. It can cause pain and discomfort and interfere with daily life and activities such as walking. Spasticity is a result of upper motor neuron lesions and is seen commonly in survivors of stroke and brain trauma, and individuals with cerebral palsy, multiple sclerosis, and spinal cord injuries. Despite its ubiquity the phenomena is not well understood. However, the most referred to definition describes spasticity as "a velocity-dependent increase in tonic stretch reflexes with exaggerated tendon jerks, resulting from hyper-excitability of the stretch reflexes."

Qualitative, subjective measures are commonly used in the clinical setting to assess spasticity, most notably the Modified Ashworth score, which has been shown to have inconsistent reliability, relying heavily on the examiner's experience, and is inaccurate for the lower limbs. Furthermore, these subjective scores do not account for the velocity-dependence of spasticity, which is a key differentiator against other symptoms such as rigidity. Consequently, there is a need for an objective measure of spasticity that can provide a more accurate and reliable alternative or supplement to the current clinical practice, in order to improve the evaluation of treatment and rehabilitation for spasticity.

To address this need, a system was developed, validated and applied for modeling the spasticity in the lower-limbs of an affected individual. An experimental setup consisted of a brace-handle system with integrated force sensors for passive actuation of each leg segment, stretching spastic muscles to assess the severity of the condition. The setup included wearable sensors sEMG and IMUs – recording muscular activity and limb segment kinematics respectively during these motions. From the data, onsets of muscular activity and subsequently the trigger points of spastic reflexes were identified, which were mapped onto the calculated joint kinematics. Based on threshold-control theory, stretch reflex threshold (SRT) models of spasticity were created for each muscle by plotting the joint velocities and positions and using regression analysis to create a dynamic threshold in the kinematic space that divided the regimes of spastic and non-spastic motion. These muscle-specific models were combined by muscle groups, leading to the creation of a novel, data-based measure that characterizes the severity of spasticity of a group of muscles. The models and measures were found to agree with the expected changes from different conditions of muscle stretch, and different levels of spasticity in the included subjects, but required more data for statistical validation.

The muscle-specific models were then implemented in a spasticity controller developed for use in neuromuscular simulations, in addition to further modeling of spastic reflex characteristics.

The controller was applied in a scenario simulation of the same passive movement spasticity assessments used to collect the original data, which provided additional validation of the methodology and results of the modeling. The spasticity controller was also applied in a previously developed reinforcement-learning walking agent, to see the effects of spasticity on simulated gait. Following modification and training of the new agents, the spatio-temporal parameters of gait were analyzed to determine the differences in healthy and spastic gait, which agreed with expectations and further validated the spasticity modeling.

This thesis presents a system to accurately and reliably model spasticity, establishing a novel, objective measure to better characterize spasticity, validating it through demonstrations of its use that may be extended in future work to accomplish better understanding of spasticity and provide invaluable improvements to the lives of affected individuals through practical applications.

Acknowledgements

I would like to sincerely thank my supervisor, Dr. Arash Arami, for his guidance and patience during the two plus change years of my master's studies. It would not have been possible without his encouragement and support throughout the development and progression of this thesis.

I would like to thank Dr. Duane Cronin and Dr. Ehsan Hashemi for taking valuable time out of their schedules by agreeing to be part of the readers committee for my thesis.

I would like to thank my colleagues in the Neuromechanics and Assistive Robotics Laboratory for their contributions and assistance in my master's studies and research.

I would like to thank the Natural Sciences and Engineering Research Council of Canada and the Centre for Bioengineering and Biotechnology at the University of Waterloo in part for funding my research.

I would also like to thank my wonderful family for their love and support, especially through this turbulent time which happened to make up the majority of my career at the University of Waterloo, which was nevertheless enjoyable and memorable.

Table of Contents

List of Figures

List of Tables

Chapter 1:

Introduction

Upper motor neuron syndrome (UMNS) is a set of symptoms that can follow stroke, brain injury or spinal cord injury (SCI), which can result in damage to the descending motor pathways from the motor cortex to the spinal cord. UMNS can also be seen in other neurological disorders including multiple sclerosis and cerebral palsy. Common symptoms included in UMNS are muscle weakness and endurance issues, and hyper- or hypo-tonia (increased or decreased muscle tone). An affected individual can suffer from problems with motor control, including worsened speed and accuracy of body movement.

Spasticity is a common symptom of upper motor neuron lesions, which can be described by increased muscle tightness and stiffness, and a hyperexcitability of the reflexes that causes involuntary contraction of the muscles or jerky movements. Spasticity presents in varying degrees of severity, and it can interfere with daily activities, movement or speech of an affected person, and can cause discomfort or pain [2]. Approximately 42% of stroke patients develop spasticity within six months of the onset of stroke [3], and spasticity affects about 65% of patients with MS [4], and about 70% of individuals living with SCI [5]. Spasticity in the long-term can lead to secondary complications such as problems with posture or muscle contractures [6], which are deformities caused by persistently shortened muscles and tendons.

A commonly accepted definition of spasticity is lacking in the literature, especially in the neurology and biomechanics communities. In a review of 250 studies [7], 35% simply equate spasticity with increased muscle tone, and nearly the same number either fail to define it or use their own definitions of spasticity. However, over 30% of studies refer to Lance's [8], [9] definition of spasticity, i.e., "a velocity-dependent increase in tonic stretch reflexes with exaggerated tendon jerks, resulting from hyper-excitability of the stretch reflexes." These three features are essential for characterizing spasticity, especially because it is also important to differentiate spasticity from other symptoms that may seem similar but are fundamentally distinct. Rigidity is another common symptom, seen in Parkinson's disease. It is characterized by increased muscle resistance occurring through the range of motion [10] and does not depend on the velocity or acceleration of movement [2]. Spasticity must also be distinguished from clinically defined flexor synergy as described by Twitchell [11] and Brunnstrom [12]. An example of flexor synergy in the clinical sense, which should not be mistaken with synergy in the context of motor control, is an abnormal coactivation of shoulder abductor muscles with elbow flexor muscles [13].

Other factors may contribute to increased muscle activity seen in spasticity, such as cutaneous or pain-related reflex mechanisms [14].

There is also a lack of consensus about the mechanisms involved in spasticity [14]. For instance, what neurological and physiological factors are involved, and how much do they contribute to the condition? It is challenging to answer the above question as the lesions affect different pathways in a patient-specific way and the subsequent adaptation in the spinal network varies across patients. The contribution of the spinal excitatory and inhibitory mechanisms and supraspinal (both inhibitory and excitatory) pathways to spasticity are still not fully understood and require further investigation.

Treatment for spasticity often involves rehabilitation, which is generally aimed at reducing the reflex hyperexcitability, normalizing muscle tone and improving motor control [15]. Medication can be effective, such as injections of botulinum toxin type A, which inhibits the signals to your muscles and therefore the spasticity. However, it must be continuously administered, which can become very expensive. Additionally, the peak of effectiveness is followed by a longer period where the spasticity symptoms gradually re-emerge, which can lead to adverse effects such as frustration, sleep loss and depression [16].

Assessing spasticity is essential for patient follow up, especially to evaluate the effectiveness of treatment by medication or rehabilitation [17], [18], and to improve our understanding of the underlying factors of spasticity. Clinicians today use qualitative measures to assess spasticity, most notably the Modified Ashworth Scale (MAS), which tends to be very subjective, relies heavily on the examiner's experience, and is inaccurate, especially for the lower limbs [19]. Instead, obtaining an objective, quantitative measure of spasticity would be better suited for assessment and following up the effects of treatment and rehabilitation.

1.1 Outline and Objectives

The main goal of this research was to develop a quantitative model of spasticity that can be used to accurately predict spastic behaviour in an individual's lower limb based on threshold control hypothesis [20]. To accomplish this goal, three primary objectives were established:

1) Develop wearable instrumentation and algorithms that will allow for modeling spasticity in a subject, and technically validate them to ensure accurate and reliable modeling.
2) Develop a protocol for spasticity experiments, consisting of passive movements of the joints in an individual's leg at different poses and speeds, using the instrumented handles and recording the required data.
    a) Collect data in collaboration with the Toronto Rehabilitation Institute involving individuals with SCI.

3) Develop models and extract features that characterizes spasticity, then combine them into a quantitative score that will supplement existing clinical measures of spasticity.

A new objective was also added following changes to the situation (see Section 3.1.4):

4) Develop a neuromuscular simulation controller of spasticity and apply it to simulations of scenarios, including passive spasticity assessments and walking.

Chapter 2 presents a review of the current state of research and application in assessing spasticity. Instead of a systematic review of the overall research, the focus is on identifying different approaches for quantitative modeling of spasticity, including the key measures used, their strengths and limitations, challenges, and future directions for spasticity research. Representative papers were selected based on modeling approaches to demonstrate the differences between the methodologies.

Chapter 3 features the methodology and results of modeling spasticity with wearable sensors. The chapter begins with the experimental design and protocol in Section 3.1, and the data processing theory and algorithms are described in Section 3.2, including a novel objective measure of spasticity. The approaches are validated in Section 3.3, and Section 3.4 describes and discusses the results of modeling.

Chapter 4 describes the functions and algorithms for simulating spasticity, in scenarios of passive movement spasticity with a virtual examiner, and a reinforcement learning walking agent. Section 4.1 introduces the background and motivation for the chapter, and Sections 4.2 and 4.3 describe the methodology for the simulations. Section 4.4 presents the results of the simulation scenarios, and Section 4.5 offers a brief conclusion on the topic.

Chapter 5 provides a conclusion to the thesis, revisiting the objectives, results and discussions of the previous chapters and directions for future research in this topic.

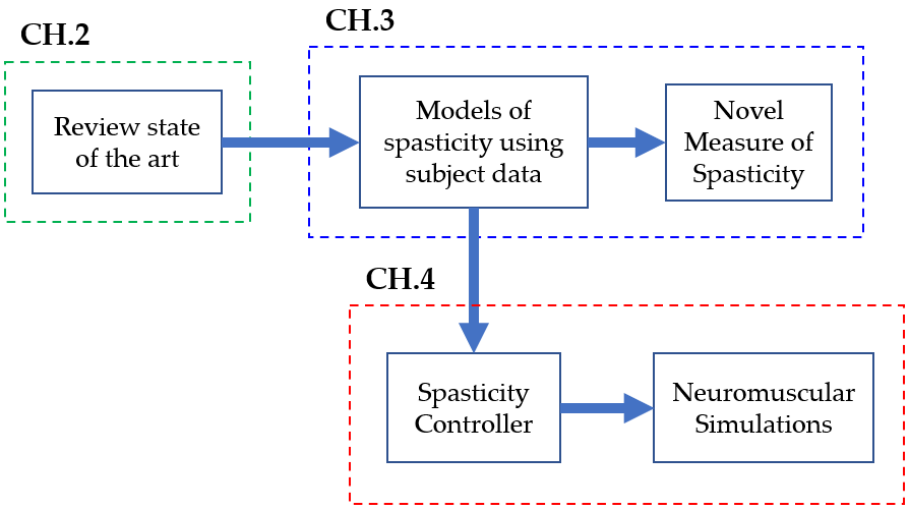

Figure 1. Overview of the progression of the research through the chapters of the thesis.

Chapter 2:

Literature Review

2.1 Subjective Clinical Measures

Qualitative measures are widely used in the clinical setting to assess spasticity, most notably the Modified Ashworth Scale (MAS) [21], [22] (see **Table 1**), which tends to be subjective, relies heavily on the examiner's experience, and is inaccurate, especially for the lower limbs [19]. Even for upper limbs, there is inconsistency in the inter-rater and intra-rater reliability. While some studies reported good inter- and intra-rater reliability [22], [23], mostly for upper limb muscles, others reported poor reliability between raters [24]. Reporting the reliability based on only two raters, as has been done in those studies, is questionable. Pandyan et al. [19] in their review suggest that both the Ashworth Scale (AS) and MAS are only good as ordinal and nominal level measures of resistance to passive movement, respectively, not measures of spasticity itself.

Such clinical scores are also unable to differentiate the previously discussed overlapping symptoms seen in UMNS. The scores are also blind to the factors that cause spasticity, therefore they could not contribute to understanding the underlying phenomena.

Table 1: Modified Ashworth Scale (MAS).

Grade	Description
0	no increase in muscle tone.
1	slight increase in muscle tone, manifested by a catch and release or by minimal resistance at the end of the range of motion (ROM) when the affected part(s) in moved flexion or extension.
1+	slight increase in muscle tone, manifested by a catch, followed by minimal resistance throughout the remainder (less than half) of the ROM.
2	more marked increase in muscle tone through most of the ROM, but affected part(s) easily moved.
3	considerable increase in muscle tone, passive movement difficult.
4	affected part(s) rigid in flexion or extension.

The Tardieu Scale is another clinical measure of muscle spasticity that can better account for the velocity-dependent characteristic of spasticity, by assessing the passive muscle response at slow and fast speeds. The Tardieu Scale and its modified version have been recently preferred over AS and MAS [25], as they better follow Lance's definition and are more sensitive to the

changes in spasticity [26], [27]. However, there is a lack of investigations of the Tardieu Scale reliability and quality as a measure of spasticity [28].

The lack of consistency and reliability of subjective measures suggest a need for an objective measure based on a quantitative approach to accurately estimate spasticity. Such objective measures could be better suited for assessment and monitoring the subsequent treatment and rehabilitation of the symptom.

2.2 Objective Approaches in Literature

To address the shortcomings of existing clinical scores, objective measures of spasticity have been investigated in recent decades. In this section, we discuss the objective approaches that have been employed to characterize spasticity, where different sensor-based quantitative measurements have been used (see **Section 2.2.1**) along with different modeling techniques (see **Section 2.2.2**) to produce outcome measures that indicate the severity of spasticity.

2.2.1 Sensors and Measurement

2.2.1.1 Electromyography

Electromyography (EMG) measures the electrical current generated in the muscles during contraction, and the signal can represent the activity of a given muscle [29]. The EMG signal is the product of a complicated process involving the nervous system and physiological properties of the muscles. The signal becomes noisy due to traveling through different tissues. Surface EMG (sEMG) uses electrodes on the skin to collect these signals, which makes it particularly prone to muscle crosstalk. Improper placement of sEMG electrodes can cause significant variations in the signal amplitude and spectral characteristics. These variations between recordings could be mistakenly attributed to the effects of a treatment or rehabilitation method [30]. Electrodes that are not aligned with the muscle fibers can also result in sEMG signals with distorted amplitude or frequencies. Staudenmann et al. [31] found that properly aligned bipolar electrodes result in the lowest root mean square difference between measured muscle forces and estimate muscle forces using the sEMG recordings. Despite the potential complications, the benefit of sEMG is the ease of use and reduced discomfort when compared to invasive techniques such as intramuscular EMG involving a needle.

Repeatability of sEMG recordings and analysis is necessary for any objective approach. Steele et al. [32] demonstrated the high repeatability of sEMG recordings and analysis of muscle synergies between clinical visits up to six weeks apart, suggesting that any change in the results of signal analysis reflects a real change in the muscular activity. Accurate detection of the onset of muscle activity is important in some approaches to quantitative modeling of spasticity, as

described in **Section 3.2**. This emphasizes the importance of EMG-based event detection algorithms.

Staude and Wolf [33] investigated three representative methods for "event" detection in EMG signals: the traditional finite moving average (FMA), two-threshold (TT) criterion, approximated generalized likelihood ratio (AGLR), as well as the cumulative sum (CUSUM) type model (with known parameters) as a comparative reference for optimal performance. The FMA algorithm uses a sliding window technique, comparing the (weighted) mean amplitude of the data to a threshold value. The TT algorithm is essentially based on the sum of two subsequent squared observations, which must pass two threshold comparisons. The AGLR algorithm gains substantial estimation performance with prior knowledge about the dynamic variance profile associated with a muscle activation accounted for at the expense of more samples required [33]. The methods were compared to a model-based (dynamic process) algorithm for better detection performance relative to the traditional methods. They compared the estimated onsets of muscle activity to the true onsets; however, their definition of the "true onsets" is unclear.

2.2.1.2 Kinematics, Force and Torque

Most investigations that quantitatively assessed spasticity used a mechanized apparatus, e.g., [34]–[38], which supports the limb during the experiments. Such an apparatus allows manual or motorized movement of the limb while recording kinematic and torque data with the integrated sensors. This approach is functional and valid for preliminary research with high reliability, but the restrictive nature of such setups would not represent all aspects of real, natural movement in daily life. More importantly, the utilized devices are typically bulky, especially if they involve robotic components [37]–[39], which is not feasible for widespread application in the clinical setting.

Recent advancements of wearable sensors and technologies allow for ubiquitously accurate monitoring of our movement, activities and physical health [40]–[45]. In recent studies of spasticity, few have used a portable system in their experiments. Some of the existing portable systems utilize a flexible electrogoniometer (based on strain gauge mechanism) [46]–[49], which is a simple method for measuring the joint angles. However, the resulting measurements would not be robust to the sensor placement; for instance, if the sensor is not perfectly aligned with the frame of motion. Electrogoniometer measurements could also result in inaccurate estimation of joint angle when the axis of rotation is changing [50], [51]. Additionally, measurement of joint angle with electrogoniometers relies on accurately identifying the center of rotation, e.g., of the knee joint [52], which changes with motion [53] and would be difficult to manually identify and track.

Inertial measurement units (IMU) were used in recent studies on spasticity [54]–[56]. IMU calibration procedures were developed [56], [57] in order to correct for imperfect placement and orientation and to produce signals that accurately represent the real motion of the limbs under study. Estimation of joint axis and angle estimation using IMU measurements has been shown to be accurate and valid when compared to camera-based motion capture systems [58], [59], or compared to magnetic tracking systems [60]. IMU-based measurement of human kinematics has also been demonstrated with high repeatability and validity, for instance in gait analysis [61], [62], and when fused with other sensors [63], and in 3D joint angle estimation [60]. Even using a single IMU has been shown to result in accurate motion analysis in studies evaluating rehabilitation exercise performance [64], [65]. As wearable sensors, IMUs are more convenient and practical for use in a clinical setting than bulkier or stationary alternatives such as the camera-based motion capture systems. IMU-based joint kinematics estimation is therefore beneficial for spasticity evaluation, due to its ease of use, reliability, and repeatability of the measurements. Wireless sEMG and IMU sensors have been combined to assess rehabilitation activities such as reaching, flexing movements and other exercises [66], [67], where high intra- and inter-subject reliability were demonstrated for the measurements [68]. IMU and sEMG sensors have also been used for load estimation in the industrial setting and showed potential in estimation of the biomechanical overload risks for manufacturing workers [69].

Many of the studies discussed in this review included in their analysis the resistive force (in many cases represented with torque) generated by the spastic muscles being investigated. Detailed in **Section 2.2.2**, some studies aimed to model and estimate the reflexive force and the EMG activity, as they reflect the magnitude of the spastic response to muscle stretch. The force or torque was also related to other outcome measures to characterize spasticity. As mentioned previously, the joint torque was often measured by a torque sensor in the experimental apparatus, otherwise the reactive force was measured by a multi-degree-of-freedom force sensor, or torque estimated by other sensors such as a dynamometer [39] or differential pressure sensor [70].

2.2.2 Quantitative Modeling

This section describes three quantitative modeling approaches of spasticity and different examples of each approach. The reviewed studies grouped based on their modeling approaches can be found in **Appendix A**, along with details on used sensors, methods, and computed measures.

2.2.2.1 Mechanical Modeling

Several studies approached modeling spasticity from a purely mechanical perspective [35], [36], [70]–[72]. Chung et al. [35] measured the resistive joint torque and angular position of the hemiplegic spastic ankle during passive dorsi- and plantar flexion motion. The slope of the

torque-angle curve (see **Figure 2**) at the dorsiflexion ROM limit represented the quasi-stiffness of the ankle joint. Additionally, the area inside the curve across the dorsiflexed ROM represented the energy loss during dorsiflexion, which was then normalized by the ROM limit. Higher stiffness and energy loss indicate higher resistive forces during the joint motion, suggesting severe spasticity. The resistive torque at the nominal limits of plantar flexion and dorsiflexion, as well as the ROM, were also considered as outcome measures, where a smaller ROM and higher torque would suggest more severe spasticity. The participating stroke subjects showed significantly higher resistive torque, stiffness, and energy loss, as well as lower ROM when compared to healthy control subjects. These passive biomechanical properties had moderate to low correlation with the MAS scores (Kendall τ = 0.294, 0.297, 0.230 for torque, quasi stiffness, and energy loss, respectively; $p < 0.05$) [35], thus could provide informative measures of the spasticity in the muscles acting on the ankle joint.

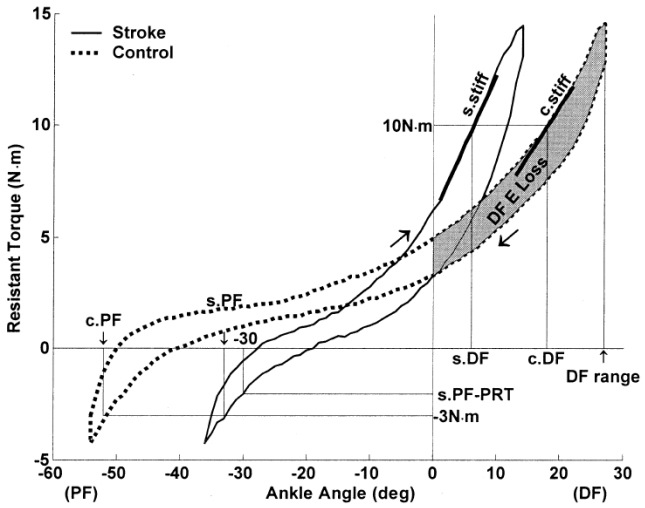

Figure 2. Representative torque-angle curves (hysteresis loops) from the experiments of Chung et al. [35]. The limit of dorsiflexion range of motion (ROM) was designated as the point of 10 Nm of resistive torque in both stroke and control subjects. The quasi-stiffnesses are the s.stiff and c.stiff slope values, respectively, for the stroke and control subjects.

Spasticity is typically characterized by the velocity-dependent increase in muscle tone, and the "catch"—the joint angle where the increased tone suddenly appears during fast passive stretching of the muscle [73]. To model this changing of muscle tone, Park et al. [71] divided the stretching motion of the elbow into three phases: pre-catch, catch, and post-catch. For the pre-catch phase, the passive elbow resistance was modeled as a linear mass-spring-damper system:

$$\tau_{pre} = m\ddot{\theta} + b\dot{\theta} + k\theta \tag{1}$$

where m is the inertial mass of the hand and forearm, and b and k are the damping and stiffness, respectively. The catch angle can be represented as:

$$\theta_{catch} = \theta_i + \frac{L}{\dot{\theta}_{pre}} \tag{2}$$

where L is the catch angle constant, θ_i is the angle at the beginning of the stretching motion, and $\dot{\theta}_{pre}$ is the average speed during the pre-catch phase. During the catch phase the elbow resistance was modeled as:

$$\tau_{catch} = h\dot{\theta}_{c\_start}\delta(t) + \tau_{pre\_end} \quad \delta(t) = \begin{cases} 1 & if\ t - t_{c\_start} < \Delta t_c \\ q\ (q < 1) & if\ t - t_{c\_start} \geq \Delta t_c \end{cases} \tag{3}$$

where h is the catch torque constant, $\dot{\theta}_{c\_start}$ is the stretching speed at the beginning of the catch phase, τ_{pre_end} the torque at the end of the pre-catch phase, q the residual torque constant, t_{c_start} the time when catch begins, and Δt_c the duration of peak torque. Finally, the elbow resistance during the post-catch phase was represented as a position-dependent torque:

$$\tau_{post} = k_{post}\left(\theta - \theta_{post\_start}\right) + m\ddot{\theta} + b\dot{\theta} \tag{4}$$

where k_{post} is the stiffness and θ_{post_start} is the initial joint angle of the post-catch phase. The model was based on analyzing the kinematics and force measurements during passive elbow stretching with four cerebral palsy (CP) participants. The MAS scores of the subjects were also assessed, and the complete model was used to simulate each subject's spasticity in a haptic device consisting of a robotic arm, motor, and controller. The clinicians then performed the MAS assessment on the haptic device, which simulated the other subjects that they had not assessed previously, to validate the results of the modeling.

2.2.2.2 Musculoskeletal and Neural Dynamics Modeling

Previous reviews on the objective characterization of spasticity showed the importance of differentiating the mechanical (musculotendon) and neural components of spasticity, especially for monitoring the effects of treatment or rehabilitation [74], [75]. Obtaining those components requires the inclusion of both biomechanical and electrophysiological signals in the assessment of spasticity.

To model the neural and physical components of spasticity, several studies have designed theoretical controllers that include the musculoskeletal geometry, musculotendon dynamics, muscle spindle, motor neuron pool and subsequent muscle activations. The theoretical controllers receive the measured kinematics as inputs to estimate the force [76] or torque [39], [77]–[79] generated by the muscles (due to reflex) for a given passive movement. The controller parameters consist of neural and non-neural parameters (e.g., muscle spindle firing rate, passive viscoelasticity, etc.) and are optimized to fit to the measured data. The estimated force or torque is

generally represented as a sum of the effects of inertial, gravitational, and active muscle forces [77]:

$$\tau_T = \tau_I + \tau_G + \tau_M \tag{5}$$

where τ_T is the measured torque, τ_I represents the torque from the moment of inertias, τ_G is the torque generated by gravity, and τ_M is the muscle torque consisting of a passive and active element, as in the following equation [77]:

$$\tau_M = \tau_{passive} + \tau_{active} \tag{6}$$

The passive torque is characterizable beforehand by a slow, passive movement (e.g., joint angle speed of 15 deg/s), which minimizes muscle activation, leaving only the passive parameters to be identified by fitting the measured torque-angle curve [77]:

$$\tau_{passive} = r(\theta)(k_{E1}e^{kE2\Delta L} + B\dot{L} + F_0) \tag{7}$$

where $r(\theta)$ is the moment arm about the joint, L is the muscle length, k_{E1} the coefficient of the elastic exponential curve, k_{E2} the rate of change of the curve slope, B the viscosity coefficient, and F_0 the elastic curve shape parameter. The active torque generated by the muscle was calculated based on the Hill-type muscle model, such as in [77]:

$$\tau_{active} = r(\theta) \cdot a(t) f_v(\dot{L}) f_l(L) \tag{8}$$

where $f_v(\dot{L})$ the relation between moment and rate of change of muscle length, $f_l(L)$ the relation between moment and muscle length, and $a(t)$ is the muscle activation function, which includes the muscle spindle and motor neuron pool models.

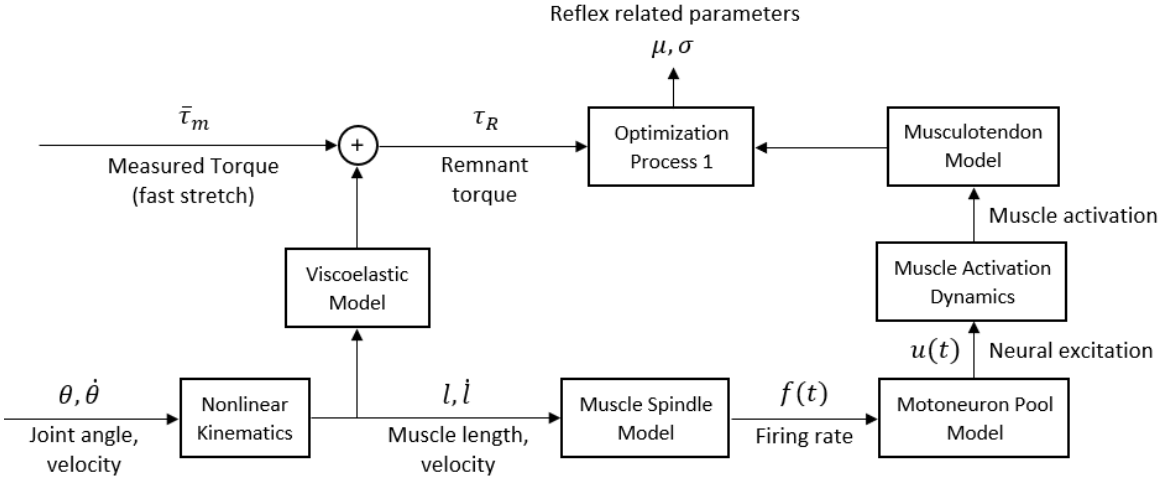

Figure 3. Example of system identification algorithm used by Shin et al. [77] for parameters characterizing the spastic reflexes, using muscle spindle, motor neuron pool, muscle activation dynamics, and musculoskeletal models to estimate the activate muscle torque generated by the spastic muscle during reflex.

Figure 3 and **Figure 4** show examples of a theoretical controller used to indirectly estimate active torque generated by spastic reflex, allowing for identification of parameters related to the reflex. These models are used to estimate the measured experimental torque at the joint, and the optimized biomechanical and neural parameters of the controller are the outputs of this type of quantitative modeling which can characterize the level of spasticity. The models are complex and while they can be used to simulate spastic behavior, they may be less applicable in clinical evaluations.

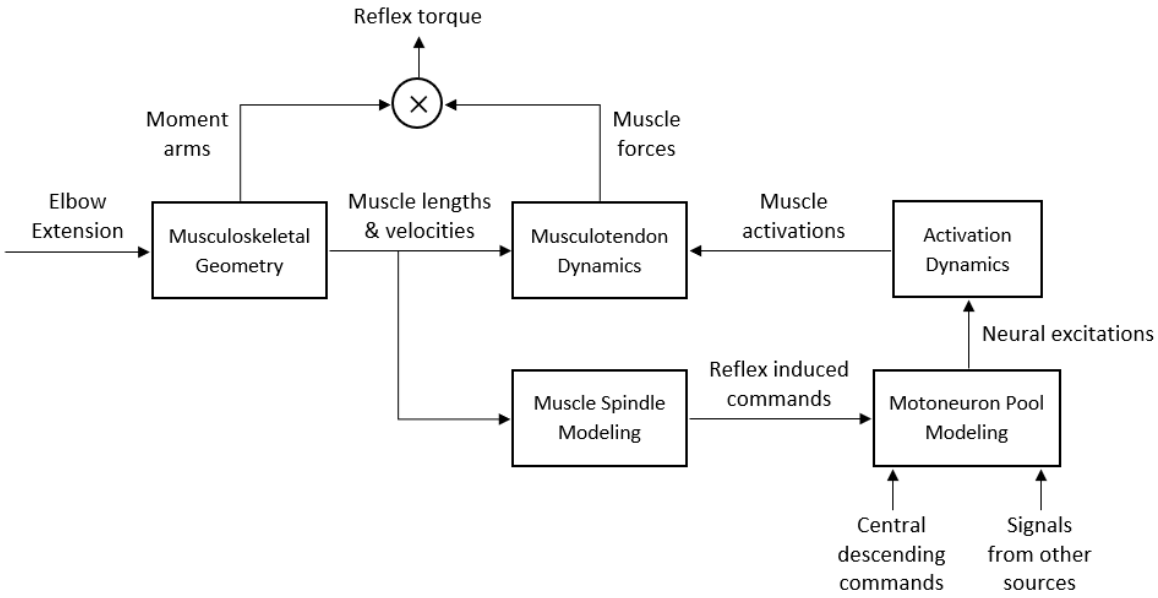

Figure 4. Another similar model used by Koo and Mak [39] that combines the moment arms of all the muscles that affect the joint movement being investigated with their active forces to estimate the resulting reflex torque.

2.2.2.3 Threshold Control Modeling

Several spasticity models have been developed based on muscle reflex models and the stretch reflex threshold (SRT). One hypothesis of how the central nervous system (CNS) controls human movement is threshold position control [20], or in a more general form, the Equilibrium Point (EP) hypothesis [80]. The EP hypothesis suggests the CNS changes the relationship between length and force in muscles to reach a new position and force equilibrium where opposing muscle forces are balanced, resulting in movement or a static posture. Specifically, it assumes the CNS controls a motor action, whether single-joint or multi-joint, by modulating the thresholds or EPs, which results in transitioning between states along a planned trajectory. Spasticity can be defined as an involuntary, velocity-dependent increase in tonic stretch reflexes, or reduction in the threshold of muscle stretch at which the tonic reflex begins and muscle force increases as a function of length. Since spasticity distorts the tonic reflex thresholds, it can adversely affect the motion control, which can be described by the EP hypothesis.

Levin and Feldman [81] used sEMG recordings to detect the onset of the elbow flexor muscle activations as a result of spastic hyperexcitability during passive extension at different speeds. In their experiment, a motorized apparatus was used to hold and passively move a participant's arm, while recording the kinematic data. **Figure 5** shows an example of a motorized setup and an example of a manual setup for investigations of the lower extremities.

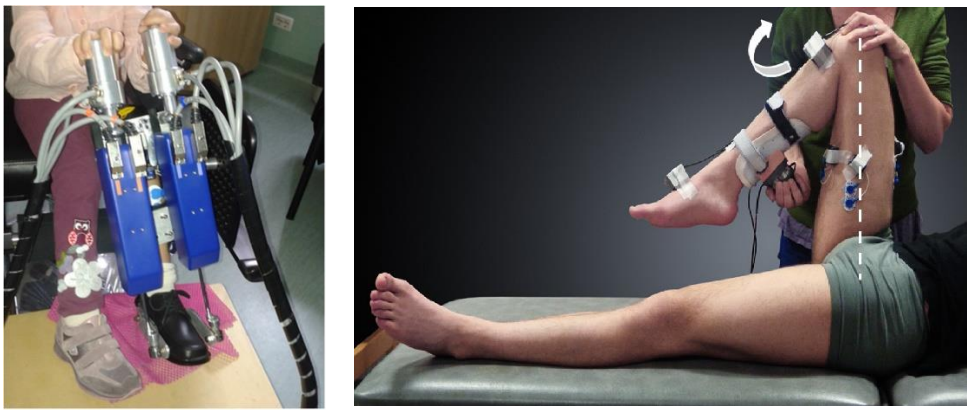

(**a**) (**b**)

Figure 5. (a) Example of a motorized setup for stretching the ankle dorsi- and plantar flexors [37] and (b) a manual setup for extending the knee joint and stretching the flexor muscles [54].

The joint angular velocity and the joint angle at the onset of spasm was used to define the dynamic stretch reflex threshold (DSRT). Repeating passive elbow extension multiple times at different speeds allowed for data-driven modeling, building a linear regression model on the combined data for a given motion and associated muscle(s). The intercept of this linear model (Equation (9)) with zero velocity represents the tonic stretch reflex threshold (TSRT) (see **Figure 6**). Several other investigations used this fundamental approach to evaluate spasticity [2], [37], [46]–[48], [56], [82], [83], based on the following equation [81]:

$$DSRT = TSRT - \mu \times Velocity \tag{9}$$

where μ represents the sensitivity of the dynamic stretch reflex threshold to velocity, and a higher μ means greater spasm sensitivity to velocity.

For an individual with spasticity, the TSRT of an affected muscle is shifted within the biomechanical range of motion of a joint, even at a relaxed state, preventing movement throughout the full range. In contrast, the TSRT for a healthy individual or unaffected muscle would lie outside the ROM. This is supported by their dynamic stretch reflexes only appearing at higher potential velocities (see **Figure 6**), in a case such as a knee tendon tap, which evokes a similar response to a very high stretch velocity of the quadriceps muscles, in excess of 300 deg/s [83], [84]. Therefore, as the quantitative outputs of the model, a lower TSRT value and higher μ

value would suggest more severe spasticity for a specific muscle. Combining the models for the muscles acting on a particular joint can provide a map of the spastic joint space [56].

The mentioned studies, including the purely mechanical approaches and musculoskeletal and neural dynamics models, investigated spasticity through passive-movement experiments. However, in daily life situations and outside of the lab setting, spasticity could also be triggered due to active movement. Thus, it is important to extend the scope of experiments to include active movements to characterize and assess spasticity in a more comprehensive capacity.

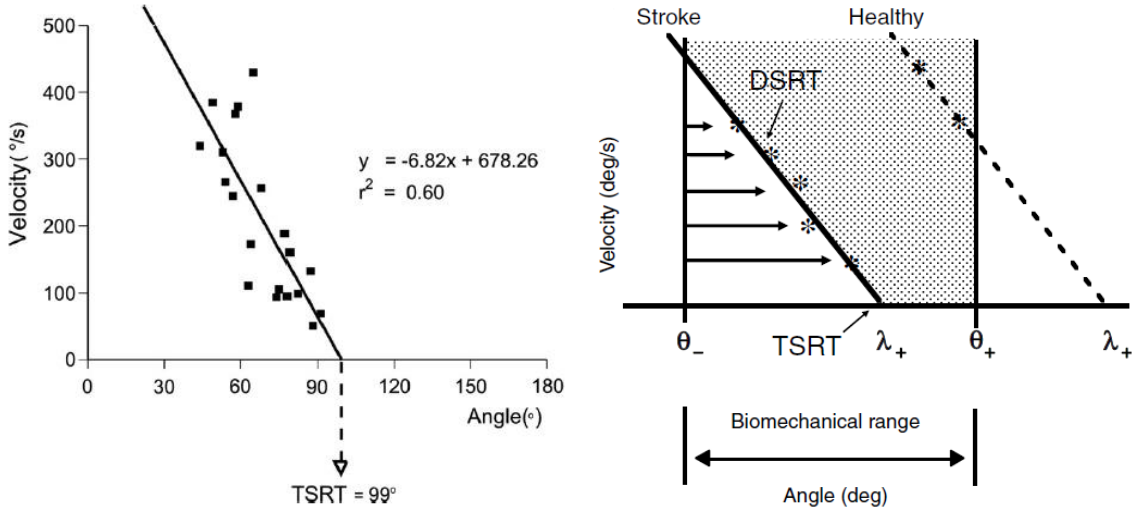

(**a**) (**b**)

Figure 6. (a) Example of tonic stretch reflex threshold (TSRT) estimation by 20 dynamic stretch reflex threshold (DSRT) points found by stretching the elbow flexor muscle biceps brachii at different velocities; (b) example of a threshold model for a post-stroke subject versus healthy person, where the TSRT lies outside the biomechanical range of the joint [48].

According to the threshold control theory, some believe that spasticity can be described as an impaired ability to regulate the tonic stretch reflex thresholds, and recent studies have begun to investigate this concept. Turpin et al. [84] tested both passive flexion and extension of the elbow joint by an experimenter, and with active, volitional elbow motion in identical conditions. Passive and active movements were performed with the same range of motion specific to each participant at a variety of joint angular velocities. Obtained TSRTs were at greater angular displacements, corresponding to more stretched muscles, in the active stretching compared to the passive stretching (by 10–40 deg), suggesting an increase in non-spastic ROM. Conversely, the slopes of the regressions (parameter μ) were increased by 1.5 to 4.0-fold, showing a higher sensitivity to velocity during volitional control. These findings suggest that during volitional motion an affected individual could stretch the muscle/extend the joint further than the during passive motion, particularly at slower speeds. However, at greater velocities the DSRTs estimated from active and passive motions are in a similar range. **Figure 7** shows a representative subject from that study.

In an earlier study on implicit learning and generalization for stretch reflexes in healthy subjects, Turpin et al. [85] found the amplitude of the stretch reflex decreases and remains attenuated by 5–12 repeated stretches, and does not increase even after 5 min of rest. This observation can be explained by the anticipation of the stretching which can result in the pre-modulation of spatial thresholds that can suppress the muscle resistance to stretch. This pre-tuning of stretch reflex is similar to the clasp-knife phenomenon [86] seen in individuals with Parkinson's disease and stroke survivors who have rigid or spastic muscles [87], [88].

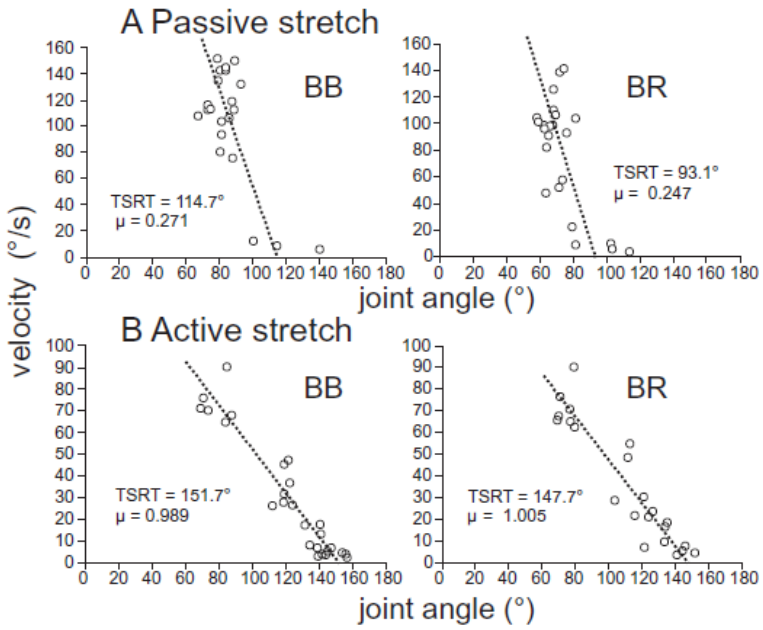

Figure 7. A representative subject in [84] where in the active stretching of elbow flexors—biceps brachii (BB) and brachioradialis (BR)—the TSRTs were found to occur at greater joint angle or higher stretch. In contrast, the sensitivity to velocity was found to be increased in both muscles, when compared to passive motion.

2.3 Discussion

2.3.1 Comparing the Approaches

Subjective measures, most commonly the AS and MAS, as well as other clinical scores, are currently used to assess spasticity in clinical practice. These scores are easy to obtain and do not require any equipment and sensors, unlike the objective approaches. However, the issue remains of their questionable reliability, weak correlation with muscle activity measurements of the reflexes [83], [89], [90], and inability to reflect the complex mechanisms of the spastic reflexes. Despite these shortcomings, subjective measures should not be totally abandoned until a reliable, objective measure is found and established, but they need to be supplemented with current quantitative approaches.

The mechanical modeling approaches represent spasticity at the joint level, usually in joint torque-kinematic space, whether by identifying biomechanical properties that differ between a healthy individual and an individual with spasticity (e.g., change in joint mechanical impedance) or representing the spastic behavior by a simulation model. The outcomes have been shown to moderately correlate with clinical scores such as the MAS [35], demonstrating the potential of this type of approach, which is also simpler and easier to use in a clinical setting than more complex modeling approaches. However, as previously discussed, the assessment of spasticity for follow up and treatment is better accomplished by differentiating biomechanical and neural components of spasticity, using both mechanical variables and electrophysiological signals [74], [75].

The resulting biomechanical and neural parameters of the musculoskeletal and neural dynamics models allow for characterizing spasticity at the muscle level. The obtained measures may allow understanding of some aspects of the neurophysiology of spasticity, and could potentially be applied to the development of treatments. For example, Shin et al. [77] arrived at optimized parameters μ which represents the muscle spindle firing rate at 50% motor neuron recruitment, and σ as the standard deviation of the Gaussian cumulative distribution that represents the function of the alpha motor neuron pool. A lower μ means a lower minimum spindle firing rate which indicates hyper-reflexia in the muscle [91]. The higher reflexive torque (increased muscle tone) found with lower μ and σ values in their experiments shows a possible relationship between those parameters and spasticity. Koo and Mak [39] showed similar results by looking at μ_0, the minimum spindle firing rate for just 0.5% neural excitation, and G_L as the muscle spindle static gain. These parameters were posited to be more physiologically meaningful in relation to spasticity. Using sensitivity analysis, μ_0 and G_L were determined as the key parameters when predicting reflex torque. Koo and Mak suggested that drug or treatment development could be focused on effectively regulating those specific parameters. Clinical scores have been used besides this modeling approach to assess the subjects' spasticity [78], and it was found that stiffness, viscosity, and reflex torque are positively correlated with AS scores. However, the authors did not include neural parameters in their torque estimation model, and instead used measured EMG to estimate the neuromuscular activity due to stretch reflex. Recent advancements in joint mechanical impedance estimation during active movements [92]–[95] would allow further investigations on how spasticity affects the modulation of joint impedance, particularly joint stiffness and viscosity, during volitional movement and walking.

From a research-oriented point of view, this type of investigation can provide meaningful details about spasticity. However, they are not likely to be clinically applicable, as also mentioned in other reviews of the literature [96], due to the complexity and time required for setup preparation and data processing. An easy to use objective assessment method that can still benefit

from high level neural and mechanical modeling could provide a more suitable solution for spasticity assessment in the clinics. This high-level approach could be based on the threshold control-based models [2], [37], [46]–[48], [56], [81]–[84], which explicitly reflect the velocity-dependence of spasticity. These models have also been shown to be moderately correlated with clinical scores, agreeing with the current practice and are generally simpler than the methods that use parameter-based estimations of spastic responses. While these models are usually acquired with robotic setups which can be complex and not available in every clinic, several studies showed the potential of using wearable sensors and inexpensive hand-held instruments to obtain such models accurately [54]–[56].

Previous studies have found that the spastic reflex is affected by the initial stretch level at the beginning of a stretching motion, given the same stretching velocity [34], [97]. Kamper et al. [34] found that with longer initial lengths of the elbow flexor muscles, the reflex threshold and stiffness were significantly reduced and increased, respectively, indicating a negative relationship between the initial muscle length and the spastic reflex. The approaches discussed in **Section 2.2.2** do not account for this observation. Future studies should incorporate varying initial stretch positions in addition to varying stretch speeds in their investigations.

More recent studies have found that the firing of muscle spindles is not necessarily unique in relation to muscle length and stretch velocity but may be more directly related to muscle force. Blum et al. [98] demonstrated that the instantaneous firing rates (IFRs) of muscle spindle primary afferents are significantly better predicted by force-related variables than muscle length-related variables, especially at higher stretch velocities. Falisse et al. [99] also found that estimating muscle activity (using EMG) during spastic reflexes in passive motion, as well as gait in children with CP, was better accomplished using measured force (applied by the examiner in passive motion and ground reaction forces in gait) than models that estimated using kinematics variables. For instance, the activity of the hamstrings was predicted significantly better in both cases by force than velocity or acceleration ($R^2 = 0.73 \pm 0.10$, 0.46 ± 0.15 and 0.47 ± 0.15, respectively). These results suggest a need for incorporating reflex generated muscle force or torque into the modeling of spasticity beyond that of estimating the measured profiles using other variables such as joint kinematics. Future investigations should aim to consider the relationship between muscle force and the spastic reflex in characterizing and assessing spasticity.

2.3.2 Effect of Spasticity Modeling on Follow-Ups and Treatment

As discussed previously, reliable and accurate assessment of spasticity by objective measures could lead to better follow-ups and treatment. Previous studies of treatment of spasticity have been limited by solely using clinical scores to evaluate the effects of the treatments. Simpson et al. [100] used the AS to evaluate the efficacy of botulinum toxin type A (BTX-A)—a common

treatment option—on the upper limb spasticity in post-stroke subjects. The experiment was randomized, double-blind and placebo-controlled, but the limitations of the AS calls into question the results that showed significant reductions in spasticity. In a recent study by Turna et al. [101] the effects of different injection techniques of BTX-A were investigated for treating ankle plantar flexor spasticity. To compare those techniques the effects of the treatment were evaluated with subjective scores including the AS, Brunnstrom stages, and Barthel index score, which again limits the reliability of the results.

Some studies have initially explored the idea of investigating the effects of treatments and management of spasticity by objective measures. Chen et al. [70] compared the spasticity in the affected biceps-brachii muscle in ten chronic stroke patients, two weeks before and after BTX-A injection. Measured by a portable device, the elbow joint kinematics, reactive torque and muscle activity were analyzed to estimate the viscosity of the muscle and the DSRTs (as a percentage of the stretch cycle). They found a significant decrease in viscosity and a significant increase in DSRT after injection. The results indicated a reduction in spasticity, which agreed with their MAS assessments performed before and after the treatment. However, Pandyan et al. [21] identified reductions in spasticity in the elbow flexors of stroke patients, which were not detected by the MAS assessments. These results reinforce the idea that clinical scores offer an insufficient and unreliable evaluation of spasticity. A better measure of spasticity can be obtained by employing quantitative evaluations that provide objective, accurate measures of spasticity and offer models that can predict spastic behavior [70]. Investigations beyond this preliminary research could potentially reveal precise relationships between dosage and the effects, allowing for an optimally effective plan to be designed for each patient [21], [70].

Several studies have investigated repetitive transcranial magnetic stimulation (rTMS) and functional electrical stimulation (FES) and their effect on spasticity. Several studies found that rTMS significantly reduces spasticity in the lower limbs, for instance, in SCI participants with the effects lasting up to a week as measured by the MAS [102], and in stroke patients [103] as measured by their own clinical scale. Franek et al. [104] found that FES improves spasticity in the hip adductors of subjects with SCI for a few days up to a few months, as evaluated by a subjective scale (scale of 1–6) and objective measures such as H reflex recruitment curves and the number and intensity of contractions, while Alfieri [105] found that not all their participants (varying cases with hemiplegia and SCI) benefitted from FES. Powell et al. [106] found that FES improves wrist extensors strength and ROM, though not specifically for spasticity as evaluated by AS, and it was unclear how long the effects lasted. A review of ten recent studies [107] found that spasticity was significantly reduced in quadriplegic and paraplegic patients by treating with FES-cycling exercise. However, the effects were primarily evaluated by MAS. Overall, there is limited evidence of the benefit of FES for spasticity, and in many cases the utilized subjective scores and

their lack of reliability (particularly for lower limbs) could have contributed to the mixed results. Objective measures of spasticity, such as the DSRT, could better evaluate and potentially prove the usefulness of FSE and rTMS for alleviating spasticity in conjunction with other treatments or rehabilitation [108].

2.4 Conclusions

Approaches that use purely mechanical modeling can provide some information on the biomechanical properties of spastic behavior but lack consideration for the neural factors of spasticity and electrophysiological activity. The musculoskeletal and neural dynamics models can provide insight into the detailed mechanisms of spasticity, such as the theoretical neural parameters involved in the spastic reflex but lack practicality and applicability in the clinical environment. The threshold control-based models can provide an easy-to-use objective method of assessment, especially with wearable sensors in the clinical setting. However, further investigations into the neural mechanisms involved in spasticity may prove beneficial for better understanding and assessing spasticity.

There is a need to develop a system that can provide an objective, accurate and reliable assessment of spasticity—especially in the lower limbs—to better evaluate the effects of treatment and rehabilitation options. Identifying an accurate and objective spasticity model for each patient allows for predicting the kinematic states that provoke spastic behavior. Such a model could inform rehabilitation programs and enable adapting the assisted movements provided by a physiotherapist or an assistive exoskeleton so that uninterrupted exercises may be achieved. Obtaining spasticity-free assisted exercises has the potential to remarkably improve the outcomes of physical rehabilitation.

Chapter 3:

Spasticity Modeling with Wearable Sensors

The first three main objectives of the thesis involve establishing a protocol for experiments to assess spasticity, developing wearable instrumentation and algorithm for modeling spasticity from subject data from those experiments, technically validating them for accuracy and reliability, performing the experiments, and finally extracting features and an objective measure to characterize spasticity. In this chapter each of these objectives are addressed and completed to produce a quantitative score that may supplement the existing clinical scores of spasticity.

3.1 In Vivo Study

3.1.1 Participants

Subjects are recruited through the Toronto Rehabilitation Institute, at the Lyndhurst Centre where the experiments will be carried out. The population will be comprised of individuals with lower-limb spasticity as a result of motor-incomplete SCI, who have assessed ASIA Impairment Scale (AIS) scores of either D or C. Subjects will additionally be individually screened by a physician to verify the subject's conditions are relevant and meaningful to the study.

Table 2: American Spinal Cord Injury Association (ASIA) Impairment Scale [109]

Grade	Type of Injury	Description
A	Complete	no sensory or motor function is preserved in the sacral segments S4-S5
B	Sensory Incomplete	sensory but not motor function is preserved below the neurological level and includes the sacral segments S4-S5, and no motor function is preserved more than three levels below the Motor Level on either side of the body
C	Motor Incomplete	motor function is preserved below the neurological level, and more than half of key muscle functions below the neurological level of injury have a muscle grade less than 3 (Grades 0-2)
D	Motor Incomplete	motor function is preserved below the neurological level, and at least half (half or more) of key muscle functions below the NLI have a muscle grade ≥ 3
E	Normal	if sensation and motor function as tested with the ISNCSCI are graded as normal in all segments, and the patient had prior deficits

3.1.2 Sensors and Equipment

3.1.2.1 Limb Kinematics Measurement

Four IMUs (Xsens Awinda) are used to measure the kinematics of the leg segments (foot, shank, thigh) as well as the pelvis. The raw signals are passed through proprietary low-pass and Kalman filtering to provide accurate and unbiased accelerometer and gyroscope data, sampled at 100 *Hz*. Post-processing algorithms have been developed to accurately estimate the joint angles and joint angular velocities from these sensor recordings. The detailed locations for placing the sensors on each segment are as follows, which are designed to minimize motion artefacts due to soft-tissue deformation:

A. Lateral side of the foot below the heel
B. flat anterior-medial part of shank
C. anterior side of the thigh, near knee
D. lateral side of the pelvis

Figure 8 illustrates the placement and orientations of the IMU sensors. The X-axis of each sensor is oriented along the length of each segment, while the Z-axis points away from the limb.

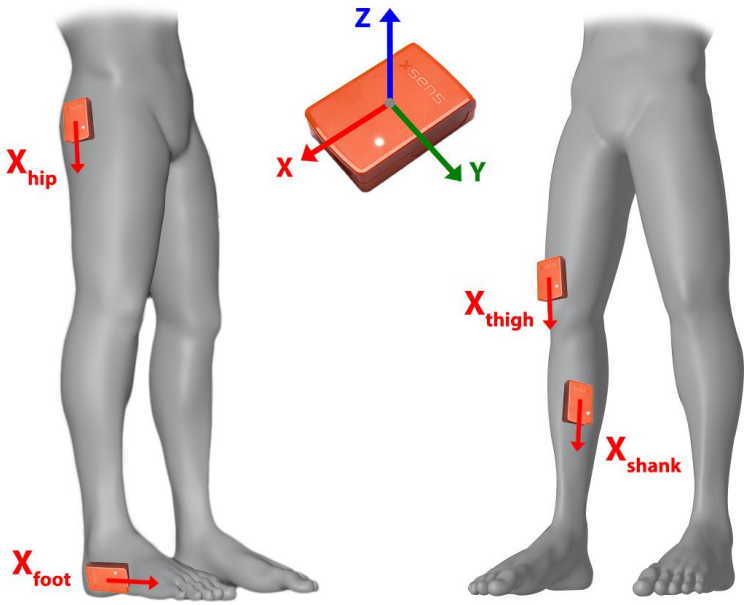

Figure 8. Placement of Xsens IMU sensors on the segments of the lower limb and hip.

3.1.2.2 Surface Electromyography Measurement

Wireless sEMG sensors (Delsys Avanti) are attached to each relevant muscle for the type of stretching motion, as described in **Table 3**. The data is recorded in the Delsys EMGworks Acquisition software, sampled at 2000 *Hz*. The EMG measurements will indicate the point at which involuntary contraction of the muscles begins, which will reveal the stretch reflex thresholds. The EMG signal itself is also a quantitative measure of muscle activation levels.

3.1.2.3 Sensor Synchronization

A spare EMG sensor which also contains a 3D accelerometer is taped to the IMU on the shank; which will be used to synchronize the EMG and kinematics recordings in post-processing by comparing the acceleration signals.

A Delsys trigger box is used to send a TTL square signal to the ADC of each force sensor, at the beginning and end of each test recording. Only the relevant data in between the two synchronization pulses will be extracted for analysis.

3.1.2.4 Instrumented Handles and Force Measurement

Three instrumented handles are designed with which the examiner moves the subject's foot, shank and thigh respectively during the tests. The handles are 3D-printed in high density from plastic material which are affixed to flexible metal braces for the shank and thigh, or another 3D-printed plastic brace for supporting the foot.

Figure 9. Experimental setup for (left to right) thigh, shank and foot. The spherical handle is attached to the bottom of the foot brace.

The interfaces between the handles and the braces are designed to house a 6 Degree-of-Freedom (DOF) force sensor (**Figure 9**). The utilized force sensors provide precise 3D force and moment measurements at the contact points between the examiner holding the handle and the brace which is fixed to the leg segment. Each force sensor is linked by an Analog to Digital converter (ADC) to a USB connection for a computer, where the forces are monitored and recorded in the OptoForce Data Visualization software. The braces of each handle are designed to be secured to the respective leg segment by Velcro straps. Each brace is covered with a layer of clinical foam on the side that will be in contact with the participant's body.

3.1.3 Experimental Protocol

The IMUs are attached to the leg segments of the leg under investigation, which is decided based on the higher MAS score (to display a greater degree of spasticity). After treating the skin with medical ethanol, the sEMG sensors are placed on the following muscles, based on SENIAM recommendations [110] (see **Appendix B**):

Table 3. Muscles and Associated Joint Motions [111]–[113].

Body Segment	Muscle name	Joint Function	Uni/Biarticular
Shank	Tibialis Anterior (TA)	Ankle dorsiflexion	Uni-articular
	Extensor Digitorum Longus (EDL)	Ankle dorsiflexion	Uni-articular
	Extensor Hallucis Longus (EHL)	Ankle dorsiflexion	Uni-articular
	Soleus (SO)	Ankle plantar flexor	Uni-articular
	Gastrocnemius Medialis (GM)	Ankle plantar flexion, assist knee flexion	Biarticular
	Gastrocnemius Lateralis (GL)	Ankle plantar flexion, assist knee flexion	Biarticular
Thigh	Biceps Femoris (BF) (long head)	Knee flexion, assist hip extension	Biarticular
	Semitendinosus (SE)	Knee flexion, assist hip extension	Biarticular
	Rectus Femoris (RF)	Knee extension, hip flexion	Biarticular
	Vastus Medialis (VM)	Knee extension	Uni-articular
	Vastus Lateralis (VL)	Knee extension	Uni-articular
	Sartorius (SA)	Hip flexion, assist knee flexion	Biarticular
Hip	Gluteus Maximus (GLM)	Hip extension	Uni-articular

An additional wireless sEMG sensor is attached to the shank IMU sensor (see **Figure 8**). Functional calibration movements for the IMUs to align the sensor frames with the anatomical frames of the leg segments (see **Section 3.2.2.1**) are performed. The participant remains in the supine position for all following steps:

1. The knee and hip are fully extended, with ankle at zero degrees; maintained for 10 seconds.
2. The shank is held securely while moving the ankle in strictly plantar/dorsi flexion for 10 seconds.
3. The ankle is moved in lateral/medial rotation while the shank is held securely but allowing for rotation along the axis of the segment; for 10 seconds.
4. The thigh is held securely while moving the knee in flexion/extension for 10 seconds.
5. The hip is moved in flexion/extension for 10 seconds.
6. The hip is moved in abduction/adduction for 10 seconds.
7. The subject is assisted to perform sit-up motions for 10 seconds.

Maximum Voluntary Contraction (MVC) is measured for each muscle. The participant is asked to perform isometric actions as strongly as possible against resistance provided by the examiner (while in supine position) for at least 5 seconds.

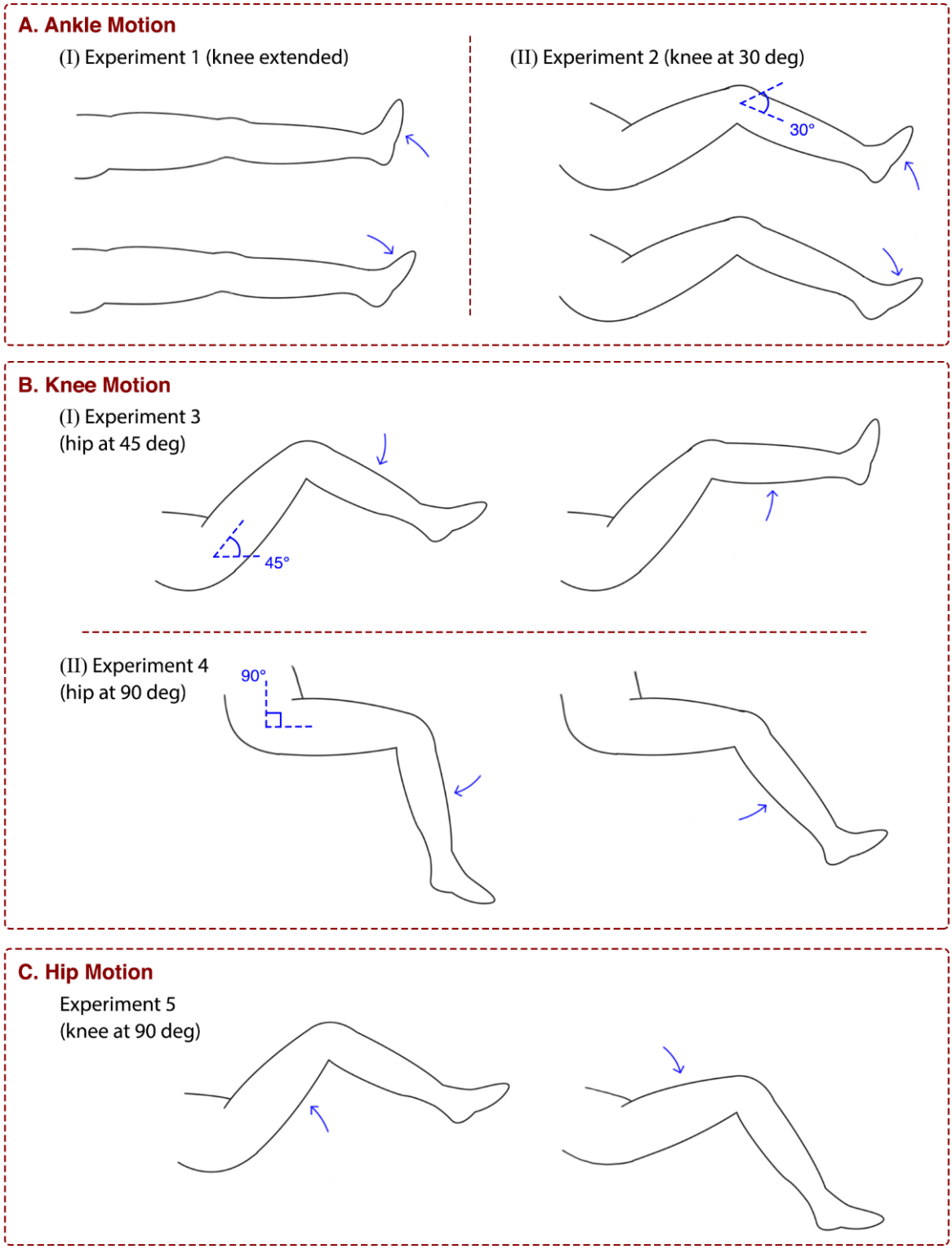

Figure 10. Experimental protocol for ankle, knee and hip motions

Passive flexion and extension movements are applied to each joint at 3 different speeds for each direction, and 5 trials are performed for each speed and direction (30 in total). At least 2 seconds of rest is allowed between each trial, and at least a further 10 seconds of rest between each set of 5 trials. Monitoring of the actual applied speed is provided by the software interface of the IMUs, to maintain as close to the desired speed as possible. The total set of trials for a given joint is repeated for different conditions of the proximal joint (see **Figure 10**):

A. **Ankle motion** – the set of trials is repeated while the thigh and shank are held at (I) knee extended (KE) at zero degrees, and (II) knee flexed (KF) at 30 degrees
B. **Knee motion** – the set of trials is repeated while the thigh is held so the hip is (I) fully extended, (II) flexed at 45 degrees, and (III) flexed at 90 degrees. The ankle is relaxed in the neutral zero degrees position throughout.
C. **Hip motion** – the shank is held to maintain 90 degrees of knee flexion while the thigh is moved to flex/extend the hip. The ankle is also maintained in a relaxed manner.

After the tests are completed, photos from the top and sides of the leg are taken beside a measuring tape for reference, including the relative geometry of the force sensors and the joints.

3.1.4 Special Note

Due to the COVID-19 pandemic, the experiments planned for the Spring/Summer of 2020 were indefinitely delayed. Despite the lifted restrictions in 2021, participants could not be recruited. Therefore, previously collected data (see **Section 3.4**) was used for the processing and results in this chapter.

3.2 Data Processing

All data was processed using MATLAB versions R2020b and R2021a [114].

3.2.1 Electromyography

3.2.1.1 Signal Filtering

Each EMG signal was passed through a high-pass filter with a cutoff frequency of 20 *Hz*, which removes motion artifacts [115]. Other types of artifacts such as ECG artifacts were not observed in the data and did not require filtering. The high-pass filter also zeroes the mean, correcting any baseline shift that can result from common issues such as suboptimal electrode placement or non-relaxed muscles at recording start [116]. The filtered signal was then full-wave rectified, which is simply taking the absolute value. The baseline correction and full-wave rectification are necessary for the next step of obtaining the envelope of the signal.

The signal must be low-pass filtered to obtain the signal envelope. A moving average filter was applied, which is a simple type of Finite Impulse Response (FIR) filter. Specifically, the root mean squared (RMS) was calculated at each instance of the sliding window over the signal. The RMS method is preferred for smoothing to produce an envelope as it reflects the mean power of the raw signal [117], [118]. Conventionally the sliding window is centered, but a left-anchored sliding window was used instead because it better preserved the onsets in EMG activity (see the next section), with a window size of 50 *ms* which is considered effective for reflex studies [116].

3.2.1.2 Spastic Reflex Identification

For modeling the spastic behaviour, the onsets of muscle activity must be determined. For each signal, the mean μ_{base} and standard deviation σ_{base} of the baseline noise were calculated by selecting an of the signal where the muscle should be relaxed with no activity. A two-threshold (TT) criterion was applied to determine when the signal rises above the baseline noise, representing an onset of activity:

$$threshold_1 = \mu_{base} + 3\sigma_{base} \tag{10}$$

$$threshold_2 = \mu_{base} + 6\sigma_{base} \tag{11}$$

where the signal must first rise above $threshold_1$, then remain above $threshold_2$ by 100 *ms* after to be considered as reliable muscle activity, and not an artifact or anomalous spike. The time points when the first threshold is crossed are taken as the onsets of muscle activity. Because of the nature of EMG signals, the algorithm may select points that are not onsets, or miss other onset points. Therefore, a manual review follows where points are rejected or added, using an additional version RMS signal with a wider window of 300 *ms* which helps by showing the overall shapes of the activations (see **Figure 11**), as well as the corresponding kinematics (see **Figure 14**) to further verify when the reflexes are expected to occur, based on the stretching motions.

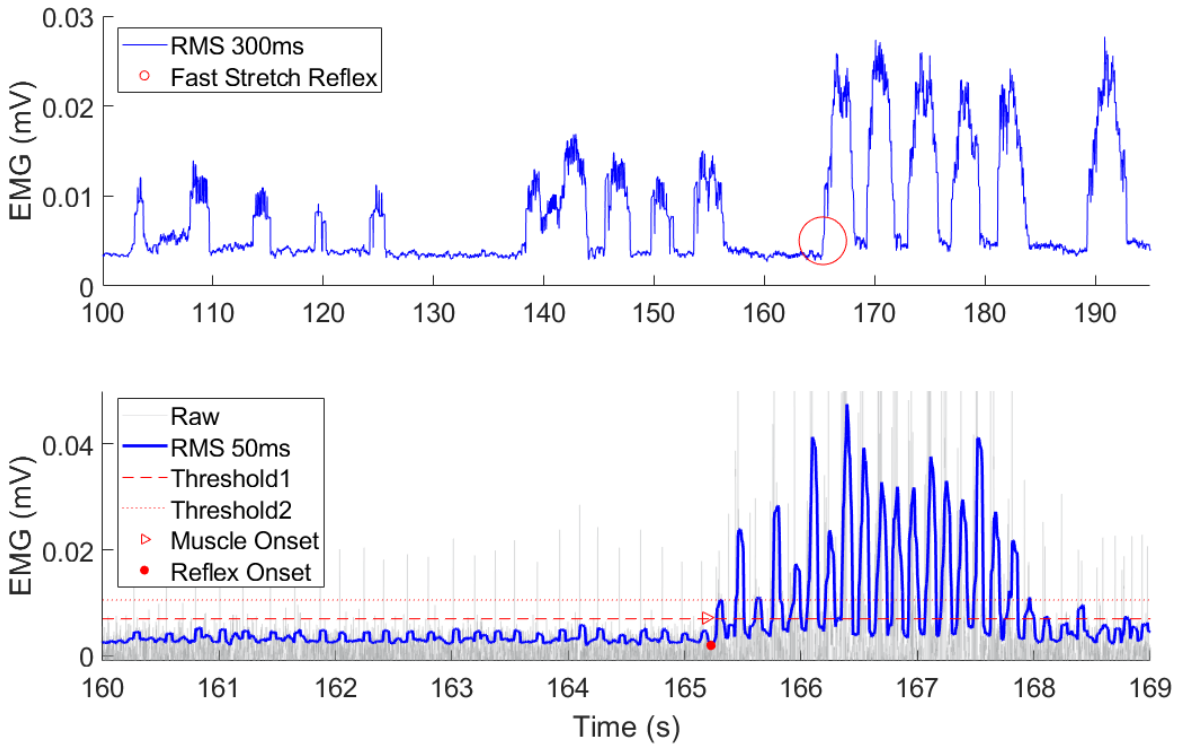

Figure 11. Example S01 KF GM muscle reflex point selection at first fast stretch motion

A latency exists between the onsets of muscle activity and when the spastic reflex is triggered. This "nervous delay" was treated as a constant, which is sufficient for the scope of this research. An average latency of 50 *ms* [119], [120] was therefore subtracted from each muscle onset to determine the "reflex onsets" that are characterized by the EMG signal.

3.2.2 Inertial Measurement Units

3.2.2.1 Functional Calibration

The geometry of human limb does not allow for placement that gives perfect alignment of IMUs relative to the true reference frames of motion for a given limb. The sensors are placed on the flattest part of the limb (**see Section 3.1.2.1**) to minimize shaking/noise in the motion data. This results in an assumedly constant misalignment from the limb frame, which can be corrected by a process that requires performing two functional calibration movements.

The first calibration motion for a given segment is performed along the flexion-extension (F-E) axis of the proximal joint, as described in (see **Section 3.1.3**). Given the data from the IMU's gyroscope, or our vector of observations $\vec{\omega}$, we can estimate the primary direction of movement by determining the vector along which there is the greatest variance in angular velocity, using Principal Component Analysis (PCA). First, we must obtain the covariance matrix of the angular velocities:

$$\mathrm{cov}(\vec{\omega}) = \Sigma = \begin{bmatrix} \mathrm{cov(x,x)} & \mathrm{cov(x,y)} & \mathrm{cov(x,z)} \\ \mathrm{cov(y,x)} & \mathrm{cov(y,y)} & \mathrm{cov(y,z)} \\ \mathrm{cov(z,x)} & \mathrm{cov(z,y)} & \mathrm{cov(z,z)} \end{bmatrix} \tag{12}$$

Using Singular Value Decomposition (SVD) (in MATLAB) we can separate the covariance matrix into its orthonormal singular vectors and singular values:

$$\Sigma \xrightarrow{\mathrm{SVD}} \mathrm{USV^T} \tag{13}$$

where the columns of U are the left singular vectors, or eigenvectors of Σ, the columns of V are the right eigenvectors, and the diagonal elements of S (returned as a vector) are the singular values, or the square of the eigenvalues. The greatest singular value in S corresponds to the vector in U along which the projection of the data yields the greatest variances, u_1. Assuming the accuracy and consistency of the calibration movement, this eigenvector can be taken as the direction of the performed motion. We can then calculate the axis a_1 and angle of rotation θ between u_1 and Z_0 (the limb frame F-E axis):

$$a_1 = \frac{u_1 \times \mathrm{Z}_0}{\|u_1 \times \mathrm{Z}_0\|} = [a_x \quad a_y \quad a_z] \tag{14}$$

$$\theta_1 = \cos^{-1}(u_1 \cdot \mathrm{Z}_0) \tag{15}$$

If $\theta_1 > 90°$, a_1 should be in the opposite direction and $\theta_1 = 180° - \theta_1$. These parameters can be used as a rotation matrix to transform the data:

$$\mathrm{R}_1 = \begin{bmatrix} c\theta_1 + {a_x}^2(1-c\theta_1) & a_x a_y(1-c\theta_1) - a_z s\theta_1 & a_x a_z(1-c\theta_1) + a_y s\theta_1 \\ a_y a_x(1-c\theta_1) + a_z s\theta_1 & c\theta_1 + {a_y}^2(1-c\theta_1) & a_y a_z(1-c\theta_1) - a_x s\theta_1 \\ a_z a_x(1-c\theta_1) - a_y s\theta_1 & a_z a_y(1-c\theta_1) + a_x s\theta_1 & c\theta_1 + {a_z}^2(1-c\theta_1) \end{bmatrix} \tag{16}$$

The remaining two axes of motion must also be corrected to the limb frame. The second calibration data is obtained either by an abduction-adduction (A-A) motion, or vertical standstill with the theoretical A-A axis pointed along or orthogonal to the direction of gravity, depending on which is more convenient/reasonable to perform for the given limb segment (see **Section 3.1.3**). Rotation R_1 is initially applied to the second calibration data to correct the F-E axis. If the second calibration is by A-A motion, PCA is performed again to determine the direction of motion in the data. In the resulting eigenvector u_2, we must first zero the second element, or project it to the plane that is normal-defined by the F-E axis:

$$u_{2,proj} = [u_{2x} \quad 0 \quad u_{2z}]^T \tag{17}$$

This step is to ensure the second calibrating rotation is purely about the reference axis and does not misalign the previously corrected F-E axis. Afterwards, a_2 and θ_2 can be found

between $u_{2,proj}$ and the limb axis Z_0 in the same manner. Finally, this gives us R_2 and therefore the total calibrating transformation:

$$R_{total} = R_2 R_1 \tag{18}$$

If the second calibration data is vertical standstill, we can instead obtain the mean direction of acceleration in the data (after initially applying the R_1 transformation). This gravity vector can then be corrected using the same process to true vertical direction to give us R_2 and the total transformation R_{total}, which is applied to the kinematic data for all trials of a subject.

3.2.2.2 Kinematics Analysis

To model the spastic behaviour, the kinematics of each limb segment about a joint, and consequently the joint kinematics must be extracted from the IMU accelerometer and gyroscope data that are calibrated to the limb reference frames (see previous section).

The acceleration data is first looked at to find "rest points" where there is nominally zero motion. The gravity vector, which is nominally zero along the F-E axis, is used to determine the standstill orientation at each of these rest points. Specifically, the orientation is defined as the angle θ' about the F-E axis with respect to the global horizontal:

$$X > 0, Y > 0 \quad \rightarrow \quad \theta = \tan^{-1}\left|{}^{Y}/_{X}\right| \quad \rightarrow \quad \theta' = -(90° - \theta) \tag{19}$$

$$X > 0, Y < 0 \quad \rightarrow \quad \theta = \tan^{-1}\left|{}^{X}/_{Y}\right| \quad \rightarrow \quad \theta' = -(180° - \theta) \tag{20}$$

$$X < 0, Y < 0 \quad \rightarrow \quad \theta = \tan^{-1}\left|{}^{Y}/_{X}\right| \quad \rightarrow \quad \theta' = 90° + \theta) \tag{21}$$

$$X < 0, Y > 0 \quad \rightarrow \quad \theta = \tan^{-1}\left|{}^{X}/_{Y}\right| \quad \rightarrow \quad \theta' = \theta \tag{22}$$

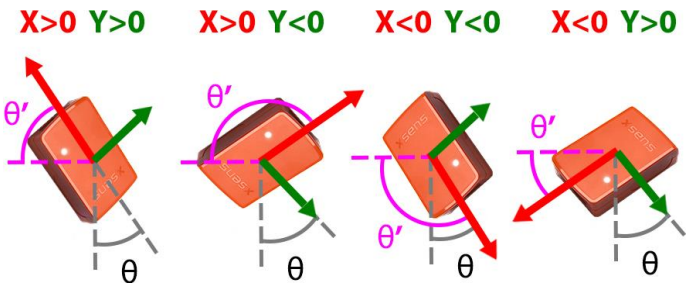

Figure 12. Orientation of IMU or limb segment w.r.t the horizontal using the sensor acceleration

Depending on the joint angle definition, which are derived from the International Society of Biomechanics standards [121] (see **Figure 13**), we can simply compare each of the two relevant joint segment's orientation to obtain the joint angle at each rest point:

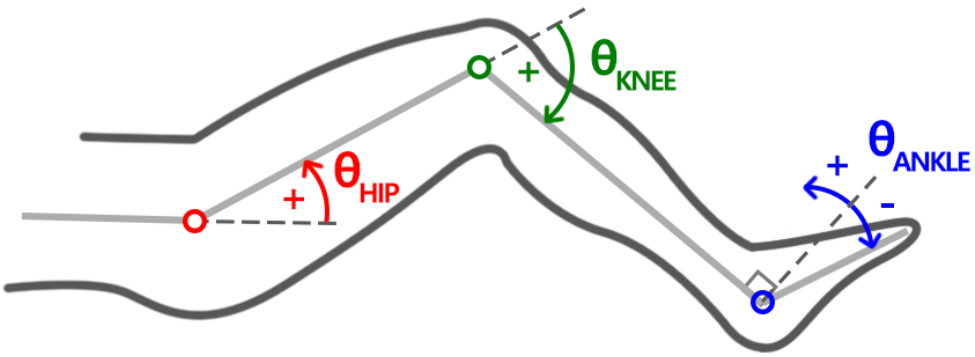

Figure 13. Joint angle definitions for the lower limb.

To determine the joint kinematics, the limb segment orientations θ'_0 at the first rest point are each converted to a rotation matrix about the F-E axis or Z_0:

$$R_{Z_0} = \begin{bmatrix} cos(\theta'_0) & -sin(\theta'_0) & 0 \\ sin(\theta'_0) & cos(\theta'_0) & 0 \\ 0 & 0 & 1 \end{bmatrix} \tag{23}$$

which can be converted to a quaternion (see **Appendix C.1)** to represent the initial orientations of each limb segment. From this initial quaternion, strapdown integration (SDI) [122] is used to update the limb quaternions at each next sample based on the next angular velocity vector. SDI requires the assumption that the sampling frequency f of angular velocities in the sensor data is sufficiently high that the rotation is small from sample to sample, and therefore the angular velocity can be treated as constant between two samples. Setting i as the current sample number, and $\vec{\omega}_i$ as the current angular velocity:

$$\vec{\omega}_{i+1} = \vec{q}_i \otimes \left(\frac{\vec{\omega}_i}{f}\right) \otimes \vec{q}_i^{\,-1} \tag{24}$$

$$\vec{\Phi}_{i+1} = \begin{bmatrix} 1 & \frac{\vec{\omega}_{i+1}}{2} \end{bmatrix} \tag{25}$$

$$\vec{q}_{i+1} = \vec{\Phi}_{i+1} \otimes \vec{q}_i \tag{26}$$

where $\vec{q}_{i+1}$ is the next sample quaternion, and $\otimes$ indicates quaternion multiplication (see **Appendix C.3**). Because we are interested in the purely sagittal movement (about the nominal F-E axis of the joint), the proximal segment's F-E axis is taken as the reference to which to correct the distal segment's F-E axis orientation. First, each segment's quaternion must be converted to a rotation matrix (see **Appendix C.2**):

$$\vec{q}_{proximal} \rightarrow R_{proximal} = [X_{proximal} \quad Y_{proximal} \quad Z_{proximal}] \tag{27}$$

$$\vec{q}_{distal} \rightarrow R_{distal} = [X_{distal} \quad Y_{distal} \quad Z_{distal}] \tag{28}$$

$$\theta_{correction} = \cos^{-1}(Z_{distal} \cdot Z_{proximal}) \tag{29}$$

$$if\ \theta_{correction} > 180° \rightarrow \theta = \cos^{-1}(Z_{proximal} \cdot Z_{distal}) \tag{30}$$

$$\vec{a} = {Z_{thigh} \times Z_{distal}} \Big/ {|Z_{thigh} \times Z_{distal}|} \tag{31}$$

Using the angle and axis of correction we can find the correction matrix $R_{correction}$ (see **Eq. 16**), to obtain a temporary, sagittal-corrected quaternion of the distal segment. We can then find the angle of rotation between the proximal and corrected distal quaternion:

$$R_{distal,temp} = R_{correction} * R_{distal} \rightarrow q_{distal,temp} \tag{32}$$

$$Q_{12} = Q_1^* \otimes Q_2 = \vec{q}_{distal,temp}^* \otimes \vec{q}_{proximal} \tag{33}$$

$$\theta_{joint} = 2\tan^{-1}\frac{\|[Q_{12b} \quad Q_{12c} \quad Q_{12d}]\|}{Q_{12a}} \tag{34}$$

The resulting joint angle data $\theta_{joint}(t)$ must then be corrected for drift that occurs in the sensors, which is assumed to be linear, based on the rest point joint angles we calculated previously. Starting from the first two, between each pair of rest points t_k and t_{k+1} a simple linear function is added to the joint angles to correct both ends to the rest point angles:

$$\theta_{joint,cor}(t) = \theta_{joint}(t) + \left[\frac{\theta_{k+1} - \theta_k}{t_{k+1} - t_k}t + \theta_k - \theta_{joint}(t_k)\right]; \quad t_k \le t < t_{k+1} \tag{35}$$

The resulting $\theta_{joint,cor}(t)$ represents our final, drift-corrected joint positions for the given passive motion trial. The corrected joint angle data is then numerically differentiated with the time data to determine the joint velocities $\dot{\theta}_{joint}(t)$.

3.2.3 Modeling Muscle Spasticity

In **Chapter 2** we concluded that the threshold control-based models can provide an objective method of assessment and have the advantage of featuring the key characteristic of spasticity, namely the sensitivity to muscle stretching velocity. Using our subject data, the accurate joint kinematics are obtained from the IMUs, and for each muscle, the onsets of spastic reflexes were found by identifying onsets of muscle activity (see **Section 3.2.1.2**) in the corresponding EMG signal of the set of stretching motions. The same time points are selected on the kinematic data to obtain the joint position and velocity at each triggering point of a spastic reflex (see **Figure 14**). Each point is one of the DSRTs in the reflex threshold model (see **Eq. 9**) used to represent the

muscle's spasticity, which first requires plotting the DSRTs together for a given muscle in a specific condition of stretching motions.

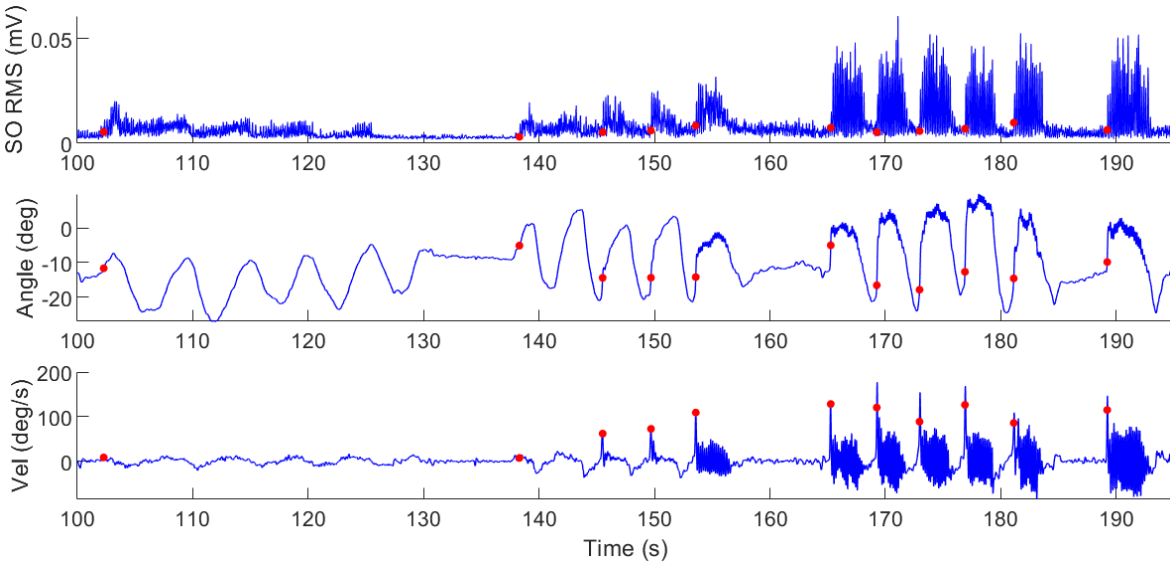

Figure 14. Example S01 KF SO muscle reflex points (red) selected on the RMS-EMG signal, then on the joint kinematics

The sensitivity of spasticity to velocity means that at greater joint velocities or muscle stretching velocity the range of motion becomes more limited, past which a spasm is triggered. In a plot of velocity versus position, a negative slope is therefore expected of any linear model fit to the data. Any trends between points that are vertical (which represents rigidity) or horizontal (which represents nothing) violate the definition of spasticity. Therefore, a criteria was established to exclude outliers: if any point is separated from the other points that lie on the expected trend, by more than 50 *deg/s* along the same position or angle, it is excluded.

A robust linear regression is finally used to fit a model to the included data points. The function *fitlm* in MATLAB is utilized, which is set to use a bisquare weight function for the robust fitting, reducing the effect of outliers aside from the already excluded points. The *x*-intercept of the resulting linear model, or the joint angle at zero velocity is the TSRT, while the negative inverse of the slope is the velocity sensitivity or μ of the muscle (see **Eq. 9**).

3.2.4 Objective Measure of Spasticity

For a given condition of the proximal joint, an objective measure of spasticity can be constructed by combining the stretch reflex models of a muscle group. The plot of velocity versus position represents the kinematic space of a joint. The limits of biomechanical range of motion of the joint [123] are set as the x-axis boundaries. For the y-axis, the range of velocity in a typical gait are defined as the boundaries. The gait data included in the OpenSim software was taken as a representative pattern for the joint velocities.

The fitted models for the members of the muscle group are plotted together on the bounded kinematic space, on the side of the x-axis that contain the joint velocities where the muscles are being stretched (e.g. for ankle plantarflexors, the positive velocity range). For each muscle model, the area on the "outside" the fitted line represents the spastic kinematic space of the muscle (see **Figure 6**). Therefore, the area outside all the models of the combined plot represents the spastic kinematic space. The ratio of this spastic kinematic area $A_{spastic}$ divided by the total kinematic space of the muscle group A_{total} is taken as a simple but objective, joint "Kinematic Spasticity Score" (KSS) for that muscle group:

$$KSS = \frac{A_{spastic}}{A_{total}} \tag{36}$$

As we have taken a typical gait as a determining factor in the measure, it can be augmented by taking the distribution of joint velocity in a gait cycle to weight our kinematic spaces.

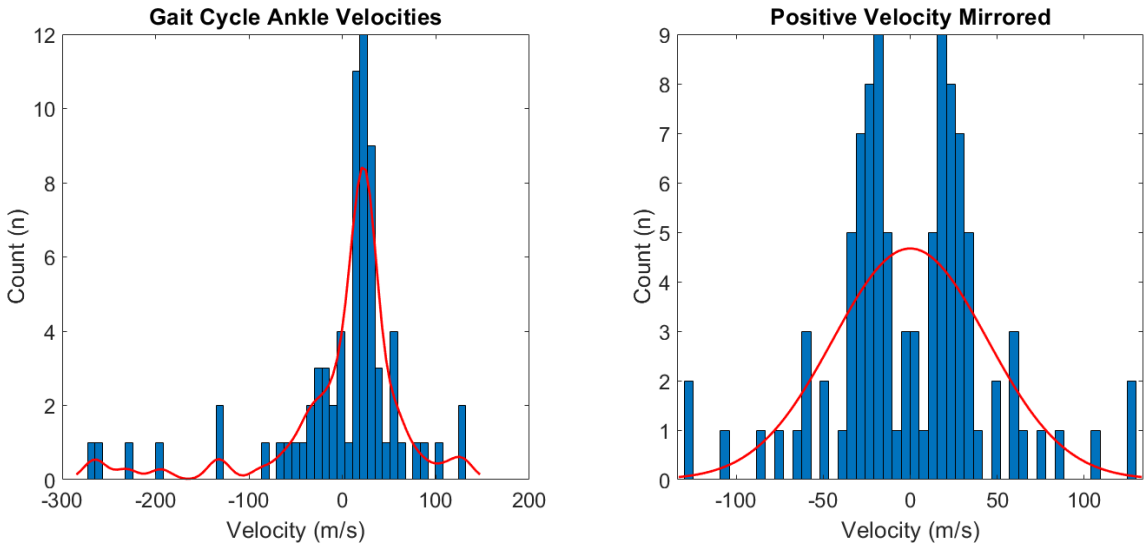

Figure 15. Ankle gait cycle velocities and distribution for weighting the kinematic space

The implication of weighting by velocity distribution is that the kinematic space that is most crossed during gait should be considered more significant in determining the measure of spasticity. However, in reality the worst case is when spasticity is present at zero velocity. To account for this, the range in gait velocities where a muscle group is stretched is mirrored about zero velocity. The resulting fitted Gaussian distribution has a mean of zero velocity and can be used to weight the kinematic space.

Additionally, one of the real consequences of spasticity is inhibited motion which is caused by the involuntary flexing of the triggered muscles. The force a muscle can exert is proportional to its biological cross-section [124], therefore the influence of a muscle on the real effects of spasticity can also be taken as proportional to the cross-section. The weight is defined for each

muscle as the ratio of its cross-sectional area to the total cross-section of the muscle group. Finally, each muscle model's spastic kinematic area is then calculated using the velocity-distribution weighting, and all the separate spastic areas are combined by each muscle's weight to result in the more biomechanically meaningful, "modified KSS" measure:

$$MKSS = \frac{A_{VM,spastic}}{A_{VM,total}} \tag{37}$$

where $A_{VM,spastic}$ is the gait velocity and muscle-weighted spastic kinematic area, and $A_{VM,total}$ is the velocity weighted total kinematic area.

3.3 Validation of Kinematics

To validate our sensor integrity, functional calibration and kinematics analysis protocol and algorithms, we compared our results to the VICON Motion Capture system. The Xsens Awinda IMUs were placed to track the motion of the thigh, shank and foot, and the VICON system was setup to capture the motion of the leg at the same time.

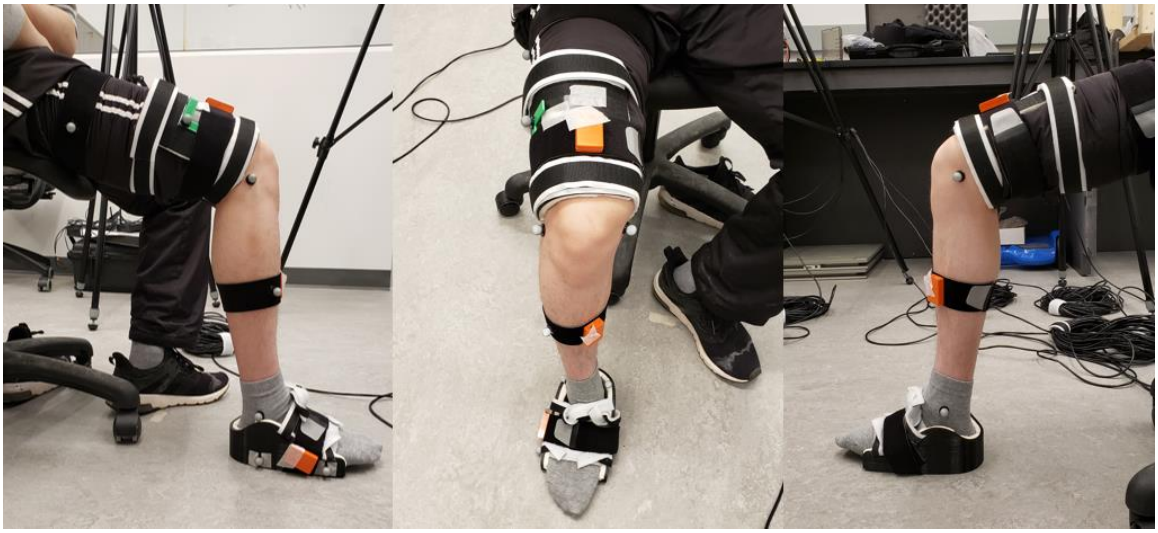

Figure 16. Validation setup for Xsens IMUs and algorithms against VICON motion capture

Both ankle and knee motions were performed during these validation trials. Similar to the method for syncing the sEMG and IMU sensors, the two systems were synchronized for post-processing by a light tap of the foot on the ground at the beginning and end of each trial. These taps which can be clearly identified in the data and used to shift the clocks to match, and ensure the clocks remain synchronized by the end of the trial and correct them if they are not.

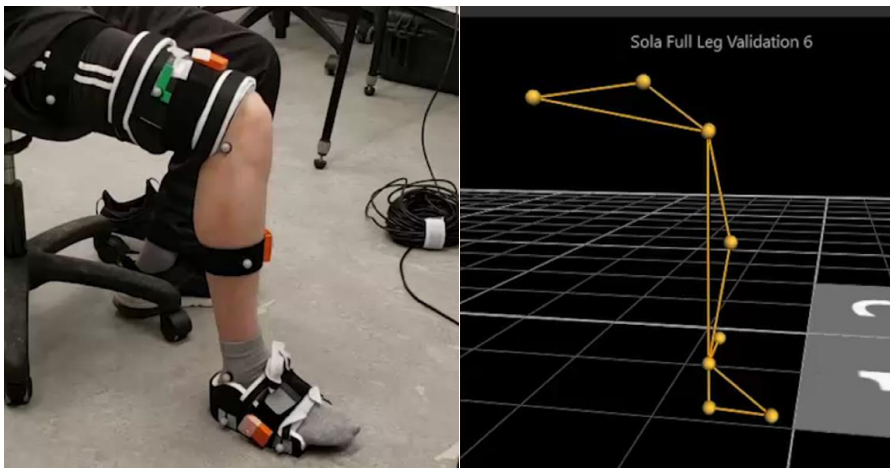

Figure 17. Comparison of motion tracking setup and representation in-software

Figure 17 illustrates how the physical dots on the left correspond to the tracked points in the VICON system on the right. In post-processing, the highlighted vectors were used to represent the thigh, shank and foot. For determining the knee or ankle joint position, the proximal and distal segment vectors were projected to the plane that is perpendicular to the joint F-E axis. The angle between them is then simply calculated according to the biological joint definition.

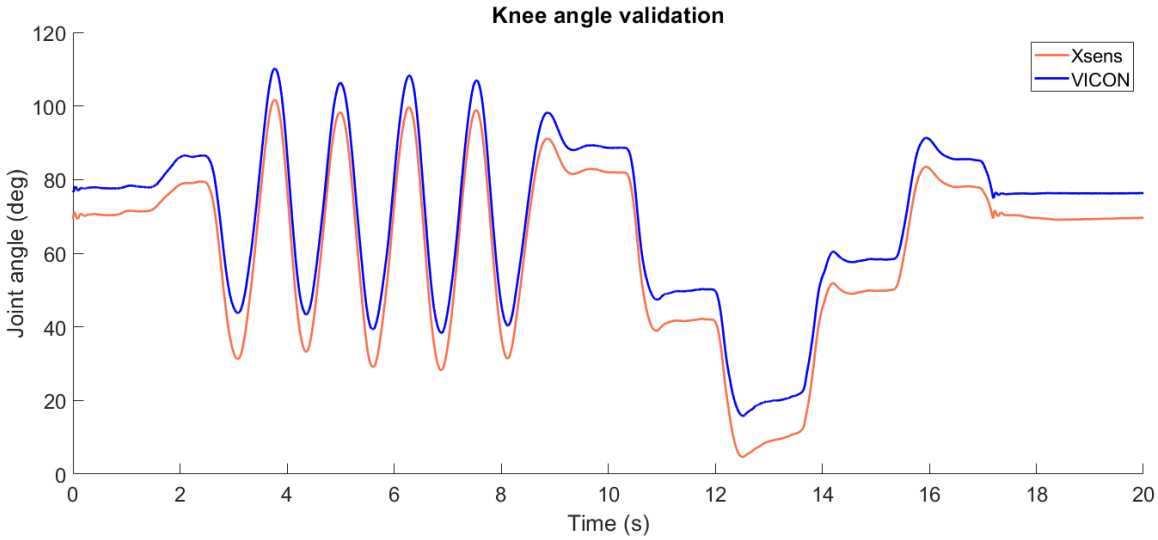

Figure 18. Xsens knee joint angle compared with VICON joint angle

Because of imperfect placement of the tracking dots for the VICON system (relative to the limb segments), a constant shift is expected between the result of calculating kinematics for the VICON data and the IMU data. The underlying algorithms for a gyroscope also means an additional minor and varying difference is expected during motion, and this effect increases with more speed. The compared results from post-processing for Xsens and VICON can be seen in **Figure 18**. In that example, the mean difference between the calculated knee angles is 8.04 *deg*,

with a relatively small standard deviation of 1.45 *deg*. This difference between the calculated joint positions is treated as the expected constant shift, and subsequently subtracted to visualize and calculate the variance (see **Figure 19**). Once corrected, the mean difference and standard deviations are 1.13 *deg* and 0.91 *deg* respectively.

More of the variance between Xsens and VICON can be accounted for by the simple physical irregularities, where due to the fat and muscles of the leg, the orientation of the dots for VICON and the Xsens IMUs do not stay constant relative to each other, where this effect becomes more pronounced with faster motion. Overall, the difference between motion tracking and IMU can be seen as minimal with expected variance, and the post-processing algorithms for IMU data as validated.

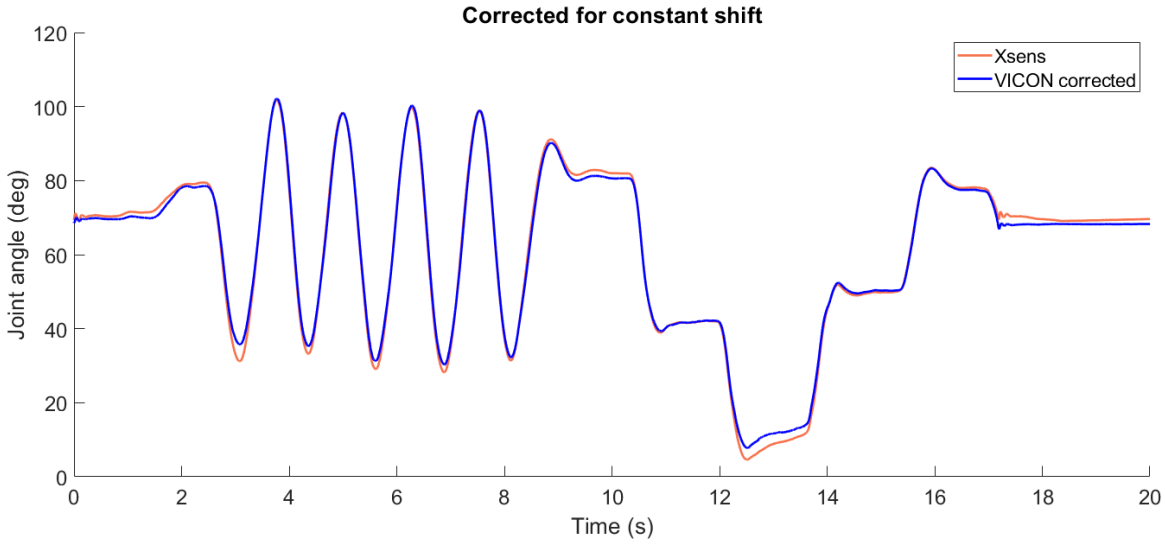

Figure 19. VICON trajectory corrected by mean difference with Xsens

3.4 Results

The data used in this section was previously collected at Imperial College London, as part of the project "EU FP7 Symbitron: Symbiotic Man-Machine Interaction in Wearable Exoskeletons to Enhance Mobility for Paraplegics" [125]. In the available data, two subjects (S01, S06) were found to have clear spastic behaviour in their EMG data and are included in these results.

Table 4. Subject information and clinical scores.

Subject		S01	S06
Etiology		Non-traumatic	Traumatic
Lesion Level		T10	L1
AIS Score		D	C
MAS	**Left Ankle**	2	3
	Right Ankle	n/a	3

For these subjects, spastic behaviour was observed for the ankle only, and commonly in the left ankle. Additionally, plantarflexion stretches were not performed, therefore only the left plantar flexor muscles could be modelled and grouped to create the measures of spasticity. In each of data set of stretching trials, a minimum of three different stretching speeds were performed, with at least 5 stretches per speed (see **Figure 14**).

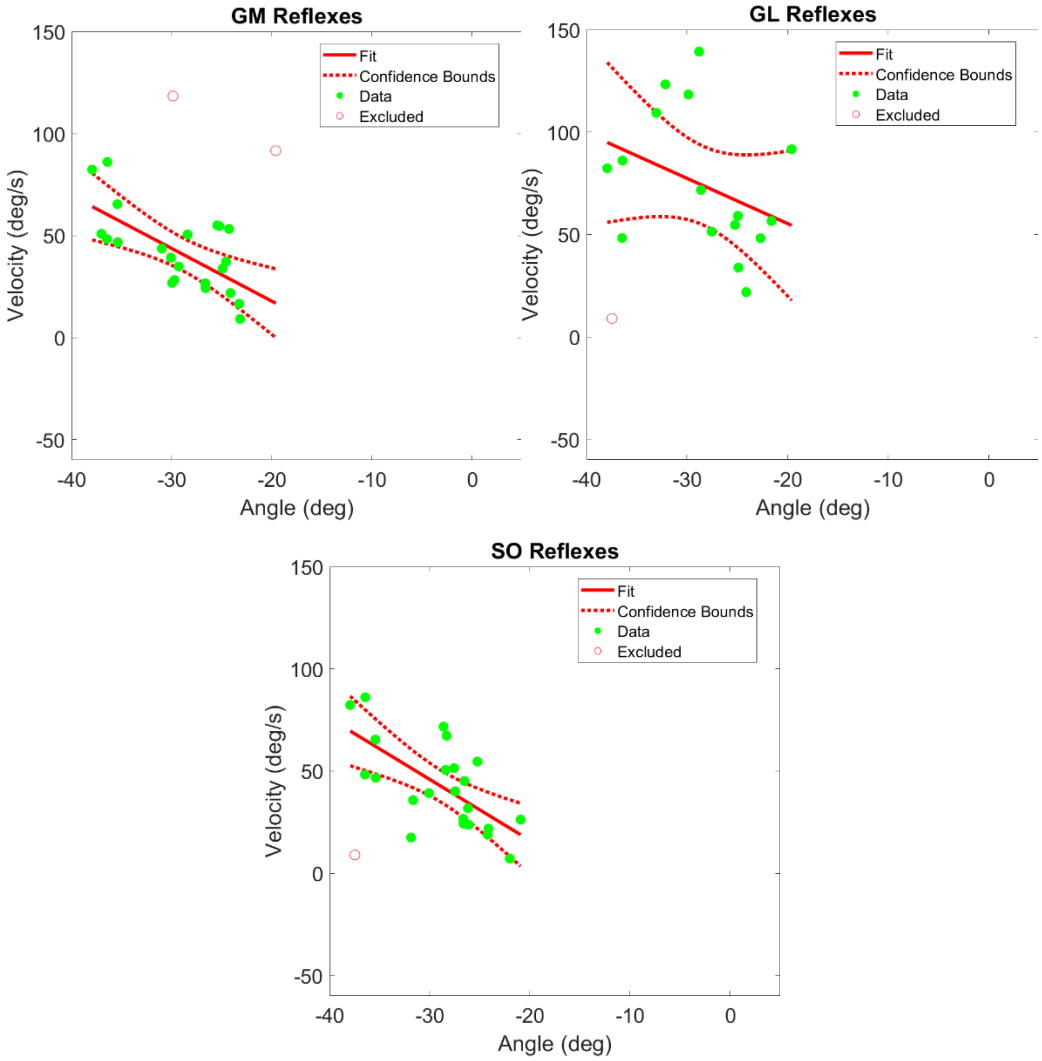

Figure 20. Subject S06 ankle plantarflexor SRT models for knee flexed at 30 degrees

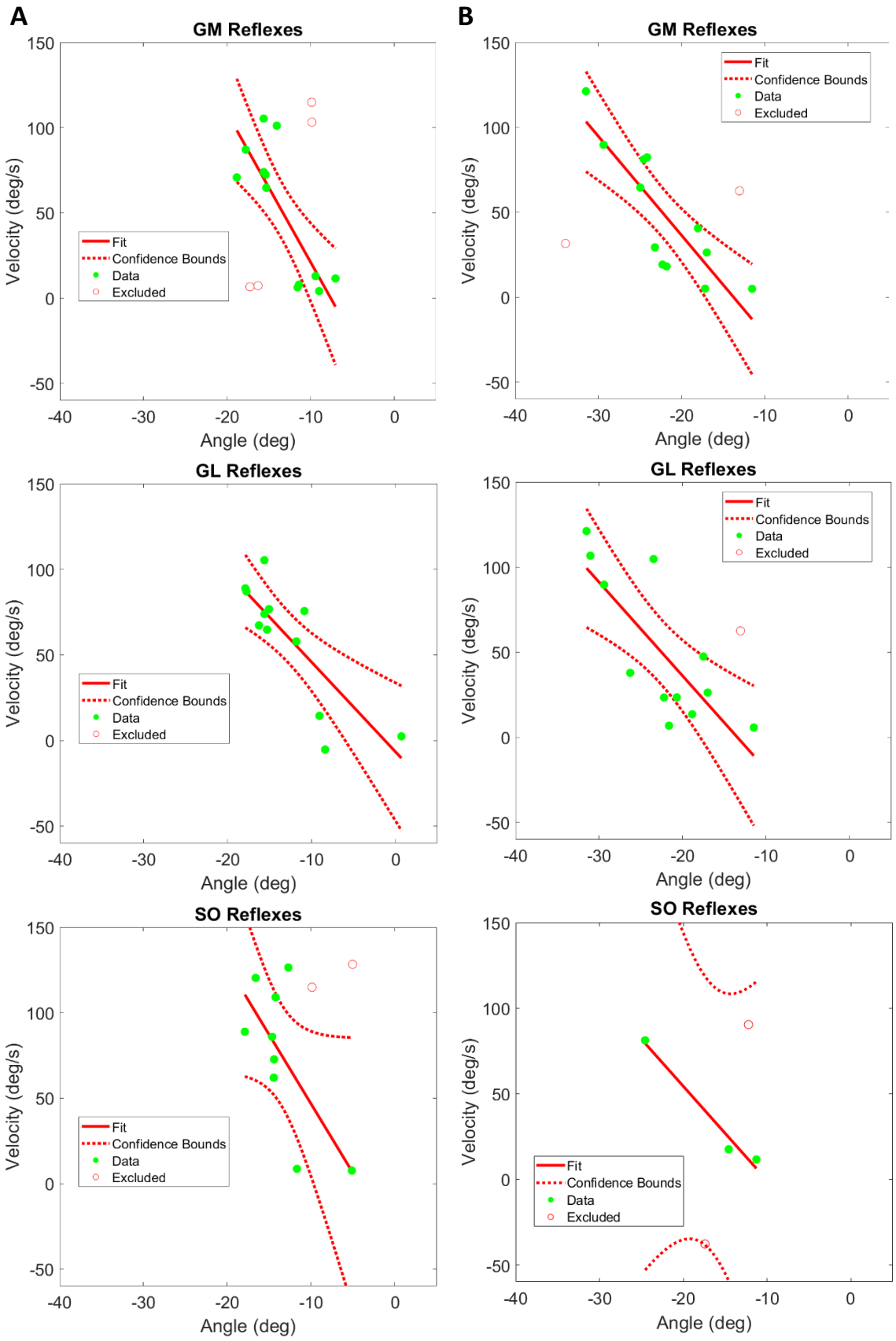

Figure 21. Subject S01 ankle plantar flexor SRT models for (A) KF at 30 degrees, (B) KE.

Table 5. Subject S01 plantar flexor models

Proximal Joint	Knee Flexed (30°)			Knee Extended (0°)		
Muscle	GM	GL	SO	GM	GL	SO
TSRT	-7.598	-0.265	-4.230	-13.768	-13.431	-10.132
μ	0.114	0.211	0.124	0.172	0.182	0.182

Table 6. Subject S06 plantar flexor models

Proximal Joint	Knee Flexed (30°)		
Muscle	GM	GL	SO
TSRT	-13.097	5.047	-14.598
μ	0.387	0.453	0.336

The individual muscle SRT models were combined to form the KS measure of the plantarflexor muscle group, for each subject and condition:

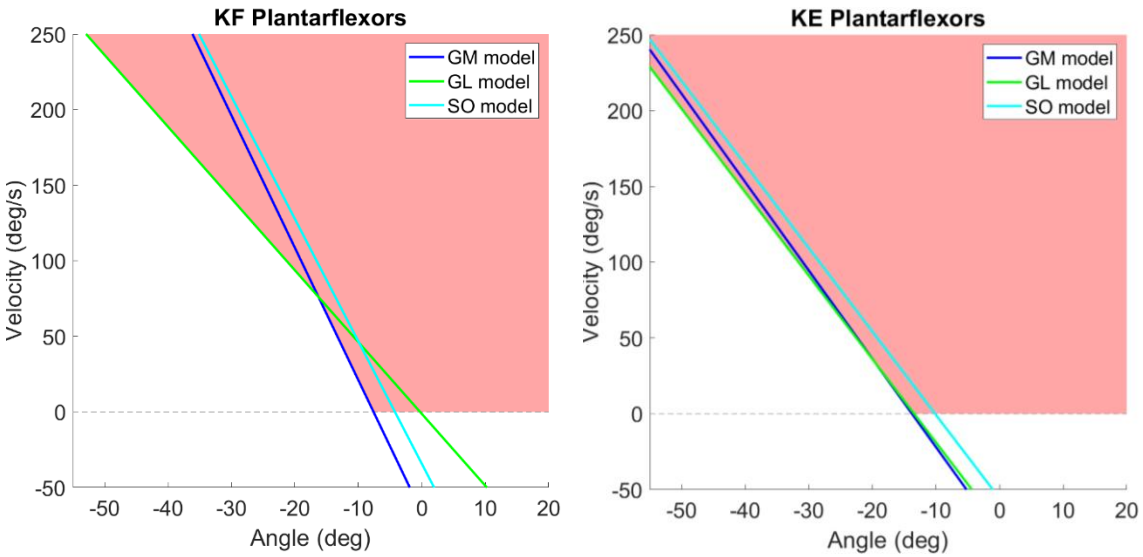

(a) (b)

Figure 22. Subject S01 combined SRT models for (a) KF at 30 degrees, (b) KE conditions

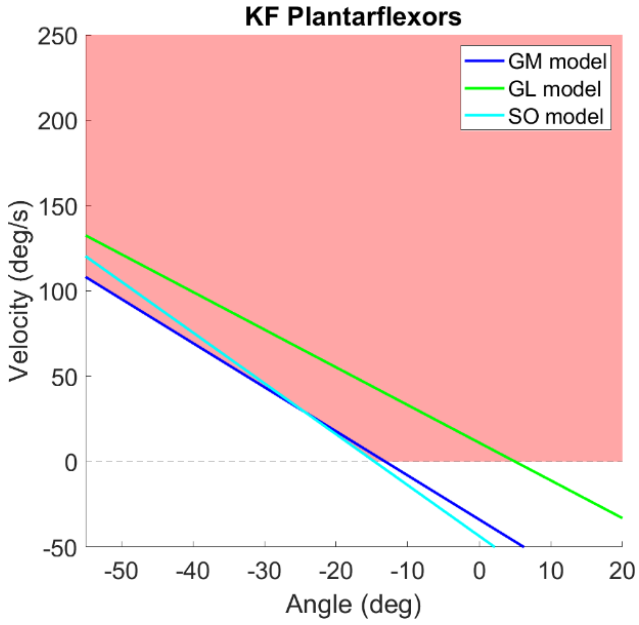

Figure 23. Subject S06 combined SRT models for knee flexed at 30 degrees

The KSS measure was further refined into the MKSS score by weighting with gait cycle velocities and relative muscle cross-sectional areas:

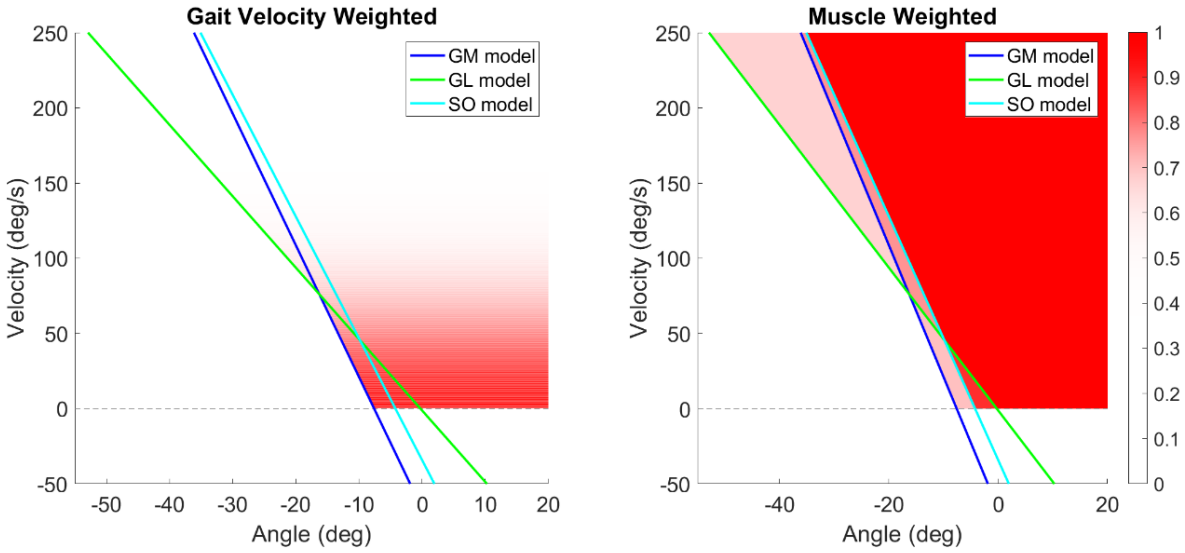

Figure 24. Example S01 knee flexed measures weighted by (a) velocity distribution and (b) muscle cross-sections. Bright red represents the maximum weighting.

Table 7. Objective measures of spasticity and MAS Scores.

Subject	S01		S06	
Condition	Knee Flexed (30°)	Knee Extended (0°)	Knee Flexed (30°)	Knee Extended (0°)
KSS	63.61	74.67	88.02	n/a
MKSS	45.44	59.15	76.06	n/a
Ankle MAS	2		3	

3.4.1 Statistical Analysis

For each individual muscle model, a one-way ANOVA was performed to determine the *F*-statistic of the coefficient of the independent variable – angular velocity – which is also measures the significance of the model itself.

Table 8 and **Table 9** also report two correlation values for the muscle models: coefficient of determination R^2 to measure the goodness of fit, as well as Spearman's rank correlation ρ as a non-parametric test because of the limited number of data points available for each model. Statistical significance is interpreted at $\alpha = 0.05$.

Table 8. Subject S01 plantar flexor model statistics

Proximal Joint	Knee Flexed (30°)			Knee Extended (0°)		
Muscle Model	GM	GL	SO	GM	GL	SO
F	17.4**	15.9**	4.93	22.5**	14.1**	25.6
R^2	0.599	0.575	0.33	0.662	0.543	0.925
ρ	-0.720*	-0.790**	-0.433	-0.874**	-0.734*	-1.00

* *p < 0.05,* ** *p < 0.01*

Table 9. Subject S06 plantar flexor model statistics

Proximal Joint	Knee Flexed (30°)		
Muscle Model	GM	GL	SO
F	14.5**	1.79	13.8**
R^2	0.369	0.049	0.368
ρ	-0.583**	-0.415	-0.617**

* *p < 0.05,* ** *p < 0.01*

The model was significant for the GM and GL muscles for S01 in both KF and KE conditions, and the GM and SO muscles for S06 KF condition. Moderate to high correlations were found for all the models except in S06 GL muscle. Spearman's ρ showed high correlations for all the models which were found to be statistically significant except for S01 SO muscle in both conditions, and S06 GL muscle. **Figure 20** illustrates the spread of data that resulted in the unsatisfactory modeling for the GL muscle in subject S06.

Due to the limited scope of the available data (see **Section 3.1.4**), only certain inferences and predictions can be made from the results for the novel spasticity measures. With a sufficiently large population, other statistical analyses could be performed both for validation and relating to other aspects of this topic, such as correlating the KSS scores with the MAS or other clinical scores used for spasticity.

3.5 Discussion

3.5.1 Spasticity Models and Measures

In both subjects, the TSRT of all muscle models show a negative shift from the knee flexed to the knee extended condition. Similarly, the KSS and MKSS measures are also greater in the knee-extended condition than when the knee is flexed. This trend is expected, as when the knee is extended, the biarticular gastrocnemius muscle is more stretched at the same joint positions than when the knee is flexed. This would cause a negative shift of the stretch-reflex model or the TSRTs as the joint range of motion is reduced. The soleus muscle is not expected to follow this trend, but with more data points it would become clearer to observe an effect or not.

As the KSS and MKSS scores suggest a worse degree of spasticity in S06 than S01, the ankle MAS scores also reflect that difference in their spasticity. It suggests a mild to moderate correlation may be observed with more data points, providing a degree of validation to our spasticity modeling and measure.

3.5.2 Limitations and Future Research

A fundamental limitation of the spasticity measures in their current form is the exclusion of the antagonist muscles. Because the dorsiflexor muscles in the data were not stretched following the same protocol as the plantarflexors, they could not be modelled in the same way. Given a more complete set of data, or the experiments detailed in **Section 3.1** are completed, the KSS and MKSS measure should be modified to include the spastic kinematic space of the dorsiflexors, else the measures reported separately for the dorsiflexor group in addition to the plantarflexor scores.

As mentioned previously, biarticular muscles are constantly stretched to a different level depending on the position of the distal and proximal joints. This constant shift of muscle stretch

affects the onsets of reflex and the resulting SRT model. Therefore, the methodology should be augmented to account for this 'shifting' of spasticity. For example, a solution would be to generate the SRT models of the GM and GL muscles at a sufficient number of different positions of the knee joint, then the relationship between the TSRT and proximal joint position could be modeled. The KSS and MKSS measures would also need be modified to account for the position of proximal joints for biarticular muscles.

The data used in this chapter were from subjects with motor-incomplete SCI, who have a limited amount of volitional motion in their lower-limbs. However, individuals with other conditions such as stroke survivors are also affected by spasticity, while retaining active movement in daily life. The tonic reflex thresholds of muscles have been found to be extended to a greater range of motion, while the sensitivity to velocities were simultaneously increased in active, volitional motion compared to passive versions of the same stretches (see **Section 2.2.2.3**). Therefore, similar to shifting by proximal joint position for biarticular muscles, the transformation of SRT models with respect to the kinematics of active motion should be modeled to provide a more comprehensive characterization of spasticity. Previous studies have also found that spastic reflexes are affected by the initial stretch level of a muscle (see **Section 2.3.1**). The dynamic reflex thresholds were found to be significantly reduced by increasingly stretched muscles before stretching motions at the same velocity. Consequently, the modeling of muscle spasticity should also incorporate the initial positions of muscle length or joint position to dynamically transform the SRT models.

Additionally, previous studies have found that spastic muscle activity can be better predicted by the applied force for actuating passive stretches, than the muscle kinematics (also see **Section 2.3.1**). These findings are not unexpected as the stretch reflex is affected by both muscle spindles and Golgi tendons which are sensitive to muscle stretch and tension respectively [126]. The relationship between spastic reflexes and the triggering muscle forces should also be included in the characterization of spasticity.

3.5.2.1 Clonus

Clonus is a common pathology that also occurs after spinal cord injury, and in many cases is accompanied by spasticity [127]. As a result, spasticity is often confused with clonus as well as rigidity in clinical practice, and while the pathophysiology of spasticity and clonus are related, they are still separate. Clonus is generally more easily induced in the more distal leg segments, at the ankles and feet [128], and presents as oscillations in the joint as a result of involuntary, rhythmic contractions of the relevant muscles. However, there are conflicting explanations; while some researchers have found that ankle clonus was the result of only gastrocnemius and soleus activations [129], others observed simultaneous activity of antagonistic muscles, where the tibialis

anterior was activated together with the plantarflexors [130], [131]. The latter agrees with the original understanding of the pathophysiology of clonus, and the hypothesis posits that a central pattern generator in the spinal cord is at least jointly responsible for clonus behaviour [128].

Table 10: SCATS scale for clonic activity

Score	Description
0	no reaction to dorsiflexion
1	mild; clonus persists for less than 3 seconds
2	moderate; clonus persists for 3 to 10 seconds
3	severe; clonus persists for more than 10 seconds

The Spinal Cord Assessment Tool for Spastic reflexes (SCATS) uses passive, fast dorsiflexion motions to assess clonus in the ankle [132], which has been shown to be a reliable tool for clinical assessment [133]. Both subjects S01 and S06 in our data were assessed with a SCATS score of 2 for their left ankles (which were analyzed in this chapter). In our data, though onsets of spastic reflex cannot be identified due to the execution of the experiments, the EMG signals of the dorsiflexor muscles can be processed to observe their activity during the stretching trials of the plantarflexors (see **Section 3.2.3**).

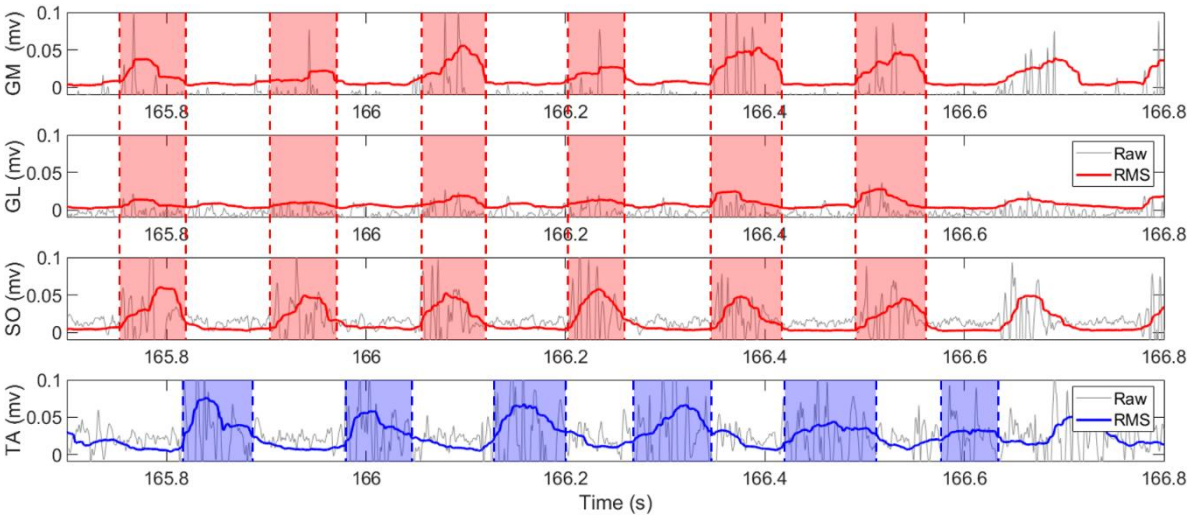

Figure 25. Example clonic behaviour in RMS-EMG data for S01 KF ankle motion

Figure 25 shows the unprocessed and RMS-envelope of the EMG signals for the three plantarflexor muscles, and the dorsiflexor tibialis anterior, during the spastic reflex of the first fast stretching motion (see **Figure 11**). The approximate simultaneous activations of the plantarflexor group are visualized in opposition to the activation of the TA muscle, which appear to follow the cyclic, alternating pattern that would produce the joints oscillations that are associated with clonus. Such joint oscillations or tremor-like behaviour were indeed observed in the footage that

was recorded for these experiments, which is corroborated by joint trajectory seen in **Figure 26**, and the clinical assessment using the SCATS scale.

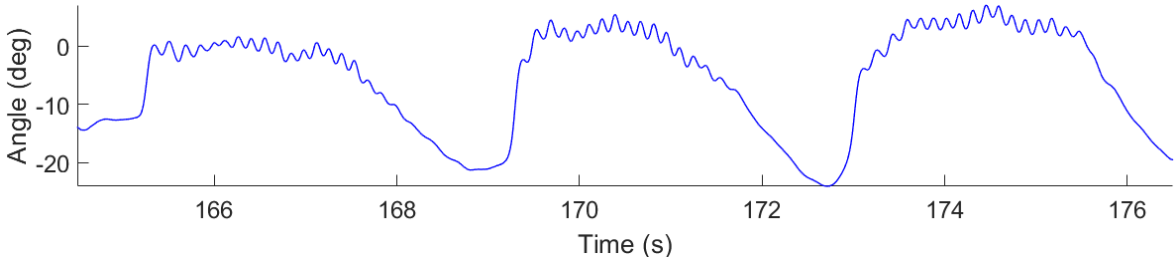

Figure 26. Clonic joint oscillations following reflex onset in first three fast stretches of S01 KF

The alternating antagonistic activations agree with the theory of a central pattern generator, however more data would be required to reach a conclusion. As the pathophysiology of clonus is thought to be separate from spasticity, their relationship and interactions must be better understood in order to begin modelling both phenomena in conjunction, which may affect the development of the objective measures for either or both symptoms.

Chapter 4:

Neuromuscular Simulation of Spasticity

4.1 Introduction

Musculoskeletal models and simulations are used for research in a wide variety of subjects, as they allow for non-invasive and inexpensive investigations into the mechanics of the human body and can therefore be invaluable for investigations that would otherwise require direct experimentation. For example, musculoskeletal modeling and simulation can potentially improve the ergonomic design of tools and consumer products [134], or provide analysis to proactively preventing occupational injuries and disorders [135]. Loading and strain in the joints and ligaments can be analyzed in other scenarios such as athletic activities [136], or in analyzing and designing joint and limb prosthetics [137], [138].

Musculoskeletal and neuromuscular pathologies can also be modeled and simulated to better understand them. For example, in anterior cruciate ligament (ACL) deficient knees the risk of osteoarthritis is increased by compressive loading in the joint [139]. OpenSim can be used to analyze the loads in the tibiofemoral joint in experimental kinematic data from ACL-deficient patients [140], [141]. The joint kinematics could then be scaled in velocity and displacement to optimize rehabilitation exercises to prevent further damage, minimize pain and discomfort and maximize recovery. The most common type of walking impairment after stroke is hemiparetic gait [142], which can be modeled and simulated and analyzed by the kinematics and kinetics in comparison to normal gait which can be simulated using the same modeling technique [143]. For a more neuromuscular example, the pathological gait as a result of multiple sclerosis can be modeled, obtaining joint kinematics and torques from simulations for analysis and designing exoskeletons to support rehabilitation [144].

The objective KSS and MKSS measures present a valuable alternative or supplement to the current clinical practices in assessing spasticity. However, the data and modeling used in creating that measure can provide further value by enabling simulation of spastic behaviour in a virtual environment. Using the same patient data as collected in **Chapter 3**, we can create models of the spastic behaviour (in addition to the SRT model) and integrate them in a spasticity controller. Once developed and validated, the spasticity controller can become a building block in developing models and simulations of impaired subjects with conditions that exhibit spasticity.

A basic yet fundamental scenario that can be simulated is a passive-movement spasticity assessment that is performed in the clinical setting, generally to rate the patient's spasticity with

subjective scores such as the MAS. In these tests, one joint is manipulated at a time by the examiner, such as the knee, to assess the spasticity in the relevant muscles as felt by the examiner, ideally moving at different speeds. By comparing the kinematics, activation levels and interaction torques in the resulting simulation to the would provide validation of those spasticity models and algorithms that produce the behaviour. The spasticity controller can be integrated into a simulation that represents more everyday functions, such as walking. By using a reinforcement-learning walking agent, the simulation can demonstrate the effects of muscle spasticity on an otherwise healthy individual's gait.

4.2 Musculoskeletal Model and Software

An OpenSim lower-limb model [145], [146] was used in the simulations. The model features 18 actuators that represent primary muscles of the lower limbs and uses 2 contact spheres on each foot to simulate the ball and heel of the foot in contact with the ground. The spasticity algorithm was developed in the MATLAB environment with integrated OpenSim API functions and a visualizer for the simulations.

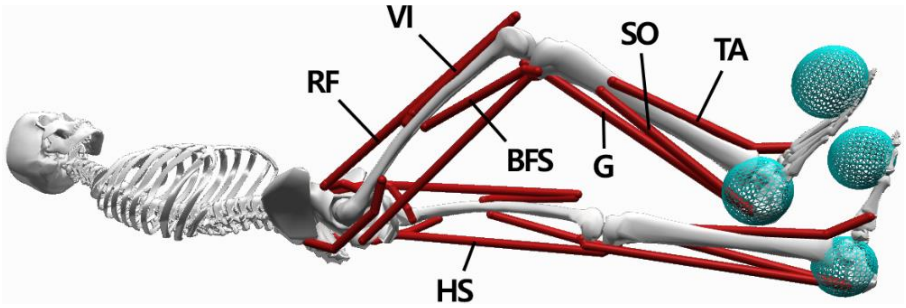

Figure 27. OpenSim model with muscles representing hamstrings (HS), biceps femoris short head (BFS), rectus femoris (RF), vastus intermedius (VI), gastrocnemius (G), soleus (S), and tibialis anterior (TA); cyan spheres are ground contacts for the balls and heels of the feet.

4.3 Methodology

The physiological models that the algorithm is based on are characteristics of a patient's spasticity, such as the sensitivity to velocity, or the range of motion where the tonic reflex persists. Similarly, the simulations were developed to represent those characteristics of a patient's spastic behaviour, not to exactly recreate the kinematic trajectories of a particular spasticity assessment test or other measurement such as gait.

4.3.1 Spasticity Controller

Spasticity can be triggered in a muscle being stretched if the kinematic variables meet the conditions as defined by the SRT models specific to each muscle of an individual. The parameters $TSRT$ and μ for each muscle model can be tuned by the user depending on their requirements.

$$DSRT = TSRT + \mu\dot{\theta}(t) \tag{38}$$

In the subject data from Chapter 3, the durations of each overall reflex and the mean activation levels as a percentage of MVC were calculated (see **Figure 28**). The mean activations and durations are each plotted against the joint velocity at the onset of those reflexes, with a robust linear regression applied to fit the data (see **Figure 29**). **Table 11** shows the strong correlations values, as well as high confidence in the positively dependent linear fit for both models.

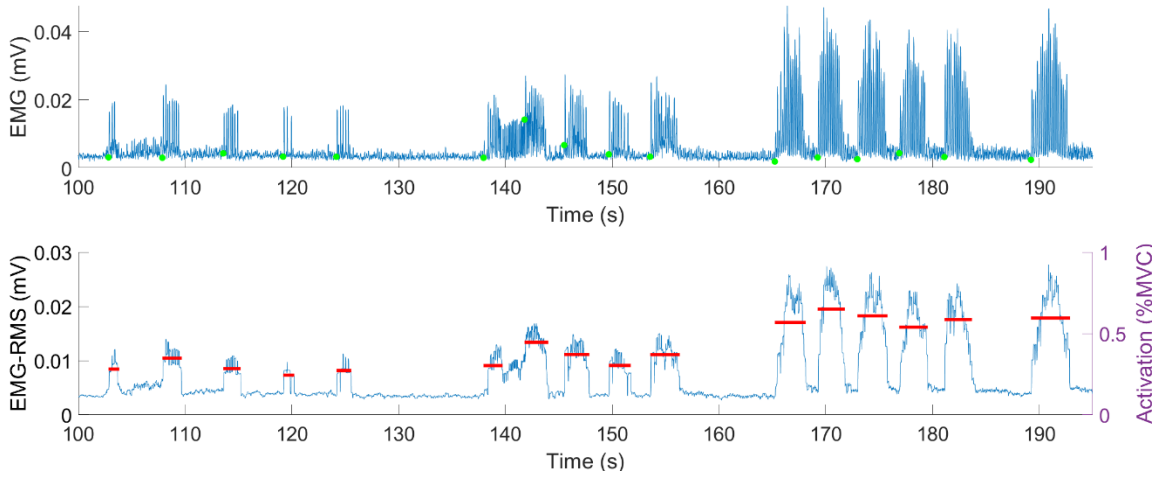

Figure 28. S01 in the KF condition; (a) filtered EMG signal of the GM muscle, (b) RMS envelope of the signal; red lines indicate duration of the reflex and the mean activation as %MVC.

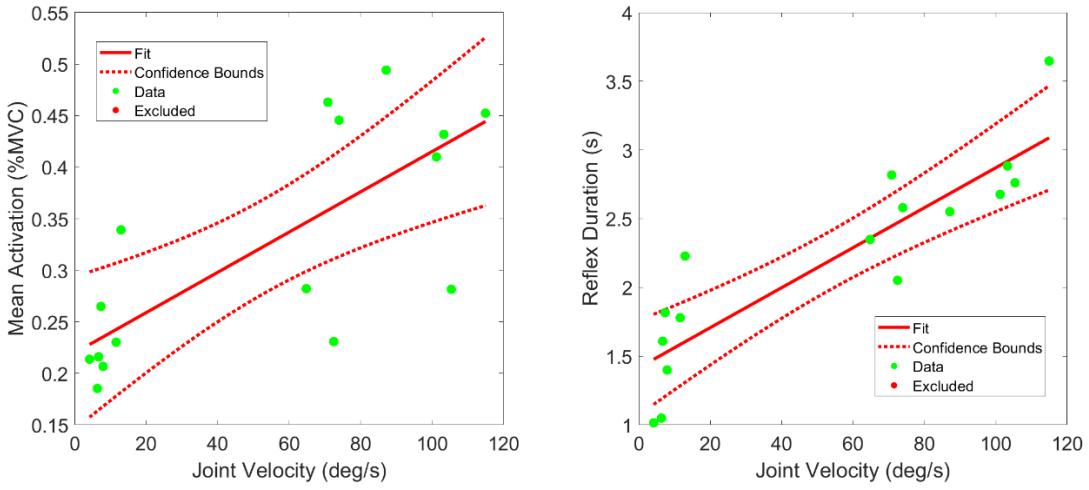

Figure 29. Robust linear regressions of the (a) mean activation as % MVC and (b) duration of the reflexes versus the joint velocity at the onset of each reflex.

Table 11. S01 reflex activation level and duration correlations and linear models

Model	Muscle	R^2	F	Spearman's ρ
Reflex Mean Activation	GM	0.477	14.7*	0.753*
	GL	0.298	5.66*	0.615*
	SO	0.595	15.7*	0.655*
Reflex Duration	GM	0.709	37.6**	0.918**
	GL	0.804	46.0**	0.685*
	SO	0.465	9.68*	0.718*

* $p < 0.05$, ** $p < 0.001$

These findings were consistent for the KE condition of S01 and S06 as well. Therefore, in this controller the spasm duration is defined as a simple linear model positively dependent on the joint velocity at the trigger point:

$$T_{reflex} = a\left|\dot{\theta}(t)\right| \tag{39}$$

$$\mu_{act} = b\left|\dot{\theta}(t)\right| \tag{40}$$

The average muscle activation during a spasm μ_{act} is also defined as linearly increasing with the joint velocity at the onset of spasm. Similar to the DSRT parameters, both model constants *a* and *b* are manually defined by the user to tune the severity of the OpenSim model's spasticity to achieve the desired behaviour. A function is then generated based on the mean activation level, where it rises from zero exponentially to a constant level, in a similar manner to how motor units are recruited in a muscle, then falls to zero in the mirror form at the end of the spasm. The constant value of this function must be equal to the modeled average activation of spasm:

$$a(t) = \begin{cases} C^t - 1 & ; \quad C^t - 1 < \mu_{act} \\ \mu_{act} & ; \quad C^t - 1 \geq \mu_{act} \end{cases} \tag{41}$$

$$C = (\mu_{act} + 1)^{10} \tag{42}$$

where the exponential constant C is determined using the assumption that the rise time for the activation is 100 *ms* (obtained by trial and error). To better imitate real-life behaviour, a random Gaussian noise is then applied to the activation using a MATLAB function, which will result in a non-smooth result for the generated reflex activation $a_{mod}(t)$. The signal to noise ratio is determined by the standard deviation of the muscle activation, which was found in the data to also be positively dependent on the onset joint velocity (see **Figure 36**).

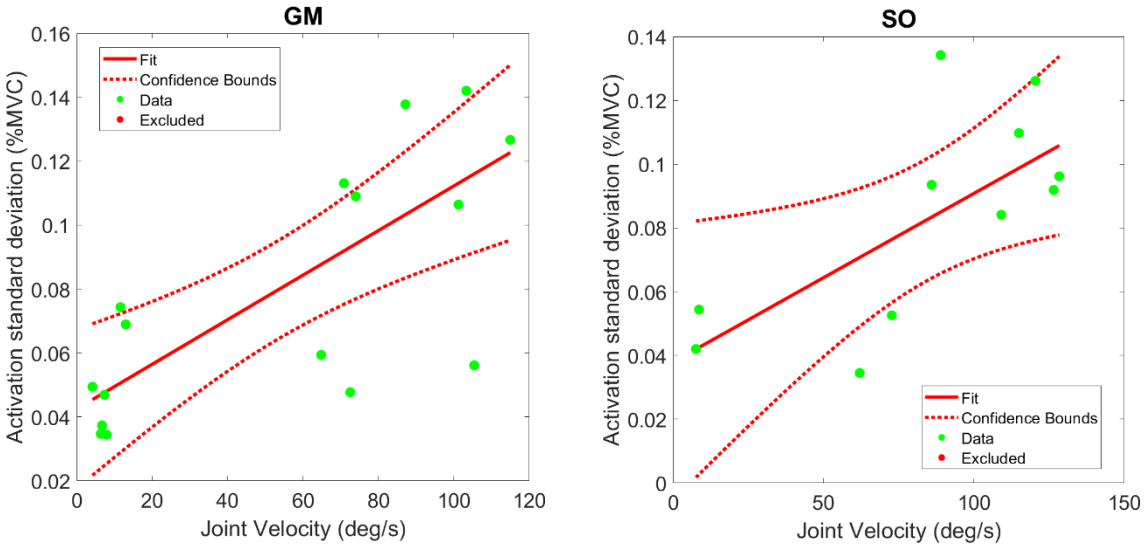

Figure 30. Examples of linear models for activation level standard deviation during reflexes versus the joint velocities at reflex onset; from S01 KF condition data.

$$\sigma_{act} = c\left|\dot{\theta}(t)\right| \tag{43}$$

Therefore, the activation standard deviation is also a user-definable linear model. With the noise applied, a simulation can be run using these instantaneous activation levels for each muscle, which will produce the spastic behaviour through the model's muscles. Alternatively, the simulation can be carried out at the joint level by further calculating the torque about the joint each muscle activation would generate. A Hill-type muscle model is used to estimate the force generated in the muscle by the activation:

$$F(t) = F_{max}\left[a(t) \cdot f_v\left(\dot{L}\right) \cdot f_l(L) + f_p(L)\right] \tag{44}$$

where $f_l(L)$ is the muscle force-normalized fiber length relationship, $f_v\left(\dot{L}\right)$ is the muscle force multiplier of normalized fiber velocity, and $f_p(L)$ the passive component of muscle force. The active muscle force-length relationship can be extracted from the OpenSim model itself:

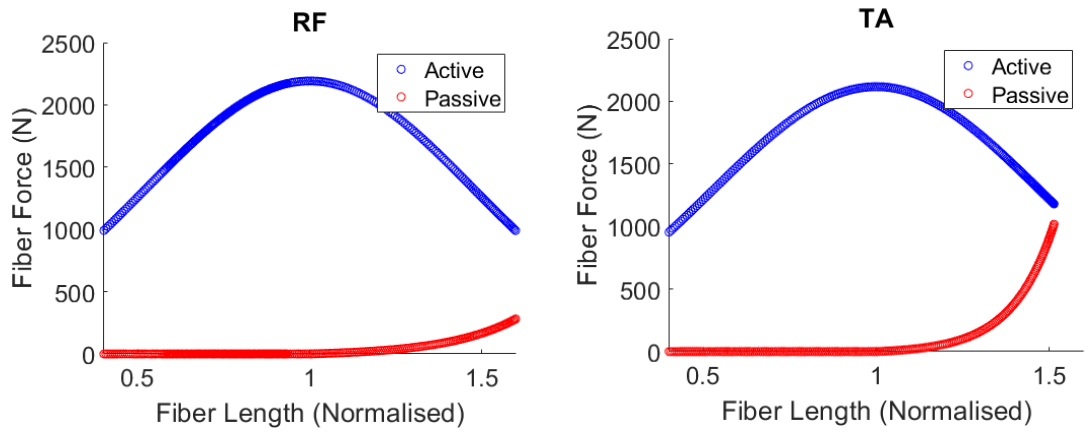

Figure 31. Example muscle force-length relationships for (a) RF and (b) TA muscles.

Normalizing the fiber force by the peak value allows the data set to be used for each muscle to interpolate for the $f_l(L)$ value at any instance. F_{max} is the maximum isometric force, which can be user defined or taken as the same peak value from the OpenSim data. For simulating reflexive activity, the passive component of muscle force is assumed to have a negligible effect. Therefore, the active force generated in a muscle is:

$$F(t) = F_{max}\left[a(t) \cdot f_v(\dot{L}) \cdot f_l(L)\right] \tag{45}$$

The function for the force multiplier of a muscle in relation to the rate of change of its length is generated based on examples from literature:

$$f_v(\dot{L}) = \begin{cases} -2 \times 10^{-8}\dot{L}^3 - 2 \times 10^{-5}\dot{L}^2 - 0.0058\dot{L} + 1.0097 & ; \quad \dot{L} \leq 0 \\ -2 \times 10^{-8}\dot{L}^3 + 2 \times 10^{-5}\dot{L}^2 - 0.0058\dot{L} + 0.9903 & ; \quad \dot{L} > 0 \end{cases} \tag{46}$$

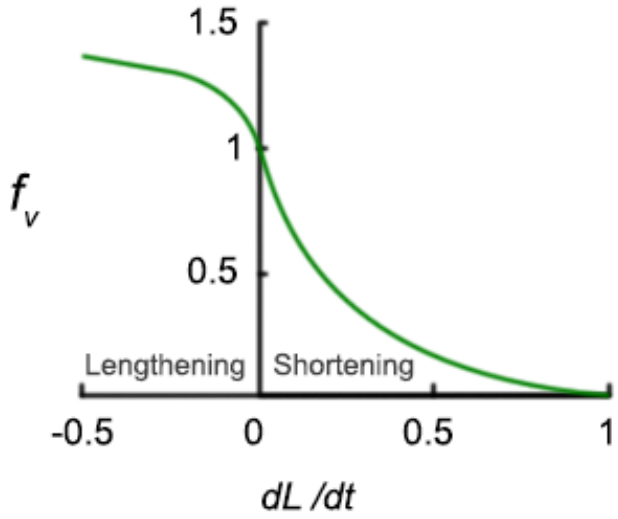

Figure 32. Example of muscle force multiplier relationship with muscle length velocity [147].

The joint torque $\tau_{reflex}(t)$ generated by the muscle reflex force can then be calculated as:

$$\tau_{reflex}(t) = r(\theta)F_{perp}(t) \tag{47}$$

$$F_{perp}(t) = \sin(LOA)\,F(t) \tag{48}$$

where $r(\theta)$ is the moment arm of the muscle acting on the limb segment joint and $F_{perp}(t)$ is the component of muscle force perpendicular to the joint, which depends on the Line of Action (LOA) angle of the muscle. The moment arm and LOA are derived from data-driven models found in the literature for each lower limb joint (see **Appendix C.4**). Finally, the joint torque can be input to a torque actuator about the joint to simulate the torque generated by the activated muscle.

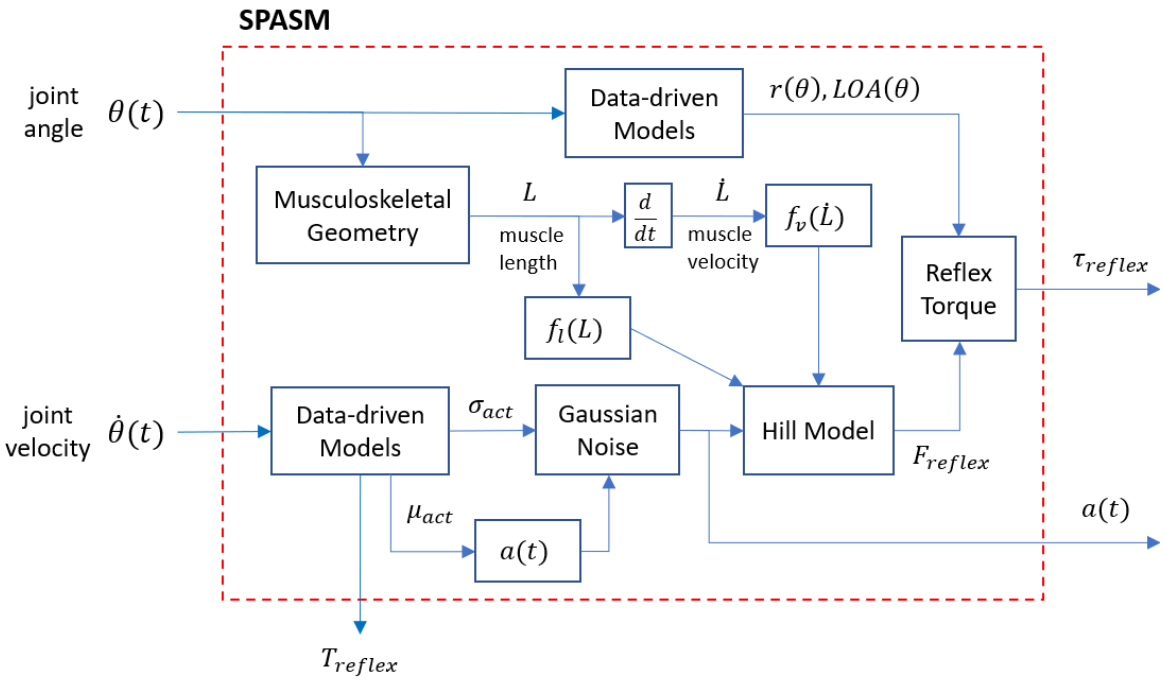

Figure 33. Block diagram of spasticity function for simulations

The models of SRT, spasm duration and activation levels can be derived from real subject data, or manually tuned to represent a theoretical subject with the desired level of spasticity in individual muscles of the knee and ankle joints. The block diagram of dynamic closed-loop spasticity can be seen in **Figure 33**.

4.3.2 Passive-movement knee spasticity test with a virtual examiner

Using the spasticity function, the objective of this section is to simulate a spasticity assessment that might be carried out by a real examiner on a subject with lower-limb spasticity. By achieving a result that reasonably represents such a test, it will provide validation of the spasticity controller. Specifically, the resulting kinematics, activation levels, and torques can be compared to the experimental data that was used to develop and tune the models in the spasticity controller. The algorithm may be adapted for other tests, but for this section the scenario of an examination of spasticity of the right knee flexor muscles will be simulated. The model is laid flat on the ground, with the left knee fully extended and the right hip held at a sagittal angle of 45 degrees. The thigh is locked in this orientation, as the knee is extended by an external actuator acting on the shank in simulation of passive knee flexor stretches to test for spasticity.

The subject's muscles are assumed to be fully relaxed when not in the spastic reflex state. In real individuals with SCI, especially incomplete SCI, the muscles may or may not be completely silent. However, this background activity, in addition to the baseline EMG noise, is negligible in terms of effect on the movement of the limbs that are being manipulated by an examiner, and as previously described the purpose of these algorithms is not to recreate those signals. Therefore,

the assumption is sufficient for the scope of this simulation. For simplicity, only the 'hamstrings' (see **Figure 27**) were considered to be spastic in this simulation.

The structure of the algorithm was built in blocks that each govern a fundamental part of the simulation. These blocks are either part of how the 'examiner agent' or 'subject model' behaves, and they will be referred to as such in this section. For a general passive-movement spasticity test scenario the algorithm flowchart is described in **Figure 34**, which also applies to the knee.

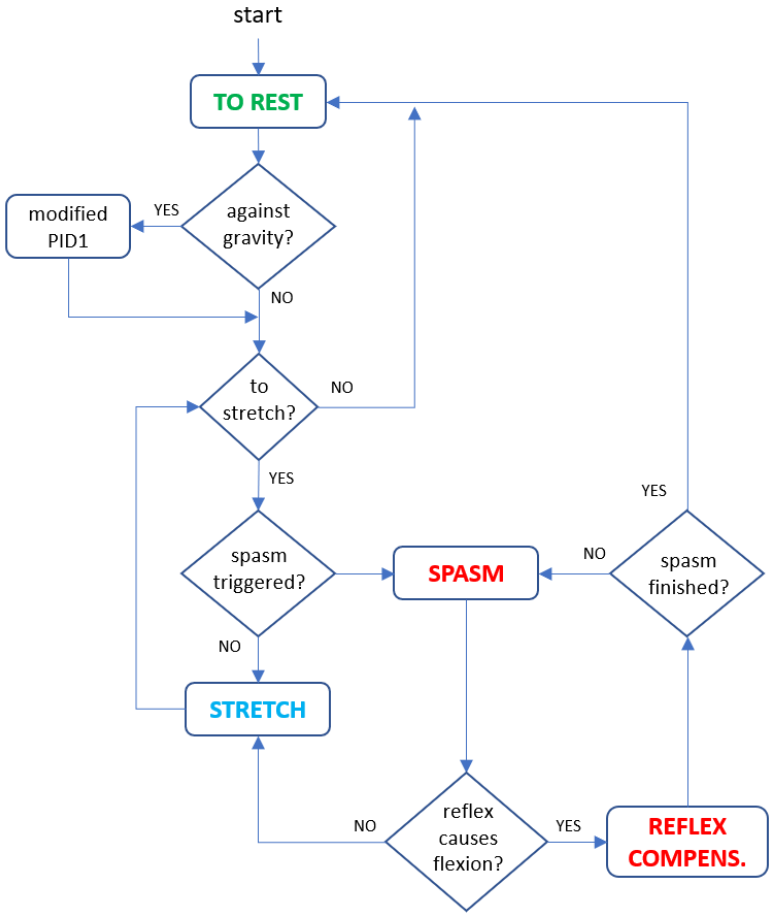

Figure 34. Passive spasticity test algorithm flowchart

The block diagram of the knee test scenario with dynamic closed-loop spasticity can be seen in **Figure 36**. The first block, "Rest", is part of the examiner agent that guides the shank to and maintains it in a resting position (user defined knee joint angle). The knee rest position θ_{rest} is the input to a PID controller which outputs an external torque to be applied about the model's knee joint. The torque about the knee due to gravity on the shank and foot at the rest position is estimated and also applied as the feedforward torque for this PID controller:

$$\tau_{grav} = -g \times [m_{shank} COM_{shank} + m_{foot}(L_{shank} + COM_{foot})] \times \cos(|\theta_{rest} - \theta_{hip}|) \quad (49)$$

where m_{shank} and m_{foot} are the mass of the respective leg segments, COM_{shank} and COM_{foot} are the centre of mass of the respectively leg segments, and L_{shank} are the length of the respective leg segments. Additionally, the PID is modified depending on if the initial direction of motion towards the desired rest position is against or with gravity.

Similar to a real passive-movement spasticity assessment, a protocol including the number of stretching motions and their range and average speed must be established and predefined in the code before execution. When each planned motion is begun, the algorithm creates a target joint trajectory based on the defined conditions to be used by the "Stretch" block. Because the examiner agent represents a human, and not a mechanized setup (see **Section 2.2.1.2** and **2.2.2.3**), the trajectory $\theta_{stretch}(t)$ from the initial position to the end of the stretch is defined as a half cosine function. The trajectory is then simply numerically differentiated to obtain the velocities $\dot{\theta}_{stretch}(t)$ of the planned motion:

$$\theta_{stretch}(t) = \theta_{peak} + \frac{\theta_{peak} - \theta_{rest}}{2}\left[\cos\left(\pi \frac{\dot{\theta}_{avg}}{\theta_{peak} - \theta_{rest}} t\right) + 1\right] \tag{50}$$

$$\dot{\theta}_{stretch}(t) = \frac{d}{dt}\theta_{stretch}(t) \tag{51}$$

where $\dot{\theta}_{avg}$ is the defined average speed, and θ_{peak} is the peak of stretch. The algorithm then utilizes another PID loop that controls for the velocity curve by applying a torque $\tau_{stretch}(t)$ to perform the stretching motion.

During stretching, the spasticity block can be triggered, which will apply a reflexive torque to the joint to simulate a spasm. If during a spasm, the reflex torque is large enough to reverse the initial stretching motion of the muscle into flexion, the "Reflex Compensation" block is enabled in the algorithm (while "Stretch" is disabled). The examiner agent will resist this strong flexion torque by applying a greater external torque than initially anticipated. In effect, the algorithm switches from controlling for the desired stretching joint velocity to a combination of attempting to stay at or above zero velocity (above or positive being in the initial direction of stretch) and at or above the joint position at which the spastic reflex started.

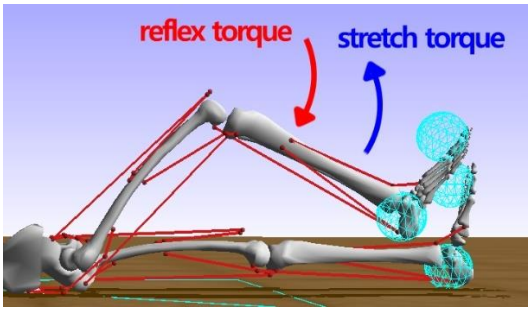

Figure 35. Knee passive spasticity assessment simulation

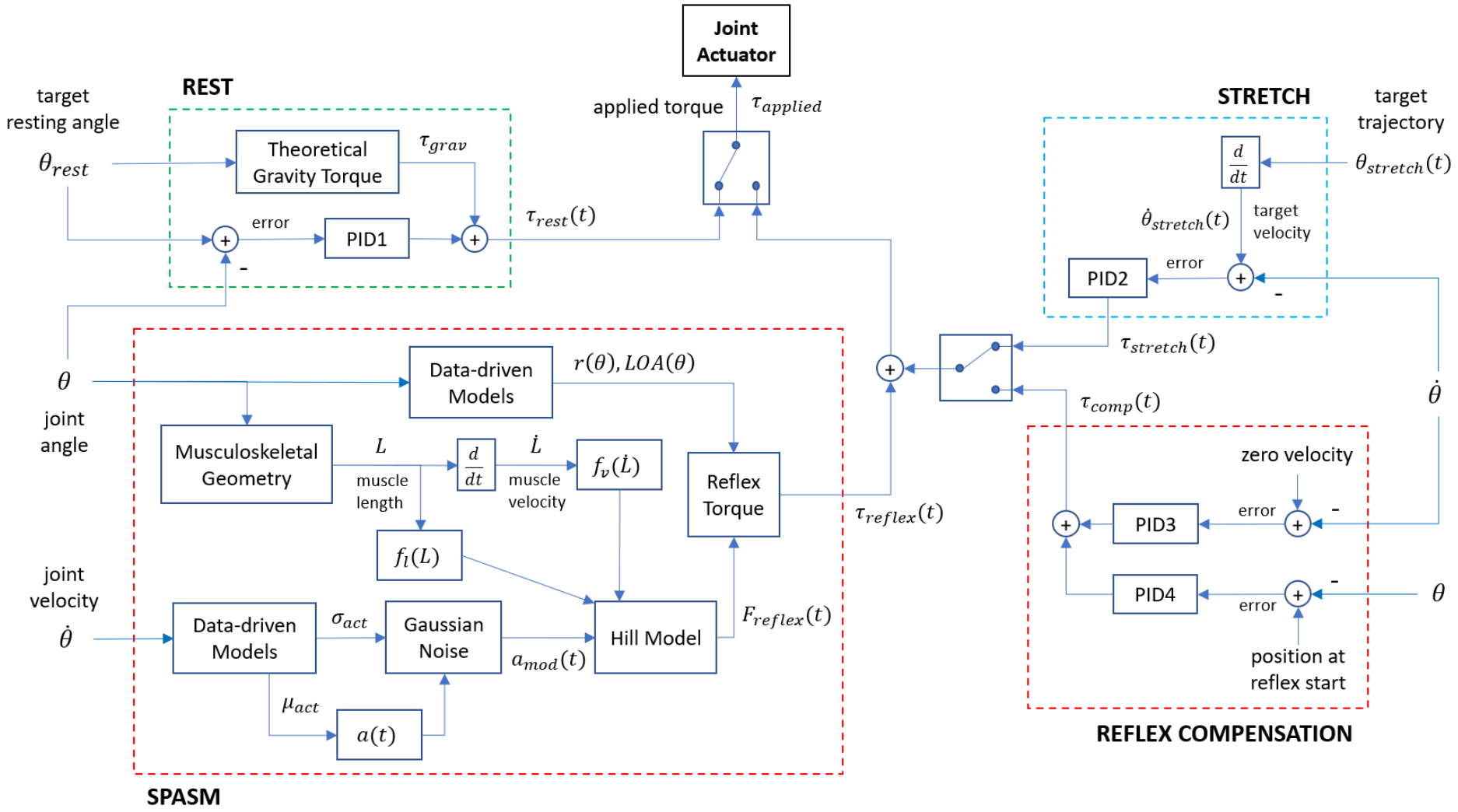

Figure 36. Technical block diagram of passive spasticity test algorithm

This alternative controller comes into effect only after a short delay from when the over-reflex condition is first met to model the neural delay between when an examiner would feel the strong reflex and begin to resist it. A constant 200 *ms* delay is used as the reaction time for the examiner agent, which is an approximate mean of reaction time for the muscles of the hand in non-athletic individuals [148].

If a spasm occurred during a stretching motion, once the spasm abates the examiner does not attempt to complete the prescribed motion, and instead returns to the rest position. If no spasm occurred, the algorithm will also switch to the "Rest" controller to return to the initial position. From there, the simulation can proceed with any more pushing motions as defined by the user.

4.3.3 Reinforcement Learning Walking Agent with Spasticity

The objective is to produce a simulation of the gait of an individual affected by lower-limb spasticity. A walking agent was developed using reinforcement learning, with an agent-environment interaction for learning an optimal control policy by maximizing a reward function. The original agent was able-bodied and trained to be capable of walking on flat ground [149]. Applying the spasticity controller with the outputs of muscle activation levels that override the activations produced by the agent's policy, we can inject spasticity to the model. The controller can be tuned with spasticity parameters from a real subject, and the gait kinematics and parameters of the simulation results can compared to the real subject's gait.

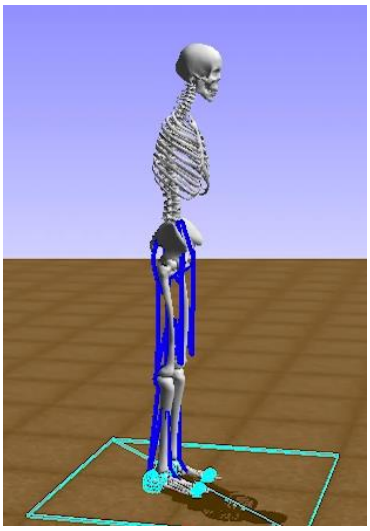

Figure 37. Updated version of OpenSim Model with two smaller contact spheres at the balls of the feet, and reduced stiffness for all spheres

The OpenSim model for this task was an updated version from what was used in the previous sections, where the contact sphere at the balls of the feet were split into two smaller spheres, and all the contact spheres had reduced stiffness values to achieve more realistic interaction with the ground during walking (see **Figure 37**). The spasticity controller was adapted for use in the

Python environment where the reinforcement learning is accomplished and was integrated into the training model and algorithms (see **Statement of Contributions**). The parameters of the spasticity controller were defined to represent a hemiplegic subject with moderate to severe spasticity in the right thigh and shank muscles. The agent must be retrained with these new perturbations introduced to its walking, which will produce a new optimal control policy that results in modified gait.

The original reward function used to train the able-bodied model was modified to allow successful training, where stability was prioritized more while forward velocity and joint velocities were prioritized less when compared to the reward function of the able-bodied agent.

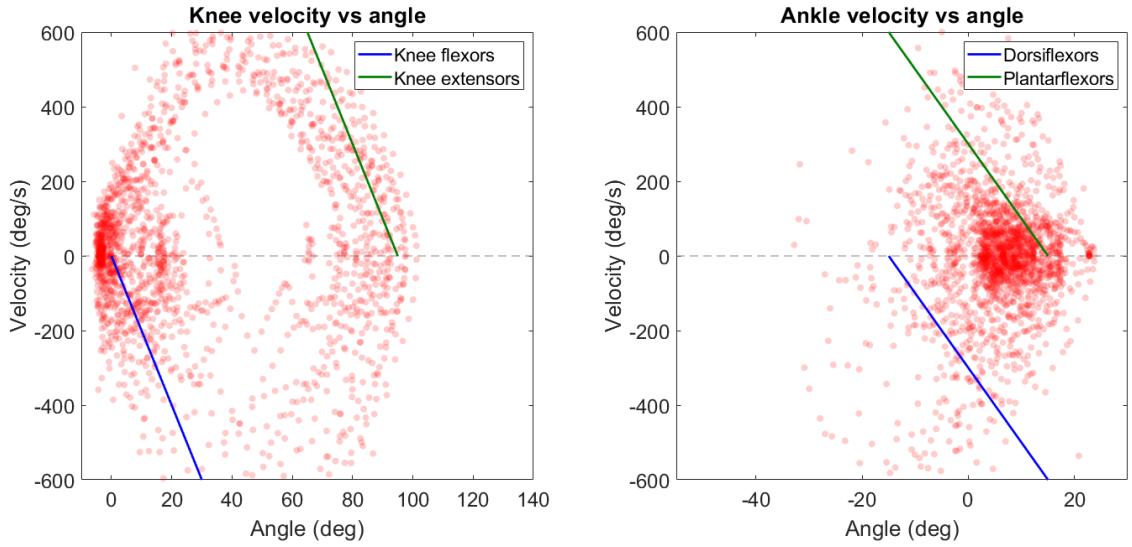

Figure 38. Example muscle group DSRT models for the (a) knee and (b) ankle, overlayed against the distribution of their respective joint velocity versus position data in a 20 second simulation of the healthy walking agent

Both extremely exaggerated spasms and spasms that virtually don't affect the gait would not be realistic nor meaningful results. To restrict the simulations to behaviour that can be expected in a real subject, the spasticity models were plotted against the distributions of joint velocity versus position data from the healthy walking agent (see **Figure 38**). This allows for optimized tuning of the spasticity parameters, while also reducing iterations of modifying the training functions.

4.4 Results and Discussion

4.4.1 Passive Assessment Simulation

The simulation was executed with a variety of input conditions, including the parameters of the muscle TSRT models which represent the severity and sensitivity of spasticity, and the planned stretching motions to be performed by the examiner agent in terms of speeds and ranges

of motion. The subject model is situated as described earlier, where the right leg knee is initially flexed with the heel resting on the simulation environment ground. When the simulation begins, the shank is raised by the examiner to reach the pre-defined rest position of the knee joint (see **Figure 35**).

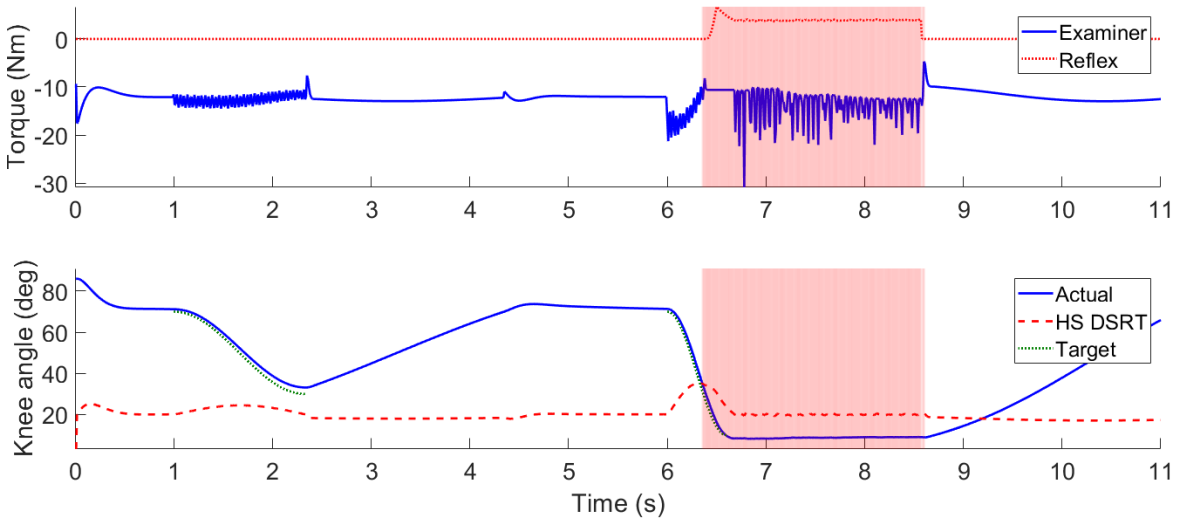

Figure 39. First simulation of two hamstring stretches. (a) Examiner agent and reflex torques, (b) knee joint position, and the DSRT threshold determined by the current joint velocity; if the joint position crosses the DSRT, a spastic reflex is triggered, highlighted in red.

Figure 39 illustrates a set of one slow and one fast stretch of the hamstrings of the human model. The first stretching motion was defined short in range and slow enough so that the joint position did not cross the DSRT and no reflex was triggered. In the second stretch, the desired velocity was set three times faster than the first and up to a range near full knee extension. The resulting spastic reflex was triggered and persisted as defined using the models in **Section 4.3.1**. The examiner agent eventually reacts and holds it at a relatively stable position.

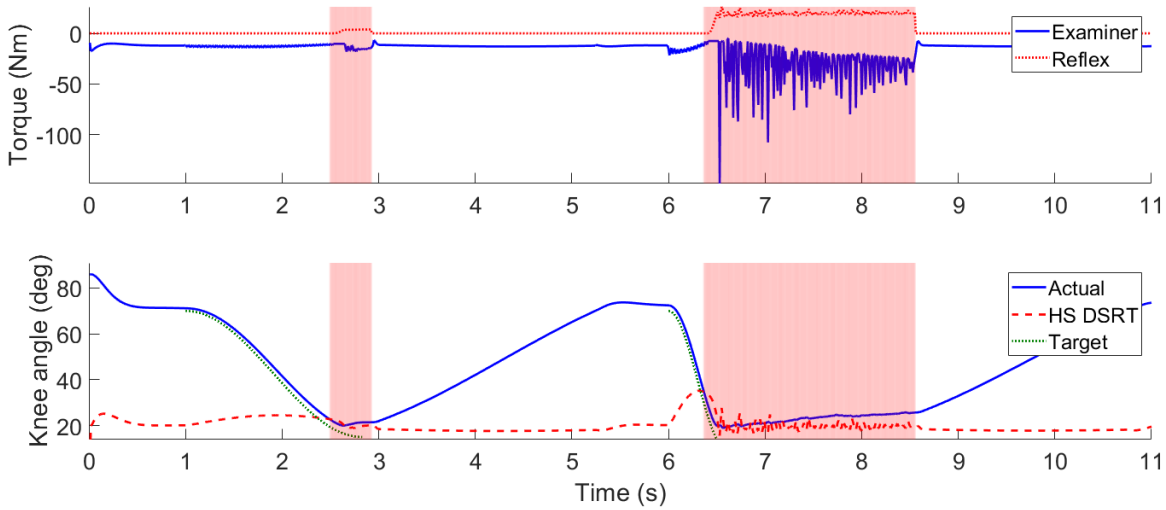

Figure 40. Second simulation with farther range for the slow stretch, and stronger reflexes.

Figure 40 shows a second set of stretches, where the range for the slow stretch was extended, and the constant for the muscle activation model was increased. The slow stretch triggered a relatively minor reflex near the end of the motion, which was short in duration but prevented reaching the target range of motion (15 *deg*). The fast stretch was defined the same as the first set, however the modified activation model produces a much stronger reflex torque which also limited the effective range of motion. The transient behaviour is also more erratic as the examiner agent attempts to prevent it and control the joint, and the opposing torques result in tremor-like motion.

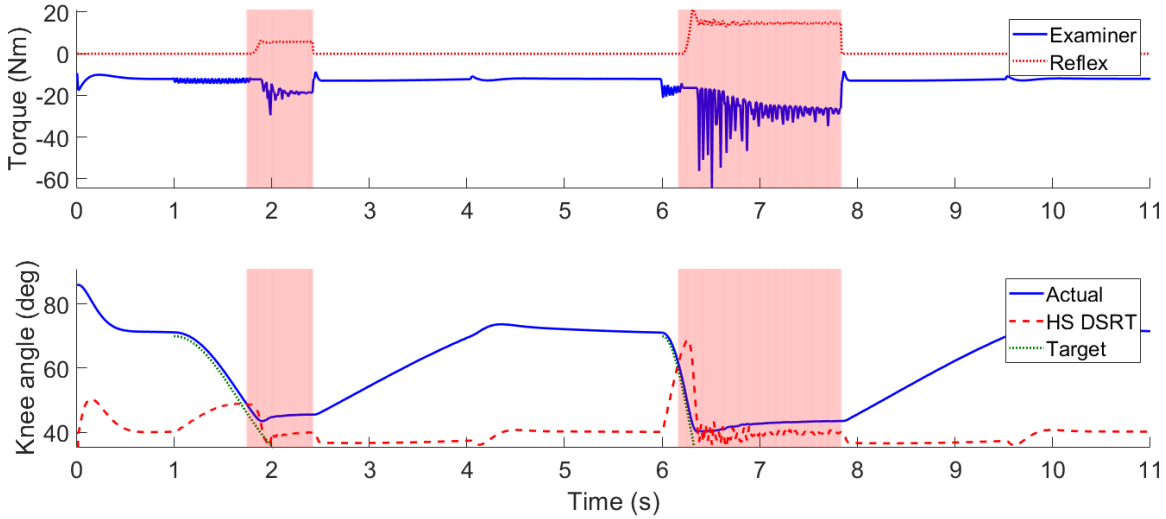

Figure 41. Simulation 3; similar to the first simulation with more severe spasticity parameters.

A third simulation is depicted in **Figure 41**, where the defined stretches and activation model are the same as the first simulation, but the SRT model parameters were increased to represent a greater severity of spasticity. For both slow and fast stretches, the DSRT threshold is crossed and the reflexes are triggered much earlier during the stretches, limiting the effective range of motion. Additionally, when compared to the second simulation the slow stretch resulted in a reflex of higher duration. In the second simulation, the reflex is triggered only near the peak when the examiner agent has already slowed down, but in the third the reflex is triggered in the middle of the motion, at peak velocity. The duration of reflexes is dependent on the triggering velocity, and results in the difference in reflex behaviour. By this same reason there is virtually no difference in reflex duration for the fast stretch for all three simulations.

The change from the first to second or third simulations can illustrate how the regime of kinematics is limited by the spasticity in a muscle, as well as show the further limiting effect of stronger spastic reflexes on joint motion. These simulations can also demonstrate the effects of differing degrees spasticity severity from subject to subject in terms of the TSRT and sensitivity to velocity, and how they affect the possible joint motion as well as spastic reflexes.

4.4.2 Walking Agent

Initially, a simulation of the healthy agent was recorded in order to compare against the results of simulating the spastic walking agent. **Figure 42** depicts the joint trajectories in a 20 second simulation of where the agent successfully walks in a manner resembling natural gait.

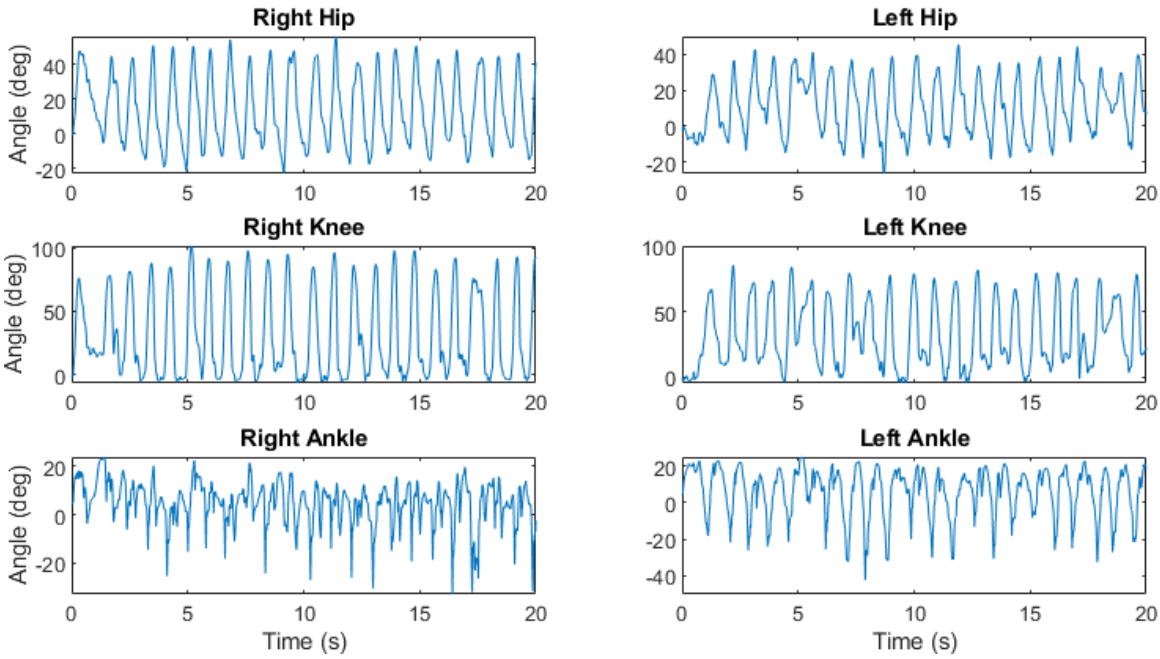

Figure 42. Joint trajectories of healthy walking agent

The spasticity controller was incorporated into the walking agent in the original Python environment, and the parameters were tuned to represent severe spasticity in the right leg based on the results of modeling in **Chapter 3** as well as other examples in literature (see **Section 2.2.2.3**). The TSRT and μ of each muscle model was set to cover approximately two-thirds of the relevant kinematic space of the healthy agent's data, which was expected to result in frequent triggering of spastic reflexes. The coefficients of the reflex activation and duration models were also tuned to result in strong reflexes that will perturb the right leg's motion to a high degree. **Figure 43** depicts the joint trajectories of a simulation of this "max" spasticity walking agent.

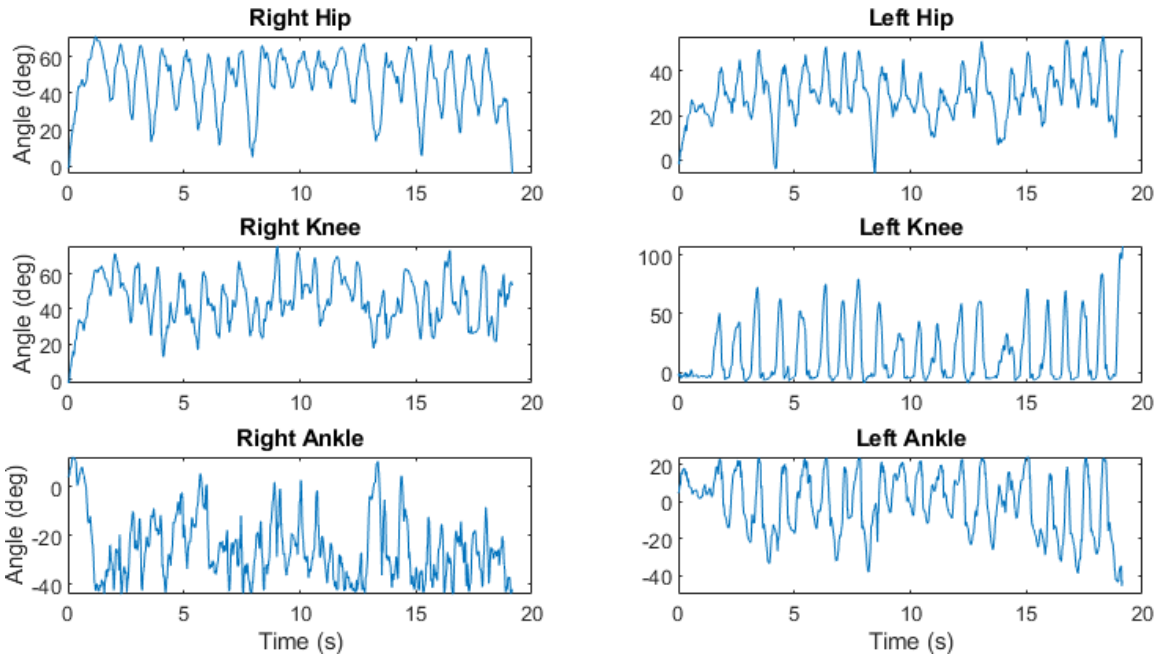

Figure 43. Joint trajectories of walking agent with severe spastic "max" parameters

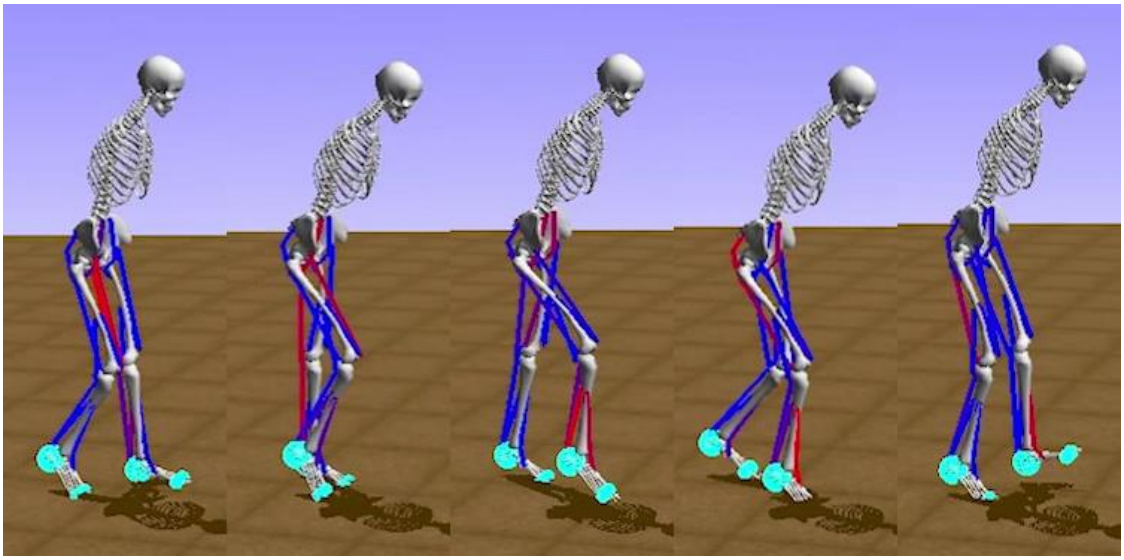

Figure 44. Example of plantarflexion at end of right leg swing, continued on toes during stance; blue indicates inactive muscles, bright red indicates fully activated muscles

The right ankle remained heavily plantarflexed through most of the gait, between 20 and 40 degrees of plantarflexion. **Figure 45** illustrates an example of this toe-walking for the right leg, where the plantarflexors are triggered and activated by onset during the swing phase, leading to a toe-strike and continuation of stance in this position. The knee range of motion (approximately 20 to 65 degrees flexion) is also limited in comparison to healthy gait where the knee is freely actuated between 100 degrees flexion and full extension. This is due to the spastic reflexes of both knee flexors and extensors that effectively cause a form of stiffness in the joint. The right hip trajectory is consequently shifted upwards to more flexion on average, to provide clearance for

the right foot during swing, due to the insufficient knee flexion and plantarflexion of the ankle. **Figure 45** depicts the SRT models used against the resulting kinematic data of this severe spasticity walking simulation.

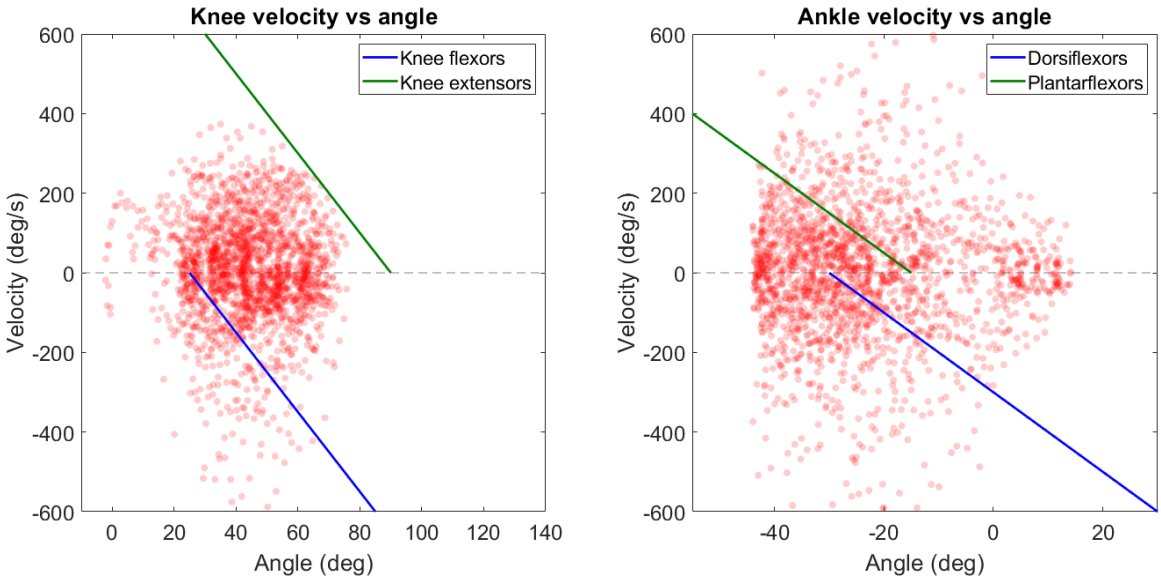

Figure 45. "Max" spasticity parameters against the resulting kinematic data

For the third type of simulations, the SRT model parameters as well as the activation and duration constants were tuned to reduce the severity of spasticity in terms of range of motion, sensitivity to velocity, and strength and time of the reflexes. This moderately affected walking agent is referred to as "50%" spasticity for the purposes of this chapter. By the resulting joint trajectories shown in **Figure 46** or the plot of SRT models and kinematic space data (**Figure 47**), it is difficult to determine the difference in gait when compared to the healthy agent.

The subsequent step is therefore gait analysis, which is necessary to further investigate the differences between the three walking agents and their simulations. Basic spatio-temporal parameters used in gait analysis are gait speed, step length and step frequency [150] . Other commonly used parameters include step duration, stride length and duration. [151]. Using the vertical position data of the calcaneus bones of the OpenSim model, we can approximate the heel strikes of each foot during the different gait conditions. From there it is straightforward to the determine the distance and time between heel strikes of the same foot (strides), and the distance and time between consecutive heel strikes of either foot (steps). The gait speed can simply be determined by the distance and time between the first and last heel strike of the simulation.

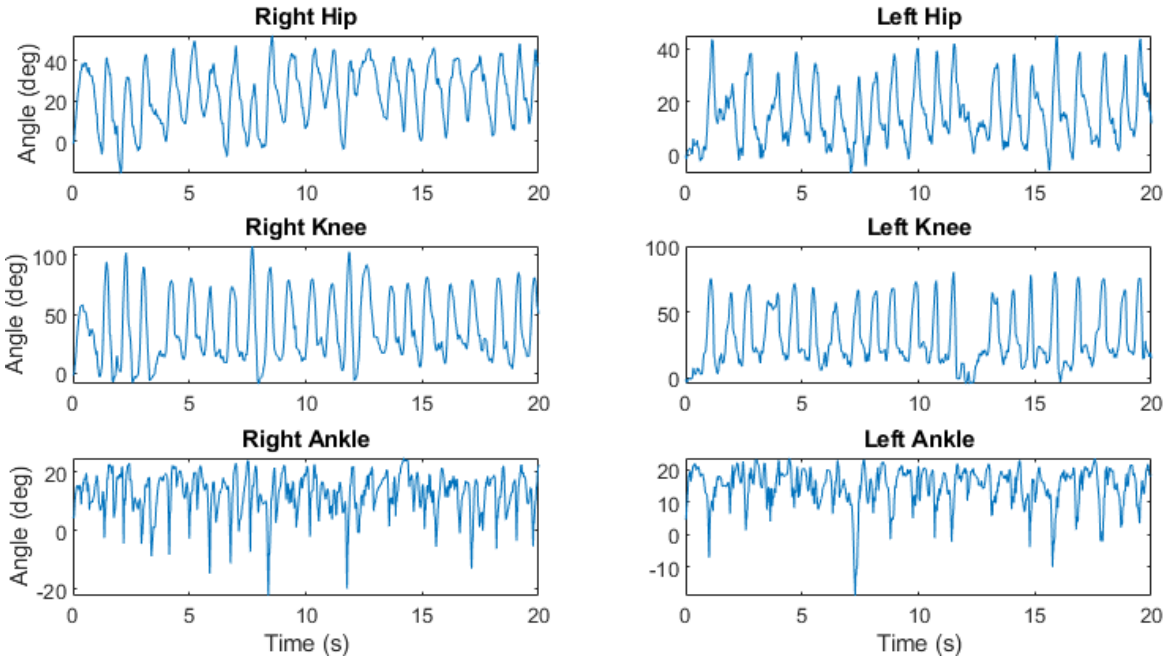

Figure 46. Joint trajectories of walking agent with less spastic "50%" parameters

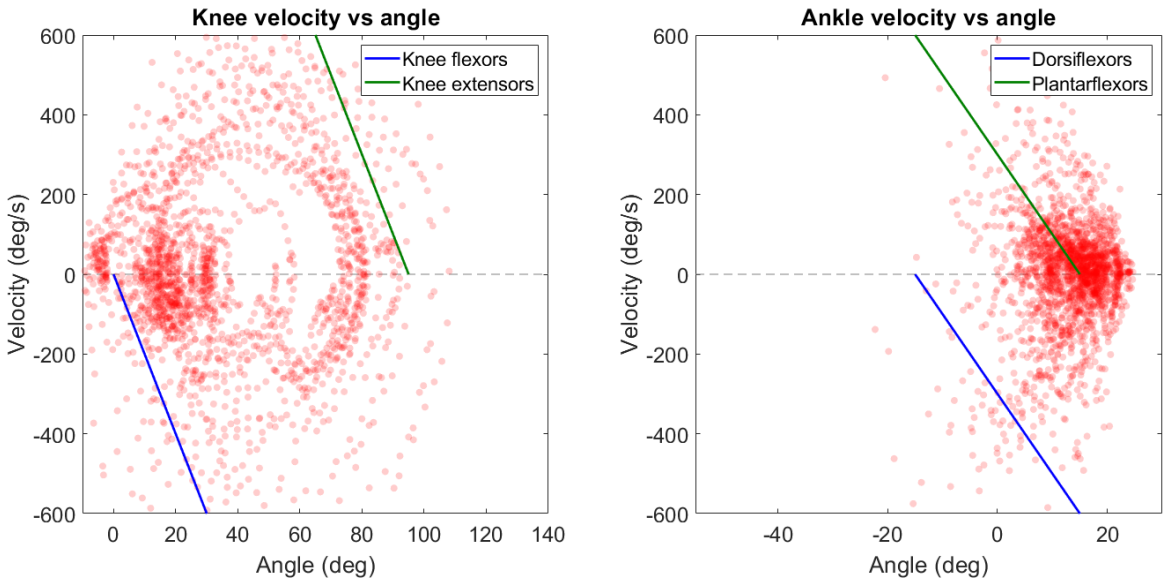

Figure 47. "50%" spasticity parameters against resulting kinematic data

Table 12. Healthy and spastic walking agent gait speeds

Walking Agent Condition	Healthy	"Max" Spasticity	"50%" Spasticity
Gait Speed (m/s)	1.235	0.8722	0.7017
Gait Distance (m)	23.75	15.92	13.39

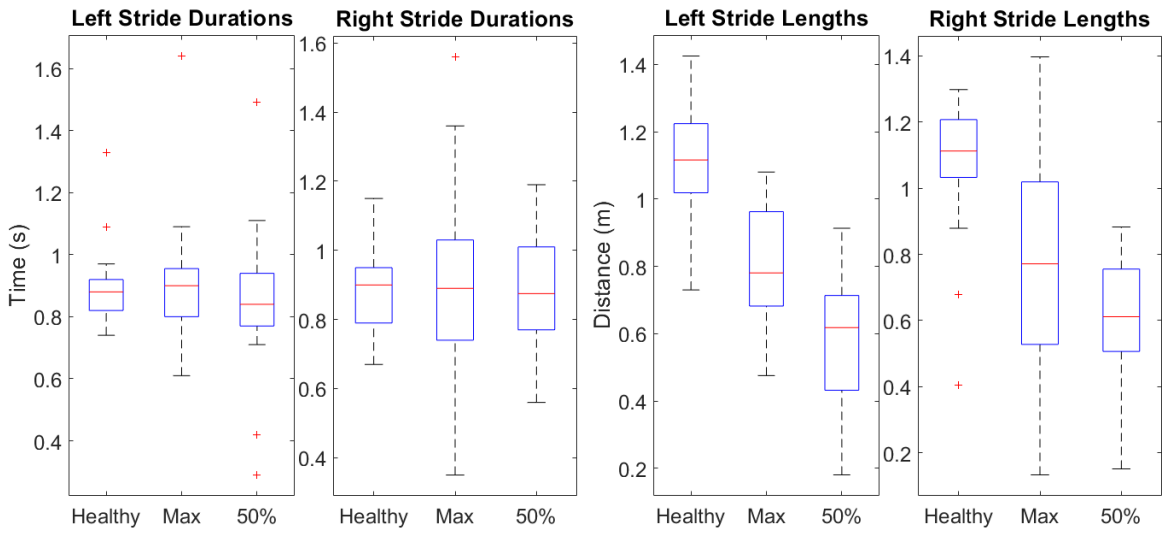

Figure 48. Stride duration and length parameters for the different walking agents

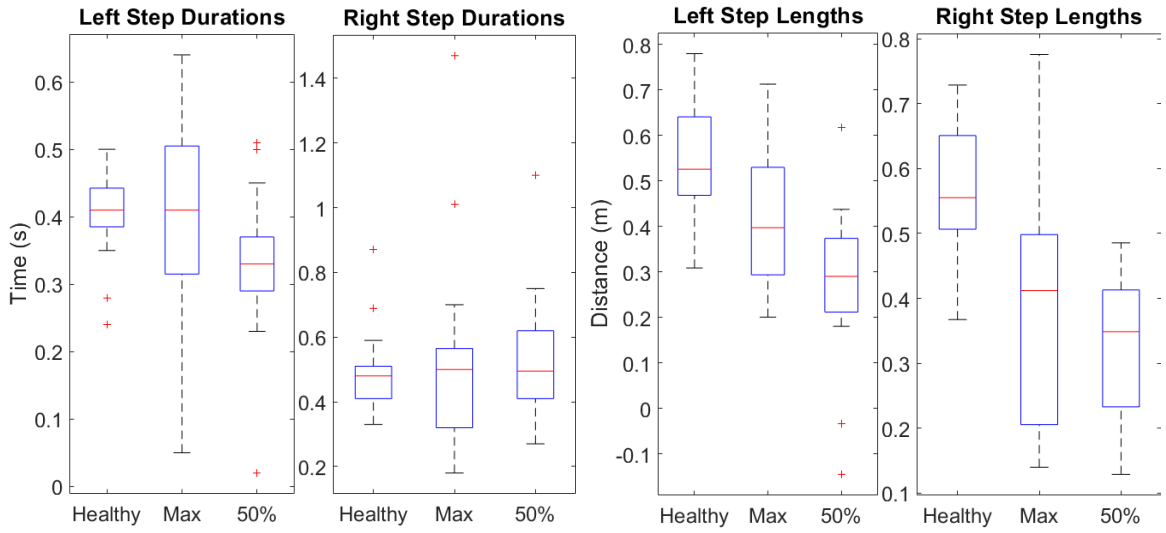

Figure 49. Step duration and length parameters for the different walking agents

The gait speed was found to be noticeably reduced in both spastic agents when compared to the healthy agent. **Figure 48** and **Figure 49** show the boxplots of the stride and step durations and lengths for both legs, comparing the data for healthy, “max” and “50%” in each parameter. One-way ANOVA was performed to determine if the means of the three groups for each gait parameter are significantly different. Post-hoc analysis was conducted using paired t-tests with a Bonferonni adjusted significance level of $\alpha = 0.0167$. Conventionally, step length and duration are single parameters for gait, but due to the right leg being impaired by spasticity and expected to behave differently, the left and right step parameters were separated.

Table 13. Post-hoc analysis of gait parameters between groups

Gait Parameter		ANOVA *p-value*		Post-hoc Test	T-test *p-value*	
		Left	Right		Left	Right
Stride	Durations	N.S	N.S	Healthy vs Max	N.S	N.S
				Healthy vs 50%	N.S	N.S
				Max vs 50%	N.S	N.S
	Lengths	< 0.001	< 0.001	Healthy vs Max	< 0.001	< 0.001
				Healthy vs 50%	< 0.001	< 0.001
				Max vs 50%	N.S	N.S
Step	Durations	< 0.05	N.S	Healthy vs Max	N.S	N.S
				Healthy vs 50%	< 0.0167	N.S
				Max vs 50%	N.S	N.S
	Lengths	< 0.001	< 0.001	Healthy vs Max	< 0.0167	< 0.0167
				Healthy vs 50%	< 0.001	< 0.001
				Max vs 50%	< 0.0167	N.S

N.S. = Not Significant (p > 0.05 for ANOVAs, p >0.0167 for Post-Hoc)

The statistical analyses show that there are significant differences between the different conditions of the walking agents in terms of stride and step lengths, for both left and right legs, but not for durations of either parameter. Post-hoc analysis showed significant differences ($p < 0.001$) for the stride and step lengths between the healthy agent and either "max" and "50%" spastic conditions. Though not indicated by the statistics, the 50% simulation did exhibit more consistently short stride or step lengths than the "max" walking agent (see **Figure 50**), which varied between short and 'normal' stride or step lengths, evidenced by the larger distributions in the boxplots (also see **Figure 51**).

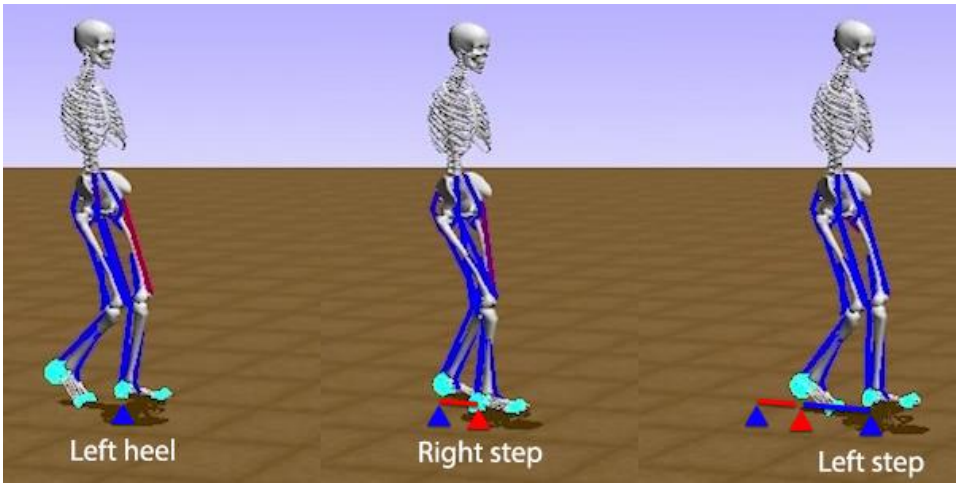

Figure 50. Example of short steps in "50%" spasticity simulation

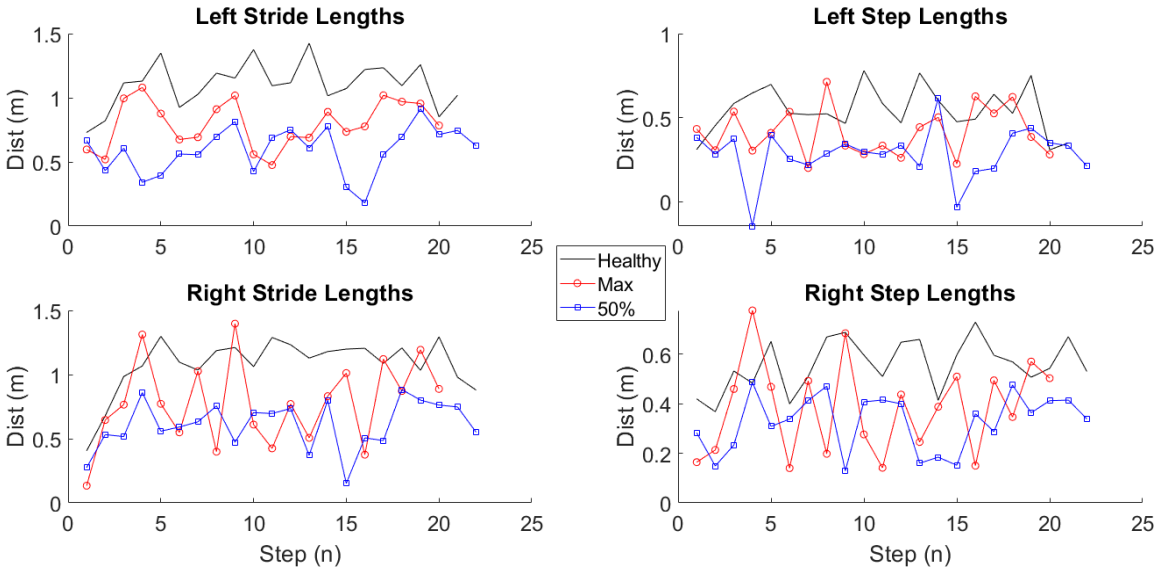

Figure 51. Step duration and length parameters for the different walking agents

Figure 49 indicated a possible trend towards shorter right step durations and step lengths within walking agents, where the different step lengths is also briefly illustrated by **Figure 50**. However, the only significant differences ($p < 0.0167$) were found between the left and right step durations for the healthy and "50%" agents.

The simulations of the healthy and impaired walking demonstrated the potential effects of spastic reflexes on gait. The consequences include restricted ranges of motion, effective stiffness in the affected joints, both which can lead to suboptimal compensations in the unaffected joints, i.e. the unaffected hip and left leg. The spatio-temporal parameters of gait can also be affected, reducing gait speed, step length and stride length. The short steps, or shuffle gait can be expected to be seen in impaired or injured gait, as well as specific conditions such as Parkinsons [152]. In real spastic hemiparetic gait, the spasticity causes difficulty in flexing the hip and knee and dorsiflexing the ankle [153]. The simulations utilized those same consequences through the implementation of the spasticity controller to affect the agent, resulting in reasonably realistic impaired gait. Therefore, the simulations of spasticity-affected gait demonstrate the validity and potential of the novel spasticity controller, especially as part of a larger, more comprehensive controller that encompasses all the neuro- and biomechanical impairments of conditions that involve spasticity, such as post-stroke, cerebral palsy or spinal cord injury.

4.5 Limitations and Future Research

To properly validate the spasticity controller, as well as the passive movement assessment simulation, instead of tuning the parameters for a hypothetical subject, the parameters of real subjects should be applied. The resulting kinematics, activation levels and interaction torques in the simulations can then be compared to the actual data from the subjects in terms of the range of values, trends and patterns in the signals. Similarly, the walking simulations should be performed using real subject parameters, followed by comparing the results to the gait data that is recorded in addition to the passive movement experiments to obtain the subjects' spasticity parameters, in terms of the actual kinematic trajectories, as well as the gait parameters. With good agreement between the simulations and the real data for a sufficient number of subjects, the spasticity controller and simulations would be validated. The degree of validation would be limited for the passive movement assessment however, as the spastic subject and examiner interact in the simulation and thus cannot be verified separately, only as lump results in comparison to the real passive movement examinations.

The passive movement assessment simulations used various assumptions for the behaviour of the examiner agent, based on observations and references from the data used to develop the spasticity models and controller. One major assumption was the resistance of the examiner in response to reflexes strong enough to overcome the initial stretching directions of the assessment scenario. The opposition of the examiner agent and spastic reflex resulted in tremor-like or oscillatory behaviour, which was similar to the kinematics observed in the data. However, as detailed in **Section 3.5.2.1**, the joint oscillations are likely due to clonus in the subjects. Observations from more data would be required to better understand the behaviour during the reflex due to passive motion by comparing of subjects with and without clonus.

As described previously, spasticity can inhibit the flexion of the hip and knee as well as dorsiflexion of the ankle. As a consequence, the stiff leg is characteristically swung medially from the body to avoid dragging of the foot, while the upper body leans in the opposite direction for balance [153]. The current walking agent and model are restricted to purely sagittal planar motion, where the legs can only move in the "X" and "Y" directions. This limitation especially affected the "max" condition simulation, which resorted to toe walking of the right foot and exaggerated hip flexion to achieve clearance. While toe-walking is seen in cerebral palsy as well as autism [154], [155], it is not necessarily associated with spasticity. Future research should incorporate motion in the third dimension, to account for the circular swing that is characteristic of stiff gait, as well as a musculoskeletal model that includes muscles to cause other motions such as inversion and eversion of the joints, which would also have to be included in the spasticity controller's models.

Other considerations for these simulations are continuations from the discussion of the spasticity modeling. Future research should include modeling of the angular shifting of the SRT models biarticular muscles by the proximal joints, transformation of the SRT model by the dynamics of volitional motion and muscle activation, as well as the dependence on the initial muscle length at the beginning of stretch, and forces imparted on and sensed by the muscles (see **Section 3.5.2**). Dynamically changing the SRT models by these additional relationships of spasticity with musculoskeletal and neuromechanical variables would add further depth and validity to the spasticity controller and simulations that include it, which could also lead to more comprehensive analysis of the results.

The existence of clonus in a subject is another possible confounding variable for the models that were used in building the spasticity controller. Specifically, the modeling of spastic activation levels and reflex durations may be affected by the presence of clonus in S01 (see **Section 3.5.3**). Once the interaction and relationship with spasticity is understood and modelled, clonus could be integrated into the spasticity controller, with a toggle that can enable or disable clonus behaviour depending on the subject or scenario being simulated.

Chapter 5:

Conclusion

The fundamental purpose of this thesis was the objective modeling of spasticity, to both better understand and characterize the symptom and the underlying mechanisms, which would improve the evaluation and follow-up for treatments and rehabilitation options. The primary objectives established for this purpose were to 1) develop wearable instrumentation and algorithms for accurate and reliable data collection and processing, and validate them, 2) develop and perform experiments involving passive movement spasticity assessments, and 3) model the resulting data and extract measures to characterize spasticity as alternatives to subjective clinical scores.

Prior to these objectives, a thorough understanding of spasticity and the state of the art for its modeling was established through a comprehensive literature review. It was concluded that threshold control theory-based models can be used for objective methods of assessing spasticity due to their inclusion of the key differentiating characteristic of spasticity from other similar symptoms, and advantages of practicality and agreement with current clinical practice.

An experimental protocol was established, using sEMG sensors, IMUs to collect muscle activity and kinematic data respectively, and brace-handle setups with integrated force sensors to passively move the subject's lower limbs while measuring the interaction forces. Algorithms were developed for the identification of spastic reflexes in the EMG data, and extraction of joint kinematics from the IMU data, validated against a motion capture system. The onsets of spastic reflexes were used to determine the kinematic conditions that trigger spasticity, which were then used to create muscle specific SRT models of spasticity. The models of a muscle group could then be combined into a novel measure or objective score of spasticity to characterize its severity. Therefore, the results satisfied the first three objectives of this thesis. Due to the COVID-19 situation, in-vivo studies were not possible leading to a limited scope of available data for spasticity modeling. This restricted the possible validation of the methodology and results.

However, the neuromuscular simulations in **Chapter 4** succeeded in providing an additional level of validation for the conclusions of the proceeding chapter. A spasticity controller was developed for use in simulations, using the previously developed models with additional modeling for generating spastic reflexes. The parameters of these models could be tuned to modify the spasticity controller for simulations of subjects with differing levels of spasticity. The controller was first used in a simulation of a passive movement assessment like the experiments in **Chapter 3**, demonstrating the validity and effects of the controller by recreating the fundamental scenario that the controller is based on. The spasticity controller was secondly integrated into a

reinforcement-learning walking agent, to simulate the walking of an individual with hemiplegic spasticity by retraining the agent to learn to walk with spasticity. The gait trajectories and parameters were compared for the healthy agent against severe and moderately affected versions of the spastic walking agent. In the impaired agents, gait speeds were reduced, and step and stride lengths were shortened, demonstrating the negative effects of spasticity on walking and providing further validation of the spasticity controller and the underlying modeling.

The methodology and findings in **Chapter 3** and **Chapter 4** share many of their limitations. The spasticity models were developed without the inclusion of antagonistic muscles, which limit the findings in the scope of the presented novel measures. Opposing muscles are also likely involved in clonus, a commonly related but separate symptom to spasticity which needs to be modeled in its interaction with and possible effect on spastic behaviour. Other factors that have been found to affect the thresholding-based modeling should be incorporated in future research, including volitional muscle activations, initial muscle stretch levels (which are further modified in biarticular muscles), and forces on muscles. Additionally, as discussed in **Chapter 2** the detailed neural and electrophysiological mechanisms should also be modeled for a more complete model of spasticity.

There was a demonstrated need to develop a system to provide accurate and reliable modeling of spasticity, and an objective measure to better assess the condition. The thesis provides a preliminary step towards that goal by showing results that clearly indicate the presented methodology merits further exploration. The presented novel measure of spasticity has the advantages of objectivity, reliability and accuracy, which will potentially improve related clinical practices such as treatment and rehabilitation. The modeling of spasticity could be applied in other ways; for example, the spasticity controller could also be applied in real life scenarios, such as an exoskeleton worn by a spastic subject to prevent regimes of motion that trigger their spasticity which can be both painful and debilitating to everyday function such as walking, or a healthy subject in order to demonstrate the effects of having spasticity. This could be utilized in daily life, or the rehabilitation exercises where exoskeletons are more necessary, such as for individuals with SCI. In conclusion, the work presented in this thesis holds the potential of further the understanding of spasticity, and improving the quality of life of the numerous individuals affected by spasticity.

References

[1] Y. Cha and A. Arami, “Quantitative Modeling of Spasticity for Clinical Assessment, Treatment and Rehabilitation,” *Sensors*, vol. 20, no. 18, Art. no. 18, Sep. 2020, doi: 10.3390/s20185046.

[2] A. A. Mullick, N. K. Musampa, A. G. Feldman, and M. F. Levin, “Stretch reflex spatial threshold measure discriminates between spasticity and rigidity,” *Clin. Neurophysiol.*, vol. 124, no. 4, pp. 740–751, Apr. 2013, doi: 10.1016/j.clinph.2012.10.008.

[3] P. P. Urban *et al.*, “Occurence and Clinical Predictors of Spasticity After Ischemic Stroke,” *Stroke*, vol. 41, no. 9, pp. 2016–2020, Sep. 2010, doi: 10.1161/STROKEAHA.110.581991.

[4] C. Oreja-Guevara, D. González-Segura, and C. Vila, “Spasticity in multiple sclerosis: results of a patient survey,” *Int. J. Neurosci.*, vol. 123, no. 6, pp. 400–408, Apr. 2013, doi: 10.3109/00207454.2012.762364.

[5] N. Sezer, “Chronic complications of spinal cord injury,” *World J. Orthop.*, vol. 6, no. 1, p. 24, 2015, doi: 10.5312/wjo.v6.i1.24.

[6] N. J. O’Dwyer, L. Ada, and P. D. Neilson, “Spasticity and muscle contracture following stroke,” *Brain*, vol. 119, no. 5, pp. 1737–1749, 1996, doi: 10.1093/brain/119.5.1737.

[7] S. Malhotra, A. Pandyan, C. Day, P. Jones, and H. Hermens, “Spasticity, an impairment that is poorly defined and poorly measured,” *Clin. Rehabil.*, vol. 23, no. 7, pp. 651–658, Jul. 2009, doi: 10.1177/0269215508101747.

[8] J. W. Lance, “The control of muscle tone, reflexes, and movement: Robert Wartenbeg Lecture,” *Neurology*, vol. 30, no. 12, pp. 1303–1303, Dec. 1980, doi: 10.1212/WNL.30.12.1303.

[9] J. W. Lance, “Symposium synopsis,” in *Spasticity, disordered motor control*, R. G. Feldman, R. R. Young, and W. P. Koella, Eds. Chicago, US, 1980, pp. 485–494.

[10] J. Jankovic, “Parkinson’s disease: clinical features and diagnosis,” *J. Neurol. Neurosurg. Psychiatry*, vol. 79, no. 4, pp. 368–376, Apr. 2008, doi: 10.1136/jnnp.2007.131045.

[11] T. E. Twitchell, “The restoration of motor function following hemiplegia in man,” *Brain*, vol. 74, no. 4, pp. 443–480, 1951, doi: 10.1093/brain/74.4.443.

[12] S. Brunnstrom, *Movement Therapy in Hemiplegia: A Neurophysiological Approach*. Medical Department, Harper & Row, 1970.

[13] J. P. A. Dewald, P. S. Pope, J. D. Given, T. S. Buchanan, and W. Z. Rymer, “Abnormal muscle coactivation patterns during isometric torque generation at the elbow and shoulder in hemiparetic subjects,” *Brain*, vol. 118, no. 2, pp. 495–510, 1995, doi: 10.1093/brain/118.2.495.

[14] A. Pandyan *et al.*, “Spasticity: Clinical perceptions, neurological realities and meaningful measurement,” *Disabil. Rehabil.*, vol. 27, no. 1–2, pp. 2–6, Jan. 2005, doi: 10.1080/09638280400014576.

[15] N. Smania *et al.*, “Rehabilitation procedures in the management of spasticity,” *Eur. J. Phys. Rehabil. Med.*, vol. 46, no. 3, p. 16, 2010.

[16] J. Jacinto, P. Varriale, E. Pain, A. Lysandropoulos, and A. Esquenazi, “Patient Perspectives on the Therapeutic Profile of Botulinum Neurotoxin Type A in Spasticity,” *Front. Neurol.*, vol. 11, p. 388, May 2020, doi: 10.3389/fneur.2020.00388.

[17] A. Harb and S. Kishner, “Modified Ashworth Scale,” in *StatPearls*, Treasure Island (FL): StatPearls Publishing, 2020. Accessed: Jul. 11, 2020. [Online]. Available: http://www.ncbi.nlm.nih.gov/books/NBK554572/

[18] C. U. Persson, L. Holmegaard, P. Redfors, C. Jern, C. Blomstrand, and K. Jood, “Increased muscle tone and contracture late after ischemic stroke,” *Brain Behav.*, vol. 10, no. 2, p. e01509, Feb. 2020, doi: 10.1002/brb3.1509.

[19] A. D. Pandyan, G. R. Johnson, C. I. M. Price, R. H. Curless, M. P. Barnes, and H. Rodgers, “A review of the properties and limitations of the Ashworth and modified Ashworth Scales as measures of spasticity,” *Clin. Rehabil.*, vol. 13, no. 5, pp. 373–383, Oct. 1999, doi: 10.1191/026921599677595404.

[20] A. G. Feldman, V. Goussev, A. Sangole, and M. F. Levin, “Threshold position control and the principle of minimal interaction in motor actions,” in *Progress in Brain Research*, vol. 165, Elsevier, 2007, pp. 267–281. doi: 10.1016/S0079-6123(06)65017-6.

[21] A. D. Pandyan, P. Vuadens, F. M. van Wijck, S. Stark, G. R. Johnson, and M. P. Barnes, “Are we underestimating the clinical efficacy of botulinum toxin (type A)? Quantifying changes in spasticity, strength and upper limb function after injections of Botox® to the elbow flexors in a unilateral stroke population,” *Clin. Rehabil.*, vol. 16, no. 6, pp. 654–660, Sep. 2002, doi: 10.1191/0269215502cr536oa.

[22] R. W. Bohannon and M. B. Smith, “Interrater Reliability of a Modified Ashworth Scale of Muscle Spasticity,” *Phys. Ther.*, vol. 67, no. 2, pp. 206–207, Feb. 1987, doi: 10.1093/ptj/67.2.206.

[23] J. M. Gregson, M. J. Leathley, A. P. Moore, T. L. Smith, A. K. Sharma, and C. L. Watkins, “Reliability of measurements of muscle tone and muscle power in stroke patients,” vol. 29, no. 3, p. 6, 2000.

[24] M. Blackburn, P. van Vliet, and S. P. Mockett, “Reliability of Measurements Obtained With the Modified Ashworth Scale in the Lower Extremities of People With Stroke,” *Phys. Ther.*, vol. 82, no. 1, pp. 25–34, Jan. 2002, doi: 10.1093/ptj/82.1.25.

[25] W. Vattanasilp, “Contribution of thixotropy, spasticity, and contracture to ankle stiffness after stroke,” *J. Neurol. Neurosurg. Psychiatry*, vol. 69, no. 1, pp. 34–39, Jul. 2000, doi: 10.1136/jnnp.69.1.34.

[26] M. Wallen, S. J. O’Flaherty, and M.-C. A. Waugh, “Functional Outcomes of Intramuscular Botulinum Toxin Type A and Occupational Therapy in the Upper Limbs of Children With Cerebral Palsy: A Randomized Controlled Trial,” *Arch. Phys. Med. Rehabil.*, vol. 88, no. 1, pp. 1–10, Jan. 2007, doi: 10.1016/j.apmr.2006.10.017.

[27] P. Filipetti and P. Decq, “Interest of anesthetic blocks for assessment of the spastic patient. A series of 815 motor blocks,” *Neurochirurgie.*, vol. 49, no. 2-3 Pt 2, pp. 226–238, May 2003.

[28] A. B. Haugh, A. D. Pandyan, and G. R. Johnson, “A systematic review of the Tardieu Scale for the measurement of spasticity,” *Disabil. Rehabil.*, vol. 28, no. 15, pp. 899–907, Jan. 2006, doi: 10.1080/09638280500404305.

[29] M. B. I. Reaz, M. S. Hussain, and F. Mohd-Yasin, “Techniques of EMG signal analysis: detection, processing, classification and applications,” *Biol. Proced. Online*, vol. 8, no. 1, pp. 11–35, Dec. 2006, doi: 10.1251/bpo115.

[30] R. Merletti, A. Rainoldi, and D. Farina, “Surface Electromyography for Noninvasive Characterization of Muscle,” *Exerc. Sport Sci. Rev.*, vol. 29, no. 1, pp. 20–25, Jan. 2001, doi: 10.1097/00003677-200101000-00005.

[31] D. Staudenmann, I. Kingma, A. Daffertshofer, D. F. Stegeman, and J. H. vanDieen, “Improving EMG-Based Muscle Force Estimation by Using a High-Density EMG Grid and Principal Component Analysis,” *IEEE Trans. Biomed. Eng.*, vol. 53, no. 4, pp. 712–719, Apr. 2006, doi: 10.1109/TBME.2006.870246.

[32] K. M. Steele, M. E. Munger, K. M. Peters, B. R. Shuman, and M. H. Schwartz, “Repeatability of electromyography recordings and muscle synergies during gait among children with cerebral palsy,” *Gait Posture*, vol. 67, pp. 290–295, Jan. 2019, doi: 10.1016/j.gaitpost.2018.10.009.

[33] G. Staude and W. Wolf, “Objective motor response onset detection in surface myoelectric signals,” *Med. Eng. Phys.*, vol. 21, no. 6–7, pp. 449–467, Jul. 1999, doi: 10.1016/S1350-4533(99)00067-3.

[34] D. G. Kamper, B. D. Schmit, and W. Z. Rymer, “Effect of Muscle Biomechanics on the Quantification of Spasticity,” *Ann. Biomed. Eng.*, vol. 29, no. 12, pp. 1122–1134, Dec. 2001, doi: 10.1114/1.1424918.

[35] S. G. Chung, E. van Rey, Z. Bai, E. J. Roth, and L.-Q. Zhang, “Biomechanic changes in passive properties of hemiplegic ankles with spastic hypertonia,” *Arch. Phys. Med. Rehabil.*, vol. 85, no. 10, pp. 1638–1646, Oct. 2004, doi: 10.1016/j.apmr.2003.11.041.

[36] L. Alibiglou, W. Z. Rymer, R. L. Harvey, and M. M. Mirbagheri, “The relation between Ashworth scores and neuromechanical measurements of spasticity following stroke,” *J. NeuroEngineering Rehabil.*, vol. 5, no. 1, p. 18, 2008, doi: 10.1186/1743-0003-5-18.

[37] M. Germanotta *et al.*, “Spasticity Measurement Based on Tonic Stretch Reflex Threshold in Children with Cerebral Palsy Using the PediAnklebot,” *Front. Hum. Neurosci.*, vol. 11, p. 277, May 2017, doi: 10.3389/fnhum.2017.00277.

[38] F. Posteraro *et al.*, “Technologically-advanced assessment of upper-limb spasticity: a pilot study,” *Eur. J. Phys. Rehabil. Med.*, vol. 54, no. 4, p. 9, 2018.

[39] T. K. K. Koo and A. F. T. Mak, “A neuromusculoskeletal model to simulate the constant angular velocity elbow extension test of spasticity,” *Med. Eng. Phys.*, vol. 28, no. 1, pp. 60–69, Jan. 2006, doi: 10.1016/j.medengphy.2005.03.012.

[40] W. Tao, T. Liu, R. Zheng, and H. Feng, “Gait Analysis Using Wearable Sensors,” *Sensors*, vol. 12, no. 2, pp. 2255–2283, Feb. 2012, doi: 10.3390/s120202255.

[41] F. Attal, S. Mohammed, M. Dedabrishvili, F. Chamroukhi, L. Oukhellou, and Y. Amirat, “Physical Human Activity Recognition Using Wearable Sensors,” *Sensors*, vol. 15, no. 12, pp. 31314–31338, Dec. 2015, doi: 10.3390/s151229858.

[42] S. Majumder, T. Mondal, and M. Deen, “Wearable Sensors for Remote Health Monitoring,” *Sensors*, vol. 17, no. 12, p. 130, Jan. 2017, doi: 10.3390/s17010130.

[43] F. Massé, R. R. Gonzenbach, A. Arami, A. Paraschiv-Ionescu, A. R. Luft, and K. Aminian, “Improving activity recognition using a wearable barometric pressure sensor in mobility-impaired stroke patients,” *J. NeuroEngineering Rehabil.*, vol. 12, no. 1, p. 72, Dec. 2015, doi: 10.1186/s12984-015-0060-2.

[44] B. Najafi, K. Aminian, A. Paraschiv-Ionescu, F. Loew, C. J. Bula, and P. Robert, “Ambulatory system for human motion analysis using a kinematic sensor: monitoring of daily physical activity in the

elderly," *IEEE Trans. Biomed. Eng.*, vol. 50, no. 6, pp. 711–723, Jun. 2003, doi: 10.1109/TBME.2003.812189.

[45] A. Pantelopoulos and N. G. Bourbakis, "A Survey on Wearable Sensor-Based Systems for Health Monitoring and Prognosis," *IEEE Trans. Syst. Man Cybern. Part C Appl. Rev.*, vol. 40, no. 1, pp. 1–12, Jan. 2010, doi: 10.1109/TSMCC.2009.2032660.

[46] K. S. Kim, J. H. Seo, and C. G. Song, "Portable measurement system for the objective evaluation of the spasticity of hemiplegic patients based on the tonic stretch reflex threshold," *Med. Eng. Phys.*, vol. 33, no. 1, pp. 62–69, Jan. 2011, doi: 10.1016/j.medengphy.2010.09.002.

[47] A. K. Blanchette, A. A. Mullick, K. Moïn-Darbari, and M. F. Levin, "Tonic Stretch Reflex Threshold as a Measure of Ankle Plantar-Flexor Spasticity After Stroke," *Phys. Ther.*, vol. 96, no. 5, pp. 687–695, May 2016, doi: 10.2522/ptj.20140243.

[48] A. Calota, A. G. Feldman, and M. F. Levin, "Spasticity measurement based on tonic stretch reflex threshold in stroke using a portable device," *Clin. Neurophysiol.*, vol. 119, no. 10, pp. 2329–2337, Oct. 2008, doi: 10.1016/j.clinph.2008.07.215.

[49] J. He, W. R. Norling, and Y. Wang, "A dynamic neuromuscular model for describing the pendulum test of spasticity," *IEEE Trans. Biomed. Eng.*, vol. 44, no. 3, pp. 175–184, Mar. 1997, doi: 10.1109/10.554764.

[50] P. Piriyaprasarth, M. E. Morris, A. Winter, and A. E. Bialocerkowski, "The reliability of knee joint position testing using electrogoniometry," *BMC Musculoskelet. Disord.*, vol. 9, no. 1, p. 6, Dec. 2008, doi: 10.1186/1471-2474-9-6.

[51] D. B. Kettelkamp, R. J. Johnson, G. L. Smidt, E. Y. Chao, and M. Walker, "An electrogoniometric study of knee motion in normal gait," *J. Bone Joint Surg. Am.*, vol. 52, no. 4, pp. 775–790, Jun. 1970.

[52] J. M. Rothstein, P. J. Miller, and R. F. Roettger, "Goniometric reliability in a clinical setting. Elbow and knee measurements," *Phys. Ther.*, vol. 63, no. 10, pp. 1611–1615, Oct. 1983, doi: 10.1093/ptj/63.10.1611.

[53] E. S. Grood and W. J. Suntay, "A joint coordinate system for the clinical description of three-dimensional motions: application to the knee," *J. Biomech. Eng.*, vol. 105, no. 2, pp. 136–144, May 1983, doi: 10.1115/1.3138397.

[54] L. Bar-On *et al.*, "A clinical measurement to quantify spasticity in children with cerebral palsy by integration of multidimensional signals," *Gait Posture*, vol. 38, no. 1, pp. 141–147, May 2013, doi: 10.1016/j.gaitpost.2012.11.003.

[55] S.-H. Schless, K. Desloovere, E. Aertbeliën, G. Molenaers, C. Huenaerts, and L. Bar-On, "The Intra- and Inter-Rater Reliability of an Instrumented Spasticity Assessment in Children with Cerebral Palsy," *PLOS ONE*, vol. 10, no. 7, p. e0131011, Jul. 2015, doi: 10.1371/journal.pone.0131011.

[56] A. Arami, N. L. Tagliamonte, F. Tamburella, H.-Y. Huang, M. Molinari, and E. Burdet, "A simple tool to measure spasticity in spinal cord injury subjects," in *2017 International Conference on Rehabilitation Robotics (ICORR)*, London, Jul. 2017, pp. 1590–1596. doi: 10.1109/ICORR.2017.8009475.

[57] J. Favre, R. Aissaoui, B. M. Jolles, J. A. de Guise, and K. Aminian, "Functional calibration procedure for 3D knee joint angle description using inertial sensors," *J. Biomech.*, vol. 42, no. 14, pp. 2330–2335, Oct. 2009, doi: 10.1016/j.jbiomech.2009.06.025.

[58] Y.-S. Cho *et al.*, “Evaluation of Validity and Reliability of Inertial Measurement Unit-Based Gait Analysis Systems,” *Ann. Rehabil. Med.*, vol. 42, no. 6, pp. 872–883, Dec. 2018, doi: 10.5535/arm.2018.42.6.872.

[59] T. Seel, J. Raisch, and T. Schauer, “IMU-Based Joint Angle Measurement for Gait Analysis,” *Sensors*, vol. 14, no. 4, pp. 6891–6909, Apr. 2014, doi: 10.3390/s140406891.

[60] J. Favre, B. M. Jolles, R. Aissaoui, and K. Aminian, “Ambulatory measurement of 3D knee joint angle,” *J. Biomech.*, vol. 41, no. 5, pp. 1029–1035, 2008, doi: 10.1016/j.jbiomech.2007.12.003.

[61] E. P. Washabaugh, T. Kalyanaraman, P. G. Adamczyk, E. S. Claflin, and C. Krishnan, “Validity and repeatability of inertial measurement units for measuring gait parameters,” *Gait Posture*, vol. 55, pp. 87–93, Jun. 2017, doi: 10.1016/j.gaitpost.2017.04.013.

[62] F. Dadashi, B. Mariani, S. Rochat, C. Büla, B. Santos-Eggimann, and K. Aminian, “Gait and Foot Clearance Parameters Obtained Using Shoe-Worn Inertial Sensors in a Large-Population Sample of Older Adults,” *Sensors*, vol. 14, no. 1, pp. 443–457, Dec. 2013, doi: 10.3390/s140100443.

[63] A. Arami, N. S. Raymond, and K. Aminian, “An Accurate Wearable Foot Clearance Estimation System: Toward a Real-Time Measurement System,” *IEEE Sens. J.*, vol. 17, no. 8, pp. 2542–2549, Apr. 2017, doi: 10.1109/JSEN.2017.2665624.

[64] O. Giggins, D. Kelly, and B. Caulfield, “Evaluating Rehabilitation Exercise Performance Using a Single Inertial Measurement Unit,” presented at the ICTs for improving Patients Rehabilitation Research Techniques, Venice, Italy, 2013. doi: 10.4108/icst.pervasivehealth.2013.252061.

[65] D. F. Whelan, M. A. O’Reilly, T. E. Ward, E. Delahunt, and B. Caulfield, “Technology in Rehabilitation: Evaluating the Single Leg Squat Exercise with Wearable Inertial Measurement Units,” *Methods Inf. Med.*, vol. 56, no. 02, pp. 88–94, 2017, doi: 10.3414/ME16-02-0002.

[66] Y. Li, X. Zhang, Y. Gong, Y. Cheng, X. Gao, and X. Chen, “Motor Function Evaluation of Hemiplegic Upper-Extremities Using Data Fusion from Wearable Inertial and Surface EMG Sensors,” *Sensors*, vol. 17, no. 3, p. 582, Mar. 2017, doi: 10.3390/s17030582.

[67] E. Repnik, U. Puh, N. Goljar, M. Munih, and M. Mihelj, “Using Inertial Measurement Units and Electromyography to Quantify Movement during Action Research Arm Test Execution,” *Sensors*, vol. 18, no. 9, p. 2767, Aug. 2018, doi: 10.3390/s18092767.

[68] C. Cifuentes, A. Braidot, L. Rodriguez, M. Frisoli, A. Santiago, and A. Frizera, “Development of a wearable ZigBee sensor system for upper limb rehabilitation robotics,” in *2012 4th IEEE RAS & EMBS International Conference on Biomedical Robotics and Biomechatronics (BioRob)*, Rome, Italy, Jun. 2012, pp. 1989–1994. doi: 10.1109/BioRob.2012.6290926.

[69] M. G. L. Monaco *et al.*, “Biomechanical Load Evaluation by Means of Wearable Devices in Industrial Environments: An Inertial Motion Capture System and sEMG Based Protocol,” in *Advances in Human Factors in Wearable Technologies and Game Design*, vol. 795, T. Z. Ahram, Ed. Cham: Springer International Publishing, 2019, pp. 233–242. doi: 10.1007/978-3-319-94619-1_23.

[70] J.-J. J. Chen, Y.-N. Wu, S.-C. Huang, H.-M. Lee, and Y.-L. Wang, “The Use of a Portable Muscle Tone Measurement Device to Measure the Effects of Botulinum Toxin Type A on Elbow Flexor Spasticity,” *Arch. Phys. Med. Rehabil.*, vol. 86, no. 8, pp. 1655–1660, Aug. 2005, doi: 10.1016/j.apmr.2005.03.019.

[71] Hyung-Soon Park, Jonghyun Kim, and D. L. Damiano, “Haptic recreation of elbow spasticity,” in *2011 IEEE International Conference on Rehabilitation Robotics*, Zurich, Jun. 2011, pp. 1–6. doi: 10.1109/ICORR.2011.5975462.

[72] Y.-N. Wu, H.-S. Park, J.-J. Chen, Y. Ren, E. J. Roth, and L.-Q. Zhang, “Position as Well as Velocity Dependence of Spasticity—Four-Dimensional Characterizations of Catch Angle,” *Front. Neurol.*, vol. 9, p. 863, Oct. 2018, doi: 10.3389/fneur.2018.00863.

[73] N. H. Mayer, “Clinicophysiologic concepts of spasticity and motor dysfunction in adults with an upper motoneuron lesion,” *Muscle Nerve. Suppl.*, vol. 6, pp. S1-13, 1997.

[74] L. Bar-On, E. Aertbeliën, G. Molenaers, B. Dan, and K. Desloovere, “Manually controlled instrumented spasticity assessments: a systematic review of psychometric properties,” *Dev. Med. Child Neurol.*, vol. 56, no. 10, pp. 932–950, Oct. 2014, doi: 10.1111/dmcn.12419.

[75] J. Burridge *et al.*, “Theoretical and methodological considerations in the measurement of spasticity,” *Disabil. Rehabil.*, vol. 27, no. 1–2, pp. 69–80, Jan. 2005, doi: 10.1080/09638280400014592.

[76] P. G. Lindberg, “Validation of a New Biomechanical Model to Measure Muscle Tone in Spastic Muscles,” *Neurorehabil. Neural Repair*, vol. 25, no. 7, p. 9, 2011.

[77] W.-S. Shin, H. Chang, S. J. Kim, and J. Kim, “Characterization of Spastic Ankle Flexors Based on Viscoelastic Modeling for Accurate Diagnosis,” *Int. J. Control Autom. Syst.*, vol. 18, no. 1, pp. 102–113, Jan. 2020, doi: 10.1007/s12555-019-0245-8.

[78] E. de Vlugt, J. H. de Groot, K. E. Schenkeveld, Jh. Arendzen, F. C. van der Helm, and C. G. Meskers, “The relation between neuromechanical parameters and Ashworth score in stroke patients,” *J. NeuroEngineering Rehabil.*, vol. 7, no. 1, p. 35, Dec. 2010, doi: 10.1186/1743-0003-7-35.

[79] R. Wang, P. Herman, Ö. Ekeberg, J. Gäverth, A. Fagergren, and H. Forssberg, “Neural and non-neural related properties in the spastic wrist flexors: An optimization study,” *Med. Eng. Phys.*, vol. 47, pp. 198–209, Sep. 2017, doi: 10.1016/j.medengphy.2017.06.023.

[80] M. L. Latash, *Fundamentals of motor control*, 1st ed. Amsterdam ; Boston: Elsevier/Academic Press, 2012.

[81] M. F. Levin and A. G. Feldman, “The role of stretch reflex threshold regulation in normal and impaired motor control,” *Brain Res.*, vol. 657, no. 1–2, pp. 23–30, Sep. 1994, doi: 10.1016/0006-8993(94)90949-0.

[82] X. Zhang, X. Tang, X. Zhu, X. Gao, X. Chen, and X. Chen, “A Regression-Based Framework for Quantitative Assessment of Muscle Spasticity Using Combined EMG and Inertial Data From Wearable Sensors,” *Front. Neurosci.*, vol. 13, p. 398, May 2019, doi: 10.3389/fnins.2019.00398.

[83] A. Jobin and M. F. Levin, “Regulation of stretch reflex threshold in elbow flexors in children with cerebral palsy: a new measure of spasticity,” *Dev. Med. Child Neurol.*, vol. 42, no. 8, pp. 531–540, Aug. 2000, doi: 10.1017/S0012162200001018.

[84] N. A. Turpin, A. G. Feldman, and M. F. Levin, “Stretch-reflex threshold modulation during active elbow movements in post-stroke survivors with spasticity,” *Clin. Neurophysiol.*, vol. 128, no. 10, pp. 1891–1897, Oct. 2017, doi: 10.1016/j.clinph.2017.07.411.

[85] N. A. Turpin, M. F. Levin, and A. G. Feldman, “Implicit learning and generalization of stretch response modulation in humans,” *J. Neurophysiol.*, vol. 115, no. 6, pp. 3186–3194, Jun. 2016, doi: 10.1152/jn.01143.2015.

[86] H. Mat Rosly, S. N. Sidek, A. Ahmad Puzi, H. M. Yusoff, N. Daud, and M. Mat Rosly, "Clasp-Knife Model of Muscle Spasticity for Simulation of Robot-Human Interaction," *IEEE Access*, vol. 7, pp. 1355–1364, 2019, doi: 10.1109/ACCESS.2018.2846595.

[87] R. Xia, D. Powell, W. Z. Rymer, N. Hanson, X. Fang, and A. J. Threlkeld, "Differentiation between the contributions of shortening reaction and stretch-induced inhibition to rigidity in Parkinson's disease," *Exp. Brain Res.*, vol. 209, no. 4, pp. 609–618, Apr. 2011, doi: 10.1007/s00221-011-2594-2.

[88] D. Burke, J. Wissel, and G. A. Donnan, "Pathophysiology of spasticity in stroke," *Neurology*, vol. 80, no. Issue 3, Supplement 2, pp. S20–S26, Jan. 2013, doi: 10.1212/WNL.0b013e31827624a7.

[89] J. F. M. Fleuren *et al.*, "Stop using the Ashworth Scale for the assessment of spasticity," *J. Neurol. Neurosurg. Psychiatry*, vol. 81, no. 1, pp. 46–52, Jan. 2010, doi: 10.1136/jnnp.2009.177071.

[90] S. Naghdi, N. N. Ansari, H. Abolhasani, K. Mansouri, N. Ghotbi, and S. Hasson, "Electrophysiological evaluation of the Modified Tardieu Scale (MTS) in assessing poststroke wrist flexor spasticity," *NeuroRehabilitation*, vol. 34, no. 1, pp. 177–184, Feb. 2014, doi: 10.3233/NRE-131016.

[91] E. S. Tehrani, K. Jalaleddini, and R. E. Kearney, "Ankle Joint Intrinsic Dynamics is More Complex than a Mass-Spring-Damper Model," *IEEE Trans. Neural Syst. Rehabil. Eng.*, vol. 25, no. 9, pp. 1568–1580, Sep. 2017, doi: 10.1109/TNSRE.2017.2679722.

[92] H. Lee, E. J. Rouse, and H. I. Krebs, "Summary of Human Ankle Mechanical Impedance During Walking," *IEEE J. Transl. Eng. Health Med.*, vol. 4, pp. 1–7, 2016, doi: 10.1109/JTEHM.2016.2601613.

[93] P. Amiri and R. E. Kearney, "Ankle intrinsic stiffness changes with postural sway," *J. Biomech.*, vol. 85, pp. 50–58, Mar. 2019, doi: 10.1016/j.jbiomech.2019.01.009.

[94] H. Y. Huang, A. Arami, I. Farkhatdinov, D. Formica, and E. Burdet, "The Influence of Posture, Applied Force and Perturbation Direction on Hip Joint Viscoelasticity," *IEEE Trans. Neural Syst. Rehabil. Eng.*, vol. 28, no. 5, pp. 1138–1145, May 2020, doi: 10.1109/TNSRE.2020.2983515.

[95] A. Arami, E. van Asseldonk, H. van der Kooij, and E. Burdet, "A Clustering-based Approach to Identify Joint Impedance during Walking," *IEEE Trans. Neural Syst. Rehabil. Eng.*, pp. 1–1, 2020, doi: 10.1109/TNSRE.2020.3005389.

[96] D. Wood *et al.*, "Biomechanical approaches applied to the lower and upper limb for the measurement of spasticity: A systematic review of the literature," *Disabil. Rehabil.*, vol. 27, no. 1–2, pp. 19–33, Jan. 2005, doi: 10.1080/09638280400014683.

[97] G. Sheean, "The pathophysiology of spasticity," *Eur. J. Neurol.*, vol. 9 Suppl 1, pp. 3–9; dicussion 53-61, May 2002, doi: 10.1046/j.1468-1331.2002.0090s1003.x.

[98] K. P. Blum, B. Lamotte D'Incamps, D. Zytnicki, and L. H. Ting, "Force encoding in muscle spindles during stretch of passive muscle," *PLOS Comput. Biol.*, vol. 13, no. 9, p. e1005767, Sep. 2017, doi: 10.1371/journal.pcbi.1005767.

[99] A. Falisse, L. Bar-On, K. Desloovere, I. Jonkers, and F. De Groote, "A spasticity model based on feedback from muscle force explains muscle activity during passive stretches and gait in children with cerebral palsy," *PLOS ONE*, vol. 13, no. 12, p. e0208811, Dec. 2018, doi: 10.1371/journal.pone.0208811.

[100] D. M. Simpson *et al.*, “Botulinum toxin type A in the treatment of upper extremity spasticity: A randomized, double-blind, placebo-controlled trial,” *Neurology*, vol. 46, no. 5, pp. 1306–1306, May 1996, doi: 10.1212/WNL.46.5.1306.

[101] I. F. Turna, B. Erhan, N. B. Gunduz, and O. Turna, “The effects of different injection techniques of botulinum toxin a in post-stroke patients with plantar flexor spasticity,” *Acta Neurol. Belg.*, vol. 120, no. 3, pp. 639–643, Jun. 2020, doi: 10.1007/s13760-018-0969-x.

[102] H. Kumru *et al.*, “Reduction of Spasticity With Repetitive Transcranial Magnetic Stimulation in Patients With Spinal Cord Injury,” *Neurorehabil. Neural Repair*, vol. 24, no. 5, pp. 435–441, Jun. 2010, doi: 10.1177/1545968309356095.

[103] J. Málly and E. Dinya, “Recovery of motor disability and spasticity in post-stroke after repetitive transcranial magnetic stimulation (rTMS),” *Brain Res. Bull.*, vol. 76, no. 4, pp. 388–395, Jul. 2008, doi: 10.1016/j.brainresbull.2007.11.019.

[104] A. Franek, B. Turczynski, and J. Opara, “Treatment of spinal spasticity by electrical stimulation,” *J. Biomed. Eng.*, vol. 10, no. 3, pp. 266–270, May 1988, doi: 10.1016/0141-5425(88)90009-X.

[105] V. Alfieri, “Electrical Stimulation for Modulation of Spasticity in Hemiplegic and Spinal Cord Injury Subjects: ES in Cerebral Vascular Accidents,” *Neuromodulation Technol. Neural Interface*, vol. 4, no. 2, pp. 85–92, Apr. 2001, doi: 10.1046/j.1525-1403.2001.00085.x.

[106] J. Powell, A. D. Pandyan, M. Granat, M. Cameron, and D. J. Stott, “Electrical Stimulation of Wrist Extensors in Poststroke Hemiplegia,” *Stroke*, vol. 30, no. 7, pp. 1384–1389, Jul. 1999, doi: 10.1161/01.STR.30.7.1384.

[107] A. R. Alashram, G. Annino, and N. B. Mercuri, “Changes in spasticity following functional electrical stimulation cycling in patients with spinal cord injury: A systematic review,” *J. Spinal Cord Med.*, pp. 1–14, May 2020, doi: 10.1080/10790268.2020.1763713.

[108] B. B. Bhakta, “Management of spasticity in stroke,” *Br. Med. Bull.*, vol. 56, no. 2, pp. 476–485, Jan. 2000, doi: 10.1258/0007142001903111.

[109] “American Spinal Cord Injury Association (ASIA) Impairment Scale,” *Physiopedia*. https://www.physio-pedia.com/American_Spinal_Cord_Injury_Association_(ASIA)_Impairment_Scale (accessed May 25, 2021).

[110] “Sensor Locations.” http://seniam.org/sensor_location.htm (accessed May 28, 2021).

[111] “Ankle joint,” *Kenhub*. https://www.kenhub.com/en/library/anatomy/the-ankle-joint (accessed May 25, 2021).

[112] “Knee joint,” *Kenhub*. https://www.kenhub.com/en/library/anatomy/the-knee-joint (accessed May 25, 2021).

[113] “Hip joint,” *Kenhub*. https://www.kenhub.com/en/library/anatomy/hip-joint (accessed May 25, 2021).

[114] *MATLAB R2020b*. Natick, MA: Mathworks, 2020. [Online]. Available: https://www.mathworks.com/help/matlab/release-notes.html

[115] S. Solnik, P. DeVita, P. Rider, B. Long, and T. Hortobágyi, “Teager-Kaiser Operator improves the accuracy of EMG onset detection independent of signal-to-noise ratio,” *Acta Bioeng. Biomech.*, vol. 10, no. 2, pp. 65–68, 2008.

[116] P. Konrad, “A Practical Introduction to Kinesiological Electromyography,” p. 61.

[117] J. V. Basmajian and C. J. De Luca, *Muscles alive: their functions revealed by electromyography*, 5th ed. Baltimore: Williams & Wilkins, 1985.

[118] C. J. De Luca, "The Use of Surface Electromyography in Biomechanics," *J. Appl. Biomech.*, vol. 13, no. 2, pp. 135–163, May 1997, doi: 10.1123/jab.13.2.135.

[119] D. M. Corden, O. C. J. Lippold, K. Buchanan, and C. Norrington, "Long-Latency Component of the Stretch Reflex in Human Muscle Is Not Mediated by Intramuscular Stretch Receptors," *J. Neurophysiol.*, vol. 84, no. 1, pp. 184–188, Jul. 2000, doi: 10.1152/jn.2000.84.1.184.

[120] E. Toft, T. Sinkjaer, and G. T. Espersen, "Quantitation of the stretch reflex," *Acta Neurol. Scand.*, vol. 79, no. 5, pp. 384–390, May 1989, doi: 10.1111/j.1600-0404.1989.tb03805.x.

[121] "Standards Documents," *International Society of Biomechanics*. https://isbweb.org/about-us/29-standards-documents (accessed May 29, 2021).

[122] J. Bortz, "A New Mathematical Formulation for Strapdown Inertial Navigation," *IEEE Trans. Aerosp. Electron. Syst.*, vol. AES-7, no. 1, pp. 61–66, Jan. 1971, doi: 10.1109/TAES.1971.310252.

[123] C. L. Brockett and G. J. Chapman, "Biomechanics of the ankle," *Orthop. Trauma*, vol. 30, no. 3, pp. 232–238, Jun. 2016, doi: 10.1016/j.mporth.2016.04.015.

[124] R. J. Maughan, J. S. Watson, and J. Weir, "Strength and cross-sectional area of human skeletal muscle.," *J. Physiol.*, vol. 338, no. 1, pp. 37–49, May 1983, doi: 10.1113/jphysiol.1983.sp014658.

[125] "Symbiotic man-machine interactions in wearable exoskeletons to enhance mobility for paraplegics | Symbitron Project | FP7 | CORDIS | European Commission." https://cordis.europa.eu/project/id/611626 (accessed May 25, 2021).

[126] J. Houk and W. Simon, "Responses of Golgi tendon organs to forces applied to muscle tendon.," *J. Neurophysiol.*, vol. 30, no. 6, pp. 1466–1481, Nov. 1967, doi: 10.1152/jn.1967.30.6.1466.

[127] J. M. Hidler and W. Z. Rymer, "A simulation study of reflex instability in spasticity: origins of clonus," *IEEE Trans. Rehabil. Eng.*, vol. 7, no. 3, pp. 327–340, Sep. 1999, doi: 10.1109/86.788469.

[128] R. Bhimani and L. Anderson, "Clinical Understanding of Spasticity: Implications for Practice," *Rehabil. Res. Pract.*, vol. 2014, pp. 1–10, 2014, doi: 10.1155/2014/279175.

[129] W. A. Cook, "Antagonistic muscles in the production of clonus in man," *Neurology*, vol. 17, no. 8, pp. 779–779, Aug. 1967, doi: 10.1212/WNL.17.8.779.

[130] J. A. Beres-Jones, T. D. Johnson, and S. J. Harkema, "Clonus after human spinal cord injury cannot be attributed solely to recurrent muscle-tendon stretch," *Exp. Brain Res.*, vol. 149, no. 2, pp. 222–236, Mar. 2003, doi: 10.1007/s00221-002-1349-5.

[131] D. M. Wallace, B. H. Ross, and C. K. Thomas, "Motor unit behavior during clonus," *J. Appl. Physiol.*, vol. 99, no. 6, pp. 2166–2172, Dec. 2005, doi: 10.1152/japplphysiol.00649.2005.

[132] E. N. Benz, T. G. Hornby, R. K. Bode, R. A. Scheidt, and B. D. Schmit, "A physiologically based clinical measure for spastic reflexes in spinal cord injury," *Arch. Phys. Med. Rehabil.*, vol. 86, no. 1, pp. 52–59, Jan. 2005, doi: 10.1016/j.apmr.2004.01.033.

[133] P. Akpinar, A. Atici, F. U. Ozkan, I. Aktas, D. G. Kulcu, and K. N. Kurt, "Reliability of the Spinal Cord Assessment Tool for Spastic Reflexes," *Arch. Phys. Med. Rehabil.*, vol. 98, no. 6, pp. 1113–1118, Jun. 2017, doi: 10.1016/j.apmr.2016.09.119.

[134] J. Rasmussen, M. Boocock, and G. Paul, "Advanced musculoskeletal simulation as an ergonomic design method," *Work*, vol. 41, pp. 6107–6111, 2012, doi: 10.3233/WOR-2012-1069-6107.

[135] C. R. Dickerson, D. B. Chaffin, and R. E. Hughes, “A mathematical musculoskeletal shoulder model for proactive ergonomic analysis,” *Comput. Methods Biomech. Biomed. Engin.*, vol. 10, no. 6, pp. 389–400, Dec. 2007, doi: 10.1080/10255840701592727.

[136] J. Kar and P. M. Quesada, “A Musculoskeletal Modeling Approach for Estimating Anterior Cruciate Ligament Strains and Knee Anterior–Posterior Shear Forces in Stop-Jumps Performed by Young Recreational Female Athletes,” *Ann. Biomed. Eng.*, vol. 41, no. 2, pp. 338–348, Feb. 2013, doi: 10.1007/s10439-012-0644-y.

[137] D. C. Ackland, A. Moskaljuk, C. Hart, P. Vee Sin Lee, and G. Dimitroulis, “Prosthesis Loading After Temporomandibular Joint Replacement Surgery: A Musculoskeletal Modeling Study,” *J. Biomech. Eng.*, vol. 137, no. 4, p. 041001, Apr. 2015, doi: 10.1115/1.4029503.

[138] M. Kia, A. P. Stylianou, and T. M. Guess, “Evaluation of a musculoskeletal model with prosthetic knee through six experimental gait trials,” *Med. Eng. Phys.*, vol. 36, no. 3, pp. 335–344, Mar. 2014, doi: 10.1016/j.medengphy.2013.12.007.

[139] D. Simon, R. Mascarenhas, B. M. Saltzman, M. Rollins, B. R. Bach, and P. MacDonald, “The Relationship between Anterior Cruciate Ligament Injury and Osteoarthritis of the Knee,” *Adv. Orthop.*, vol. 2015, pp. 1–11, 2015, doi: 10.1155/2015/928301.

[140] Z. Knoll, R. M. Kiss, and L. Kocsis, “Gait adaptation in ACL deficient patients before and after anterior cruciate ligament reconstruction surgery,” *J. Electromyogr. Kinesiol.*, vol. 14, no. 3, pp. 287–294, Jun. 2004, doi: 10.1016/j.jelekin.2003.12.005.

[141] F. R. Noyes, O. D. Schipplein, T. P. Andriacchi, S. R. Saddemi, and M. Weise, “The anterior cruciate ligament-deficient knee with varus alignment: An analysis of gait adaptations and dynamic joint loadings,” *Am. J. Sports Med.*, vol. 20, no. 6, pp. 707–716, Nov. 1992, doi: 10.1177/036354659202000612.

[142] L. R. Sheffler and J. Chae, “Hemiparetic Gait,” *Phys. Med. Rehabil. Clin. N. Am.*, vol. 26, no. 4, pp. 611–623, Nov. 2015, doi: 10.1016/j.pmr.2015.06.006.

[143] L. A. Luengas, E. Camargo, and G. Sanchez, “Modeling and simulation of normal and hemiparetic gait,” *Front. Mech. Eng.*, vol. 10, no. 3, pp. 233–241, Sep. 2015, doi: 10.1007/s11465-015-0343-0.

[144] M. Cardona and C. G. Cena, “Musculoskeletal Modeling as a Tool for Biomechanical Analysis of Normal and Pathological Gait,” in *VIII Latin American Conference on Biomedical Engineering and XLII National Conference on Biomedical Engineering*, vol. 75, C. A. González Díaz, C. Chapa González, E. Laciar Leber, H. A. Vélez, N. P. Puente, D.-L. Flores, A. O. Andrade, H. A. Galván, F. Martínez, R. García, C. J. Trujillo, and A. R. Mejía, Eds. Cham: Springer International Publishing, 2020, pp. 955–963. doi: 10.1007/978-3-030-30648-9_124.

[145] “Reinforcement learning with musculoskeletal models.” http://osim-rl.stanford.edu/docs/home/ (accessed May 25, 2021).

[146] “stanfordnmbl/osim-rl,” *GitHub*. https://github.com/stanfordnmbl/osim-rl (accessed May 25, 2021).

[147] E. M. Arnold, S. R. Hamner, A. Seth, M. Millard, and S. L. Delp, “How muscle fiber lengths and velocities affect muscle force generation as humans walk and run at different speeds,” *J. Exp. Biol.*, vol. 216, no. 11, pp. 2150–2160, Jun. 2013, doi: 10.1242/jeb.075697.

[148] R. H. Burpee and W. Stroll, “Measuring Reaction Time of Athletes,” *Res. Q. Am. Phys. Educ. Assoc.*, vol. 7, no. 1, pp. 110–118, Mar. 1936, doi: 10.1080/23267402.1936.10761762.

[149] J. Weng, E. Hashemi, and A. Arami, “Natural Walking With Musculoskeletal Models Using Deep Reinforcement Learning,” *IEEE Robot. Autom. Lett.*, vol. 6, no. 2, pp. 4156–4162, Apr. 2021, doi: 10.1109/LRA.2021.3067617.

[150] T. Oberg, A. Karsznia, and K. Oberg, “Basic gait parameters : Reference data for normal subjects, 10-79 years of age,” p. 14, 1993.

[151] M. Bertoli *et al.*, “Estimation of spatio-temporal parameters of gait from magneto-inertial measurement units: multicenter validation among Parkinson, mildly cognitively impaired and healthy older adults,” *Biomed. Eng. OnLine*, vol. 17, no. 1, p. 58, Dec. 2018, doi: 10.1186/s12938-018-0488-2.

[152] J. C. M. Schlachetzki *et al.*, “Wearable sensors objectively measure gait parameters in Parkinson’s disease,” *PLOS ONE*, vol. 12, no. 10, p. e0183989, Oct. 2017, doi: 10.1371/journal.pone.0183989.

[153] M. R. Lim, R. C. Huang, A. Wu, F. P. Girardi, and F. P. J. Cammisa, “Evaluation of the Elderly Patient With an Abnormal Gait,” *JAAOS - J. Am. Acad. Orthop. Surg.*, vol. 15, no. 2, pp. 107–117, Feb. 2007.

[154] “Toe walking - Symptoms and causes,” *Mayo Clinic*. https://www.mayoclinic.org/diseases-conditions/toe-walking/symptoms-causes/syc-20378410 (accessed May 30, 2021).

[155] W. J. Barrow, M. Jaworski, and P. J. Accardo, “Persistent Toe Walking in Autism,” *J. Child Neurol.*, vol. 26, no. 5, pp. 619–621, May 2011, doi: 10.1177/0883073810385344.

[156] R. Wartenberg, “Pendulousness of the Legs as a Diagnostic Test,” *Neurology*, vol. 1, no. 1, pp. 18–18, Jan. 1951, doi: 10.1212/WNL.1.1.18.

[157] M. F. Levin and C. W. Y. Hui-Chan, “Relief of hemiparetic spasticity by TENS is associated with improvement in reflex and voluntary motor functions,” *Electroencephalogr. Clin. Neurophysiol. Potentials Sect.*, vol. 85, no. 2, pp. 131–142, Apr. 1992, doi: 10.1016/0168-5597(92)90079-Q.

[158] A. R. Fugl-Meyer, L. Jääskö, I. Leyman, S. Olsson, and S. Steglind, “The post-stroke hemiplegic patient. 1. a method for evaluation of physical performance,” *Scand. J. Rehabil. Med.*, vol. 7, no. 1, pp. 13–31, 1975.

[159] W. Herzog and L. J. Read, “Lines of action and moment arms of the major force-carrying structures crossing the human knee joint,” *J. Anat.*, vol. 182 (Pt 2), pp. 213–230, Apr. 1993.

[160] S. G. Rugg, R. J. Gregor, B. R. Mandelbaum, and L. Chiu, “In vivo moment arm calculations at the ankle using magnetic resonance imaging (MRI),” *J. Biomech.*, vol. 23, no. 5, pp. 495–501, 1990, doi: 10.1016/0021-9290(90)90305-m.

[161] P. Procter and J. P. Paul, “Ankle joint biomechanics,” *J. Biomech.*, vol. 15, no. 9, pp. 627–634, 1982, doi: 10.1016/0021-9290(82)90017-3.

Appendices

Appendix A: Quantitative Spasticity Modeling Literature

Table A1. Reviewed mechanical approaches to modeling spasticity.

Authors	Target Population	Target Joints	Sensors	Method	Outcome Measures
Alibiglou et al. [36]	Post-stroke	Elbow and ankle	Non-wearable 6-axis force sensor, potentiometer, tachometer	Motor-driven motion; system identification model; goodness of fit evaluated by percent variance accounted for (%VAF)	Intrinsic stiffness, reflex stiffness; near-zero correlation with MAS
Chen et al. [70]	Post-stroke	Elbow	Wearable gyroscope, differential pressure sensor, sEMG sensors	Manually driven motion; phase-shifted torque-angle curve	Average viscosity (across multiple stretching speeds), muscle activity onset
Chung et al. [35]	Post-stroke	Ankle	Non-wearable 6-axis force sensor, unspecified kinematics sensors	Motor-driven motion; torque-angle curves	Resistance torque, quasi-stiffness, energy loss and ROM; low to moderately correlated with MAS
Park et al. [71]	CP (children)	Elbow	Unspecified kinematics and force sensors	Manually driven motion; model of torque during pre-, during, and post-catch phases	Replication of MAS level on simulated spastic elbow (haptic device); model accuracy evaluated by blinded assessors
Wu et al. [72]	Post-stroke	Elbow	Non-wearable potentiometer, torque sensor; wearable sEMG sensors	Manually driven motion; torque-angle curve, 4-D characterization of catch angle using torque, torque rate of change, angle and velocity; model accuracy evaluated by mean square error	ROM, stiffness, energy loss, catch angle; high correlations with MAS

Table A2. Reviewed musculoskeletal and neural dynamics approaches to modeling spasticity.

Authors	Target Population	Target Joints	Sensors	Method	Outcome Measures
Koo and Mak [39]	Post-stroke	Elbow	Non-wearable dynamometer and needle EMG electrode; wearable sEMG sensors	Motor-driven motion; parameter identification in torque estimation and sensitivity analysis; model goodness of fit evaluated by root mean square error (RMSE)	Minimum spindle firing rate for 0.5% neural excitation, muscle spindle static gain
Lindberg et al. [76]	Post-stroke	Wrist	Non-wearable stepper motor, unspecified force sensor; wearable sEMG sensors	Motor-driven motion (multiple speeds); force estimation to separate into components; re-test with ischemic nerve block	Neural component (NC) of force – model validated by NC reduces with ischemic nerve block and velocity dependence of NC; moderate correlation between NC and MAS, also integrated EMG
Shin et al. [77]	Post-stroke	Ankle	Non-wearable torque sensor, rotary encoder; wearable sEMG sensors	Manually driven motion; parameter identification in torque estimation; model goodness of fit evaluated by %VAF, normalized RSME, and R^2	Muscle spindle firing rate for 50% motor neuron recruitment, standard deviation of alpha motor neuron pool function
de Vlugt et al. [78]	Post-stroke	Ankle	Non-wearable potentiometer, force transducer; wearable sEMG sensors	Motor-driven motion (multiple speeds); parameter identification in torque estimation; model goodness of fit evaluated by %VAF, performance by repeatability	Stiffness and viscosity parameters; stiffness moderately correlated with AS at low speed, reflex torque moderately correlated with AS at fast speeds
Wang et al. [79]	Post-stroke	Wrist	Non-wearable force transducer, high-precision stepper motor; wearable sEMG sensors	Motor-driven motion (slow and fast speed); parameter identification in torque estimation; model goodness of fit evaluated by %VAF and R^2	Passive stiffness, muscle spindle firing rate for 50% motor neuron recruitment, motor neuron pool gain

Table A3. Reviewed threshold-control approaches to modeling spasticity.

Authors	Target Population	Target Joints	Sensors	Method	Outcome Measures
Arami et al. [56]	Incomplete SCI	Ankle	Wearable IMUs, 6-axis force sensors, wireless sEMG sensors	Manually driven motion at different knee angles; DSRT model for dorsi- and plantar flexor muscles; models goodness of fit evaluated by R^2	Model μ and TSRT for each muscle; spastic joint space; joint torque moderate-high correlation with DSRT angle and velocities
Bar-On et al. [54]	CP (children)	Knee and ankle	Wearable IMUs, 6-axis force sensors, wireless sEMG sensors	Manually driven motion; DSRT model and torque-angle curve; model evaluated by repeatability	ROM, max velocity, average RMS-EMG, torque, and work
Blanchette et al. [47]	Post-stroke	Ankle	Wearable electrogoniometer, sEMG sensors	Manually driven motion; DSRT model for plantar flexors	Model μ and TSRT; interrater reliability for TSRTs
Calota et al. [48]	Post-stroke	Elbow	Wearable electrogoniometer, sEMG sensors	Manually driven motion; DSRT model of biceps brachii	TSRT; moderately good intra- and interrater reliability, no correlation with MAS
Germanotta et al. [37]	CP (children)	Ankle	Non-wearable mini-rail linear encoders, unspecified torque sensor; wearable wireless sEMG sensors	Motor-driven motion; DSRT models of dorsi- and plantar flexors; goodness of fit evaluated by r correlations	Model μ and TSRT; low to moderate correlations with MAS
He et al. [49]	MS	Knee	Wearable electrogoniometer	Pendulum test [156]; estimation of swing trajectory during pendulum test	DSRT, TSRT and stretch reflex gain
Jobin and Levin [83]	CP (children)	Elbow	Non-wearable angle and velocity transducers; wearable sEMG sensors	Motor-driven motion; DSRT models of elbow flexors and extensors	TSRT; high test-retest reliability by ICC, no correlation with CSI[2]

Kim et al. [46]	Post-stroke	Elbow	Wearable twin-axis electrogoniometer, sEMG sensors	Manually driven motion; DSRT models, K-means clustering of TSRT groups	Significant differences between K-means groups (3 levels), no significant differences between groups by MAS; very high correlation between K-means groups and TSRTs
Levin and Feldman [81]	Post-stroke	Elbow	Non-wearable precision digital resolver; wearable sEMG sensors	Motor-driven motion; DSRT models of elbow flexors and extensors	Model μ and TSRT; moderate correlations with MAS
Mullick et al. [2]	Post-stroke, Parkinson's	Elbow	Non-wearable precision axial gauge; wearable sEMG sensors	Motor-driven motion [1]; DSRT models of elbow flexors and extensors; goodness of fit evaluated by R^2	Sensitivity of DSRT to velocity – high for post-stroke, near-zero for parkinsonian; zero correlation between μ and TSRT and CSI [2]
Turpin et al. [85]	Post-stroke	Elbow	Non-wearable optical encoder; wearable sEMG sensors	Manually driven (passive) and active motion; DSRT models of flexors and extensors	Velocity sensitivity μ and TSRT increased in active stretch; change in TSRT between passive and active was moderate to highly correlated with CSI [2] and FMA [3]
Zhang et al. [82]	Post-stroke, brain trauma, SCI	Elbow	Wearable IMUs and sEMG sensors	Manually driven motion; DSRT model of flexor muscle, reconstructed models of kinematic profiles; supervised single/multi-variable linear regression and support vector regression	Predicted evaluation scores (MAS) using TSRT, biomarkers from kinematics models, and combination of both; models estimation performance evaluated by mean square error

[1] Velocity profile was bell-shaped (more natural), other motor-driven apparatus used ramp-shaped motion; [2] Composite Spasticity Index [157]; [3] Fugl-Meyer Arm Assessment [158].

Appendix B: EMG Sensor Protocol

The exact placement of sEMG sensors follow the recommendations of the SENIAM project (Surface ElectroMyoGraphy for the Non-Invasive Assessment of Muscles) [110]:

Table B1. Sensor Placement of Shank Muscles

Tibialis Anterior	**Extensor Digitorum Longus**
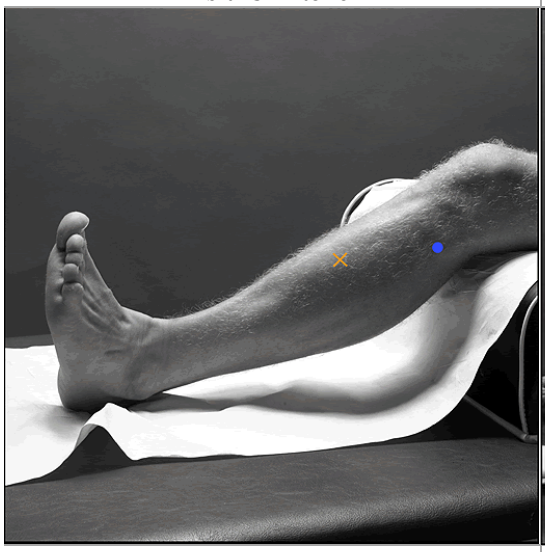	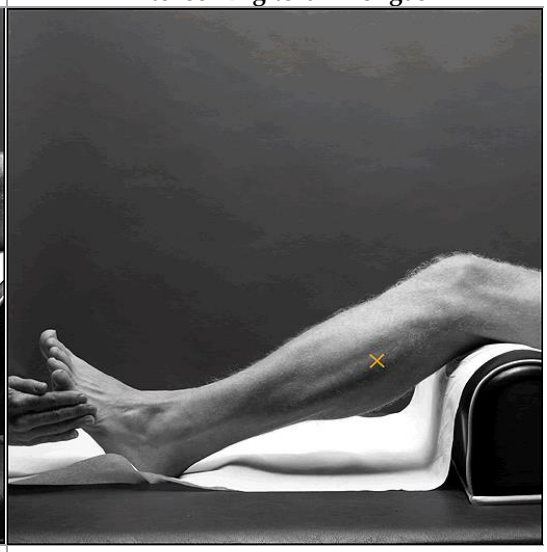
Extensor Hallucis Longus	Soleus
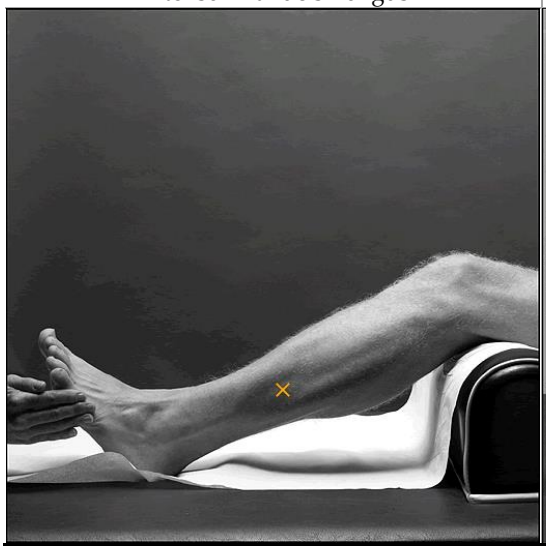	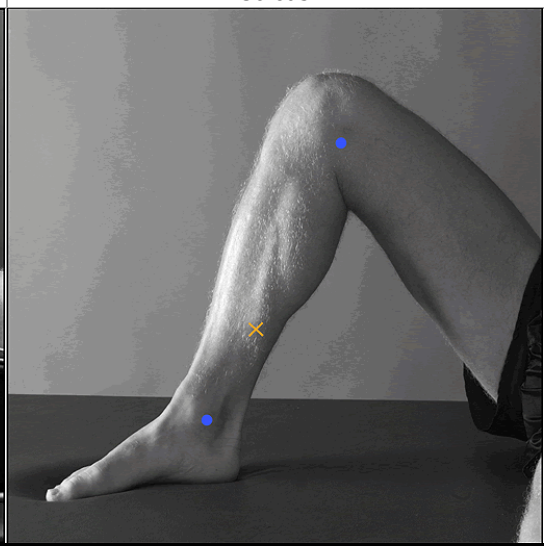

Gastrocnemius Medialis	Gastronemius Lateralis
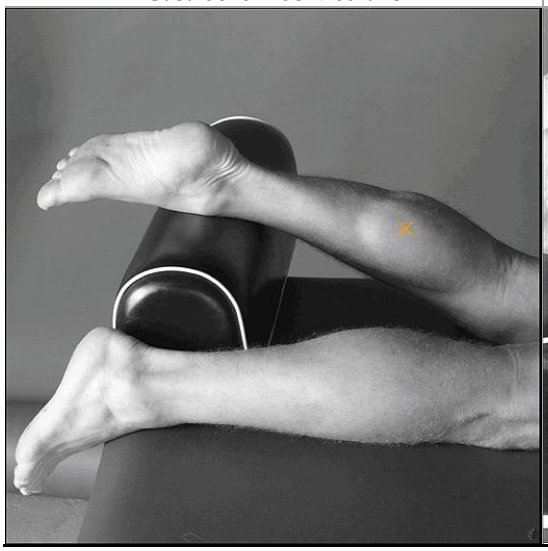	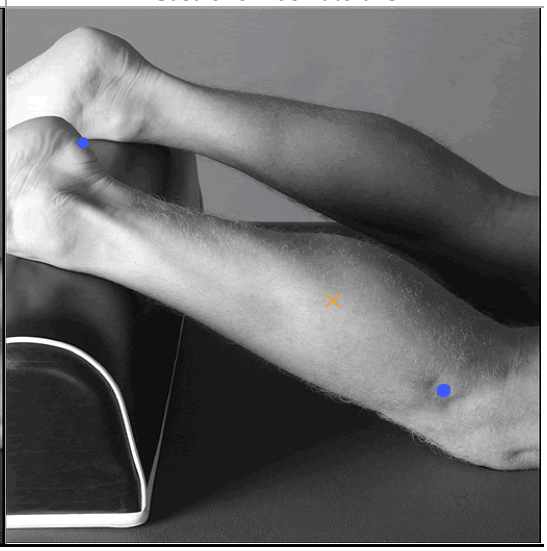

Table B2. Sensor Placement of Thigh and Hip Muscles

Biceps Femoris (long head)	Semitendinosus
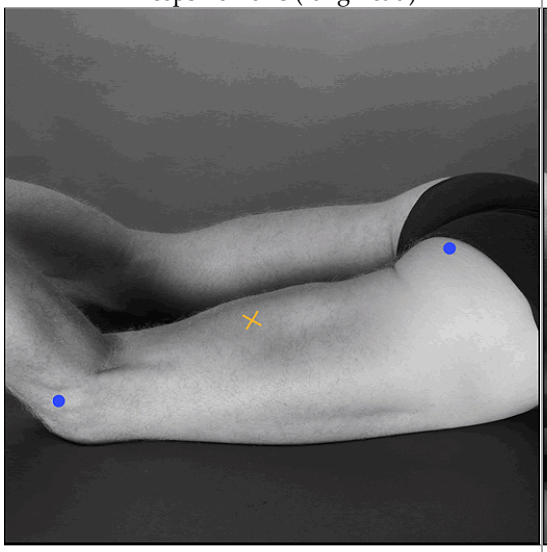	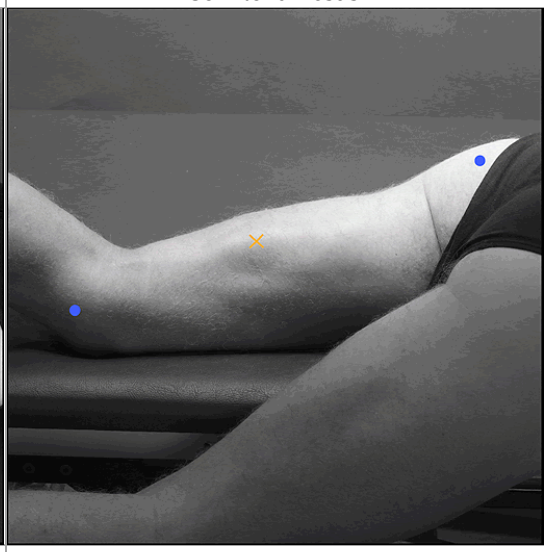
Rectus Femoris	Vastus Medialis
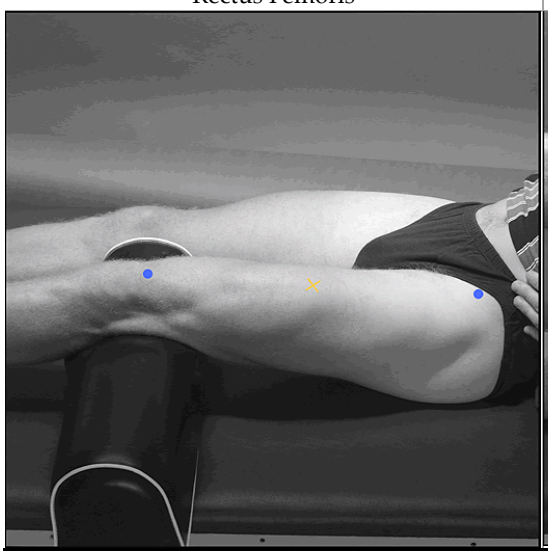	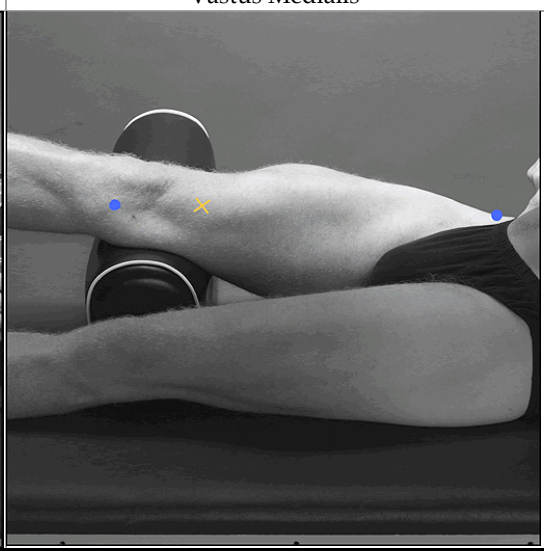

Vastus Lateralis	Gluteus Maximus
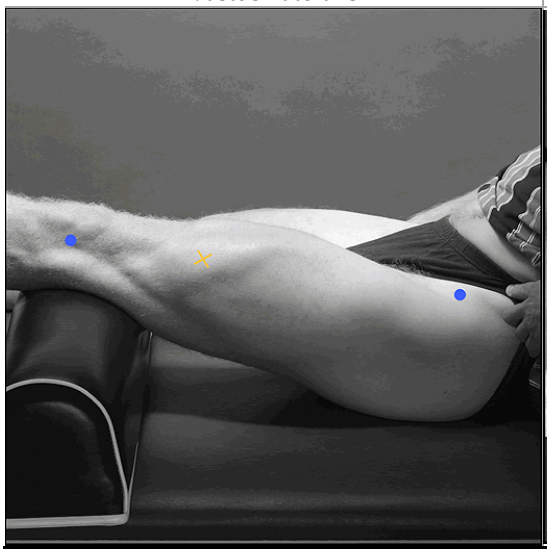	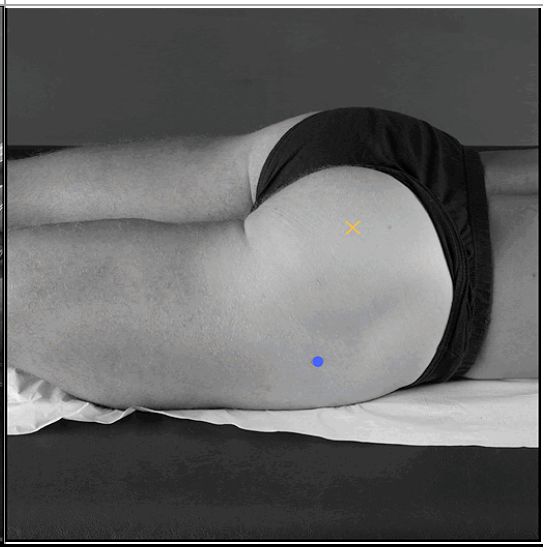

Appendix C: Supplementary Methodology

C.1 Converting Rotation Matrix to Quaternion

Given the rotation matrix is defined as:

$$\mathrm{R} = \begin{bmatrix} R_{11} & R_{12} & R_{13} \\ R_{21} & R_{22} & R_{23} \\ R_{31} & R_{32} & R_{33} \end{bmatrix} \tag{B1}$$

and a quaternion is generally defined as:

$$\vec{q} = [q_w \quad q_x\mathbf{i} \quad q_y\mathbf{j} \quad q_z\mathbf{k}] \tag{B2}$$

First, the trace T_R of the matrix must be obtained:

$$T_R = R_{11} + R_{22} + R_{33} \tag{B3}$$

If $T_R + 1 > 0$, then the quaternion can be found by:

$$s = \frac{1}{2\sqrt{T_R}} \tag{B4}$$

$$\vec{q}_0 = \left[\frac{1}{4s} \quad s(R_{32} - R_{23}) \quad s(R_{13} - R_{31}) \quad s(R_{21} - R_{12})\right] \tag{B5}$$

Otherwise, the calculation depends on largest diagonal element; if R_{11} is largest:

$$s = 2\sqrt{1 + R_{11} - R_{22} - R_{33}} \tag{B6}$$

$$\vec{q}_0 = \left[\frac{1}{s}(R_{23} - R_{32}) \quad \frac{1}{4}s \quad \frac{1}{s}(R_{12} + R_{21}) \quad \frac{1}{s}(R_{13} + R_{31})\right] \tag{B7}$$

Else if R_{22} is largest:

$$s = 2\sqrt{1 + R_{22} - R_{11} - R_{33}} \tag{B8}$$

$$\vec{q}_0 = \left[\frac{1}{s}(R_{13} - R_{31}) \quad \frac{1}{s}(R_{12} + R_{21}) \quad \frac{1}{4}s \quad \frac{1}{s}(R_{23} + R_{32})\right] \tag{B9}$$

Finally, if R_{33} is largest:

$$s = 2\sqrt{1 + R_{33} - R_{11} - R_{22}} \tag{B10}$$

$$\vec{q}_0 = \left[\frac{1}{s}(R_{12} - R_{21}) \quad \frac{1}{s}(R_{13} + R_{31}) \quad \frac{1}{s}(R_{23} + R_{32}) \quad \frac{1}{4}s\right] \tag{5211}$$

C.2 Converting Quaternion to Rotation Matrix

Given the quaternion is defined as **Eq. B1**, the corresponding rotation matrix is simply:

$$\mathrm{R} = \begin{bmatrix} {q_w}^2 + {q_x}^2 - {q_y}^2 - {q_z}^2 & 2(q_x q_y - q_w q_z) & 2(q_w q_y + q_x q_z) \\ 2(q_w q_z - q_x q_y) & {q_w}^2 - {q_x}^2 + {q_y}^2 - {q_z}^2 & 2(q_y q_z - q_w q_x) \\ 2(q_x q_z - q_w q_y) & 2(q_w q_x - q_y q_z) & {q_w}^2 - {q_x}^2 - {q_y}^2 + {q_z}^2 \end{bmatrix} \tag{B12}$$

C.3 Quaternion Multiplication

$$\begin{aligned} \vec{q}_{new} = \vec{q}_1 \otimes \vec{q}_2 &= [q_{1,w} \quad q_{1,x}\mathbf{i} \quad q_{1,y}\mathbf{j} \quad q_{1,z}\mathbf{k}] \otimes [q_{2,w} \quad q_{2,x}\mathbf{i} \quad q_{2,y}\mathbf{j} \quad q_{2,z}\mathbf{k}] \\ &= \begin{bmatrix} q_{1,w}q_{2,w} - q_{1,x}q_{2,x} - q_{1,y}q_{2,y} - q_{1,z}q_{2,z} \\ q_{1,w}q_{2,x} + q_{1,x}q_{2,w} + q_{1,y}q_{2,z} - q_{1,z}q_{2,y} \\ q_{1,w}q_{2,y} - q_{1,x}q_{2,z} + q_{1,y}q_{2,w} + q_{1,z}q_{2,x} \\ q_{1,w}q_{2,z} + q_{1,x}q_{2,y} - q_{1,y}q_{2,x} + q_{1,z}q_{2,w} \end{bmatrix}^T \end{aligned} \tag{B13}$$

C.4 Moment Arm and Line of Action

The moment arms and lines of action (LOA) of the knee flexor and extensor muscles are derived from in vivo modeling by Herzog and Read [159] using the reference frame origin as the knee joint centre:

$$r_{knee\ extensors} = 5\ cm \tag{B14}$$

$$r_{knee\ flexors} = -1.5\cos\left(\frac{3}{2}\theta_{knee}\right) + 2.5\ \ cm \tag{B15}$$

$$LOA_{knee\ extensors} = \frac{-25}{125}\theta_{knee} - 75\ \ deg \tag{B16}$$

$$LOA_{knee\ flexors} = \frac{-130}{140}\theta_{knee} + 260\ \ deg \tag{B17}$$

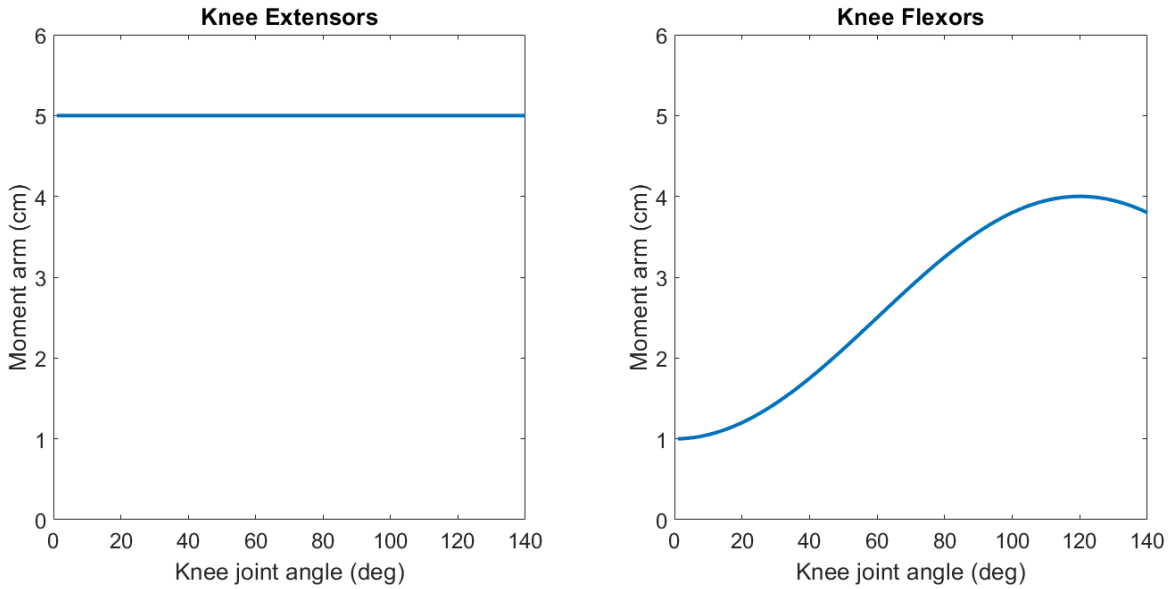

Figure B1. Moment arm of knee extensors and flexors as a function of knee angle

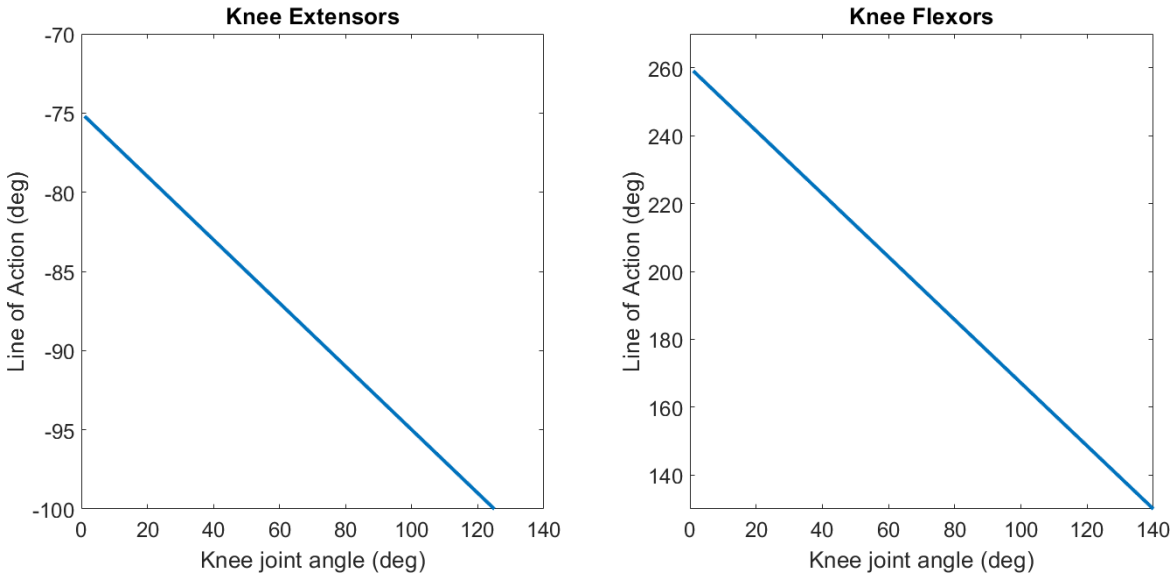

Figure B2. LOA of the knee extensors and flexors as function of knee angle.

Moment arms of the ankle plantarflexor and dorsiflexor muscles are derived from in vivo modeling by Rugg et al. [160]:

$$r_{plantarflexor} = \frac{-1.2}{50}\theta_{ankle} + 4.66 \;\; cm \tag{B18}$$

$$r_{dorsiflexor}(\theta) = \frac{1.5}{50}\theta_{ankle} + 4.8 \;\; cm \tag{B19}$$

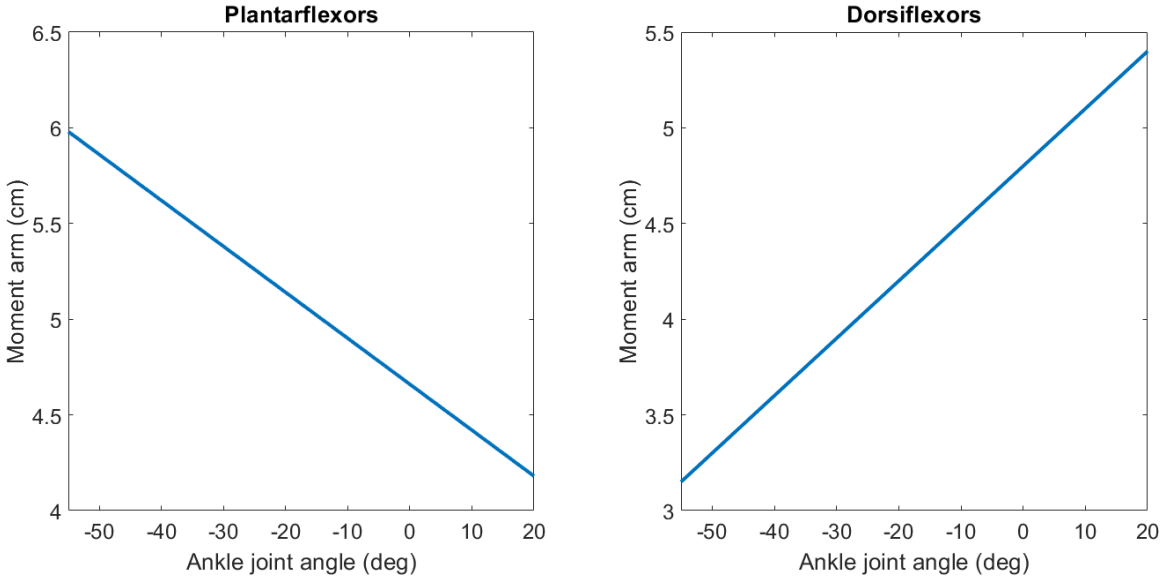

Figure B3. Moment arm of plantarflexors and dorsiflexors as a function of ankle angle

The LOA of the ankle muscles are derived from modeling by Procter and Paul [161]:

$$LOA_{plantarflexor} = \frac{-20}{45}\theta_{ankle} + 86.889 \quad deg \tag{B20}$$

$$LOA_{dorsiflexor} = \frac{4}{45}\theta_{ankle} + 36.222 \quad deg \tag{B21}$$

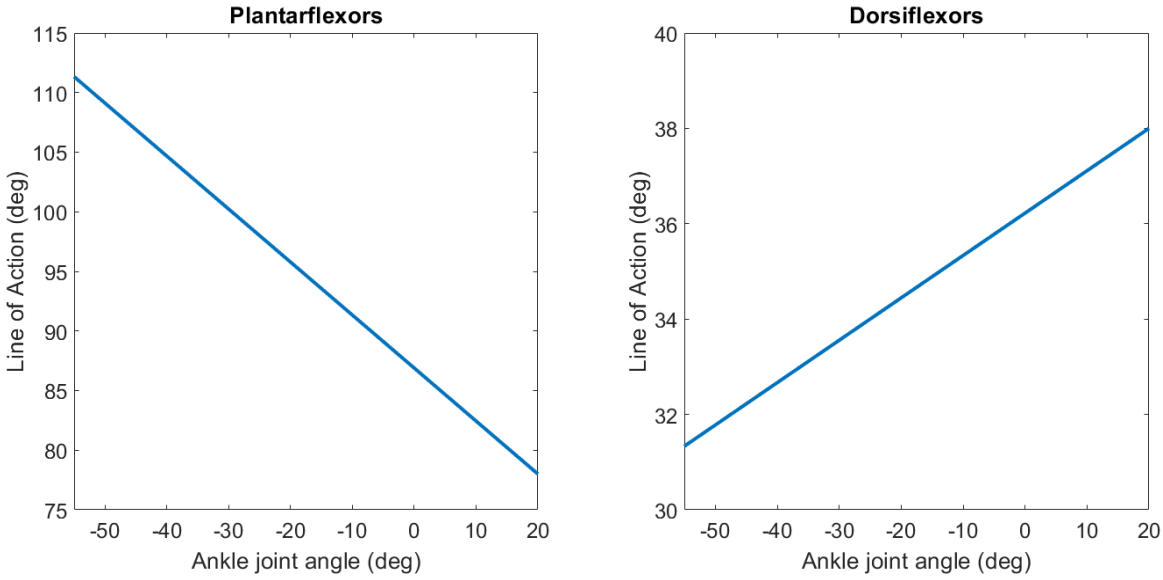

Figure B4. LOA of plantarflexors and dorsiflexors as a function of ankle angle.